ABSTRACT

SHARMA, LAVYA. Design and Development of an Unmanned Microgravity Test Platform (Under the direction of Dr. Venkateswaran Narayanaswamy).

Microgravity research enables scientists and researchers to study physical and biological phenomena in a unique environment free from Earth's gravitational influence and thus holds paramount significance. This research explores the innovative creation of a specialized Unmanned Microgravity Test Platform to conduct short-duration and repeatable research and testing while achieving microgravity conditions within the proximity to the ground. The primary focus of this study lies in executing a drop test to attain a microgravity environment by advancing the capabilities of an Unmanned Aerial Vehicle system through subtle design considerations, encompassing structural, propulsion, and control systems leveraging rapid prototyping methodology. The imperative for such a specialized platform stems from the burgeoning demand for microgravity research and experiments crucial in advancing our understanding of the universe, improving technology, and mitigating the challenges of space exploration and terrestrial endeavors.

This investigation delineates the conceptualization and engineering intricacies of the Test Platform through a meticulous design approach, achieving a balance between structural integrity, weight efficiency, and capability to induce microgravity conditions. The platform achieves enhanced performance by incorporating innovative design principles and leveraging engineering tools, enabling the UAV system to carry scientific instruments and experimental payloads. Key facets of the research include the development of a scalable UAV system adept at collecting data and executing maneuvers to conduct microgravity experiments. Rapid prototyping techniques are employed to optimize the UAV’s design iteratively, addressing challenges unique to microgravity while enhancing overall performance and reliability. This research elaborates on the systematic testing and validation of the drop conducted to attain the desired microgravity environments, exemplifying the platform's effectiveness in maintaining stability and precision during experimental operations.

Furthermore, the research aims to bridge the gap with the existing microgravity platforms and deliver an incorporation of cutting-edge technologies for enhancing the platform's functionality. The validation of the unmanned microgravity test platform is demonstrated through a series of successful trials that simulated microgravity environments. Results and data obtained from these trials underscore the platform's efficacy in providing a stable and controlled experimental setting.

In conclusion, this research endeavors to establish a comprehensive framework for designing and developing an unmanned microgravity test platform capable of achieving microgravity conditions with a drop test. The platform's versatility and adaptability make it a valuable tool for scientists and engineers engaged in orbital research, offering a unique opportunity to explore and validate technologies in a microgravity environment. The designed novel unmanned platform serves as a stepping stone for further research and applications, opening new avenues for scientific exploration and technological innovation in the realm of space research.

Keywords:

Microgravity, UAVs, Design, Drop Test, Drop Capsule, Rapid Prototyping, Drop Mechanism

Design and Development of an Unmanned Microgravity Test Platform

By

Lavya Sharma

A thesis submitted to the Graduate Faculty of
North Carolina State University
in partial fulfillment of the requirements
for the degree of Master of Science

Aerospace Engineering

Raleigh, North Carolina
2024

APPROVED BY:

_______________________________ _______________________________
Dr. Gracious Ngaile Dr. Liming Xiong

____
Dr. Venkateswaran Narayanaswamy
Committee Chair

DEDICATION

Immense expression of gratitude to my advisor and family for their unwavering support, belief, and encouragement in my academic journey. Their constant guidance, wisdom, and camaraderie have enriched my learning experience.

BIOGRAPHY

Lavya Sharma was born on 17th April 1999 in New Delhi, India. After spending her childhood in her hometown, she moved to the beautiful city of Dehradun in the foothills of the Himalayas from 2017 to 2021, to pursue her bachelor's degree in Mechanical Engineering. Her childhood dream and passion for becoming an Aerospace Engineer led her to move to United States to pursue a Master's degree in Aerospace Engineering from North Carolina State University, Raleigh, NC from 2022 to 2024. She is a traveler and enjoys hiking, trekking, stargazing, astronomy, astrophysics, history and geography.

ACKNOWLEDGMENTS

I extend my deepest gratitude to all those who have contributed to the completion of my Master's thesis in Aerospace Engineering at North Carolina State University.

First, I would like to express my sincere appreciation and gratitude to my advisor, Dr. Venkateswaran Narayanaswamy, for his unwavering guidance, mentorship, and continuous support throughout this research endeavor. Their expertise, encouragement, and constructive feedback have been instrumental in shaping the trajectory of this thesis. I am immensely thankful to the faculty members of the Aerospace Engineering Department for fostering an intellectually stimulating environment. Their commitment to academic excellence and passion for aerospace research has been a constant source of inspiration.

I owe a debt of gratitude to my peers and fellow graduate students for their camaraderie, insightful discussions, and collaborative spirit. Our collective efforts have enriched my academic experience and provided valuable perspectives. Special thanks are due to the administrative staff and library resources at North Carolina State University for their assistance and facilitation, which have greatly contributed to the success of this research. I would like to express my heartfelt appreciation to my family for their unwavering support, understanding, and encouragement throughout this academic journey. Their love and encouragement have been my pillars of strength.

Finally, I am grateful to the funding agencies or any other organizations that supported this research financially. Your contribution has been essential in making this work possible. Thank you to everyone who has played a role in this academic pursuit. Your support has been invaluable, and I am truly grateful for the collective efforts that have culminated in the completion of this thesis.

TABLE OF CONTENTS

LIST OF TABLES

LIST OF FIGURES

CHAPTER 1

INTRODUCTION

1.1. BACKGROUND

Microgravity, often referred to as "weightlessness" or "zero gravity," is the condition in which objects appear to be in a state of free fall towards a massive body, such as Earth, but are actually in a continuous state of falling and orbiting. This occurs when an object is in a state of constant acceleration due to the force of gravity, and the object and its surroundings experience the same acceleration. As a result, everything inside a spacecraft or a freely falling object appears to be weightless, as there is no apparent force acting on them. Microgravity signifies a state where the force of gravity is significantly reduced, resulting in the sensation of weightlessness for objects and individuals within that environment.

While gravity is still present & the effects are on such a small scale that they become negligible compared to the normal gravitational force experienced on Earth's surface, coining the term “microgravity”. Several factors contribute to the experience of microgravity such as a constant free fall of the object or spacecraft, which creates a sensation of weightlessness for everything inside it. Conducting experiments in a microgravity environment provides unique insights that are not achievable on Earth. This condition is commonly encountered in space, whether it be in the International Space Station (ISS), orbiting satellites, or during parabolic flights that simulate short periods of microgravity on Earth.

Harnessing and understanding the effects of microgravity contributes to advancements across various disciplines, fostering innovation and expanding our knowledge of the fundamental principles governing the universe. Microgravity allows scientists to study fluid behavior without the influence of buoyancy and convection, leading to a better understanding of fluid dynamics and heat transfer. The absence of gravitational effects helps researchers investigate the properties of materials in their purest form, leading to improved materials for use in various applications. Microgravity provides insights into how living organisms, from cells to entire organisms, respond to a weightless environment. This research is crucial for understanding human health in space and potential applications on Earth [1]. Studying the effects of microgravity on the human body is essential for planning long-duration space missions, such as missions to Mars. It helps address challenges like bone density loss, muscle atrophy, and fluid shift that astronauts experience in space [2]. Microgravity can impact biological processes, offering a unique environment for drug testing and development. This can lead to the discovery of new treatments and medications. Understanding how fluids behave in microgravity is crucial for designing spacecraft systems, including fuel transfer, life support, and waste management.

Microgravity experiments assist in testing the resilience and performance of materials that are used in spacecraft construction. Studying plant growth in microgravity can have applications for future space exploration, such as growing food on long-duration missions [3]. It can also lead to innovations in agriculture on Earth. Microgravity can enable the production of unique materials and structures, leading to advancements in manufacturing processes. Testing equipment and technologies in a microgravity environment allows for a more accurate assessment of their performance and potential issues. It provides an opportunity to study fundamental physics questions related to gravity, including its effects on various phenomena. Microgravity research and space experiments offer educational opportunities to inspire students and promote interest in science, technology, engineering, and mathematics (STEM) fields.

Figure 1.1: Astronaut aboard the International Space Station portraying the effects of microgravity on a floating glob of water

This century holds tremendous promise for the future of space exploration, with unprecedented opportunities and advancements on the horizon. It is bringing in programs like the Artemis and Mars missions, Space Tourism and Commercialization, development of satellite constellations, and missions to study the outer planets having a dynamic follow-up with a myriad of missions, collaborations, and scientific developments changing the whole game. The International Space Station (ISS) stands as the cornerstone in our pursuit of progressive developments and advancements within microgravity environments. Serving as the primary platform, it leads the way for a myriad of scientific, technological, diplomatic, and educational breakthroughs. In all this space exploration, is the focal point for encompassing scientific, technological, diplomatic, and educational domains [4]. The ISS stands as a symbol of international cooperation, involving space agencies from multiple countries, including NASA

(United States), Roscosmos (Russia), ESA (European Space Agency), JAXA (Japan Aerospace Exploration Agency), and CSA (Canadian Space Agency).

1.2. OUR ACCESS TO MICROGRAVITY:

Achieving microgravity on Earth for scientific research involves various methods and facilities. Here are some of the past and current research efforts and facilities used to simulate microgravity:

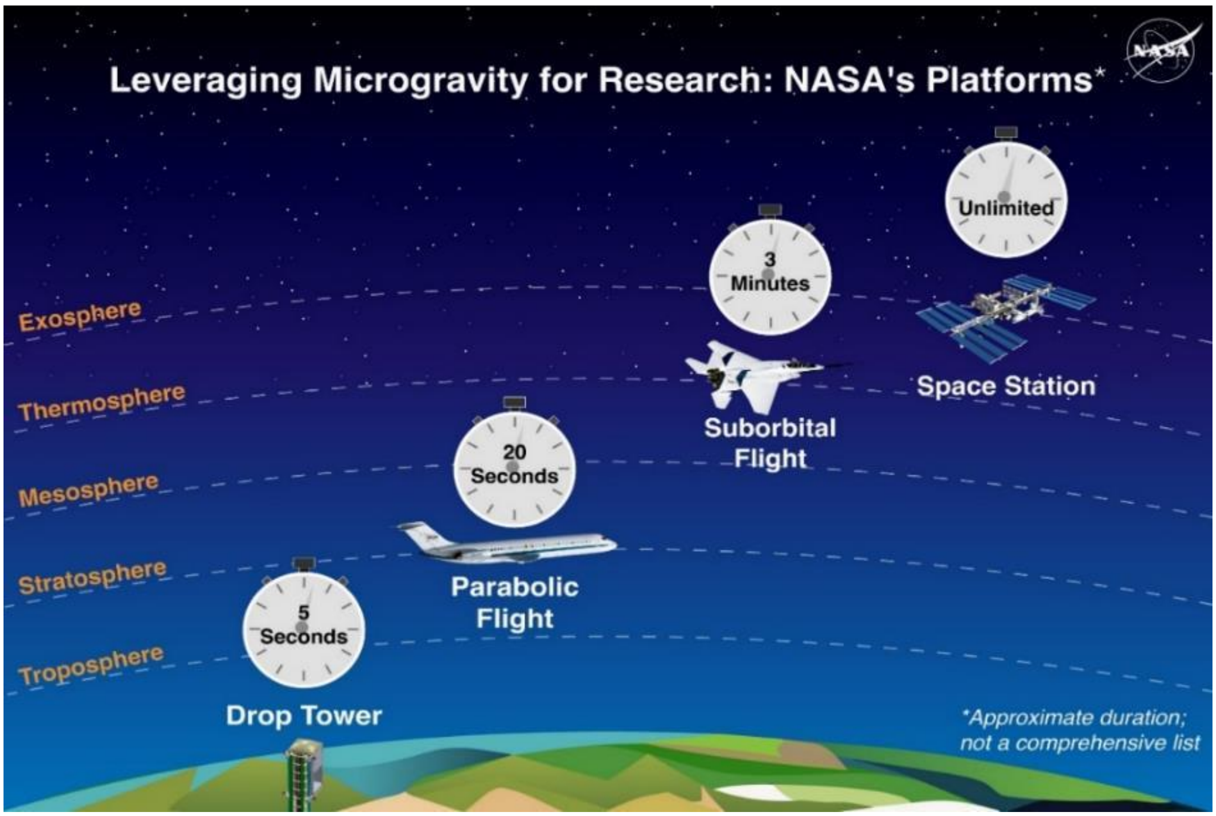

Figure 1.2: Different Platforms with their duration of microgravity

1.2.1 SPACE SHUTTLES AND SPACE STATIONS

While not on Earth, Space shuttles and space stations like the International Space Station (ISS) provide actual microgravity environments for extended periods. Space stations like the ISS serve as premier microgravity research facilities placed in low Earth orbit, where they continuously fall toward the Earth due to gravity but move forward fast enough to remain in orbit. This results in an environment of microgravity, commonly referred to as "weightlessness" or "zero gravity."

Figure 1.3: Astronauts experiencing microgravity on the International Space Station

The occupants of a space station, including astronauts and any experiments on board, experience a constant state of free fall toward the Earth. This creates a sensation of microgravity, allowing for extended periods of experimentation. Astronauts on extended missions on the ISS may experience changes in bone density, muscle mass, and other physiological adaptations due to the absence of regular gravitational stress [1]. Investigating these effects helps scientists develop strategies to mitigate health issues and maintain the well-being of astronauts during long-duration space travel. The ISS is equipped with scientific laboratories where researchers can conduct experiments in various fields, such as physics, biology, and materials science [10]. This unique microgravity environment enables investigations into phenomena that are not possible under the influence of Earth's gravity.

1.2.2 PARABOLIC FLIGHTS AND SOUNDING ROCKETS

Suborbital methods are a unique and valuable tool in the field of microgravity research. Parabolic flights involve specialized aircraft flying along a carefully choreographed trajectory, creating a series of parabolas. During a parabolic flight, an aircraft follows a specific trajectory that involves ascending steeply, reaching the apex of the parabola, and then descending rapidly making the occupants experience a brief period of near-weightlessness or microgravity.

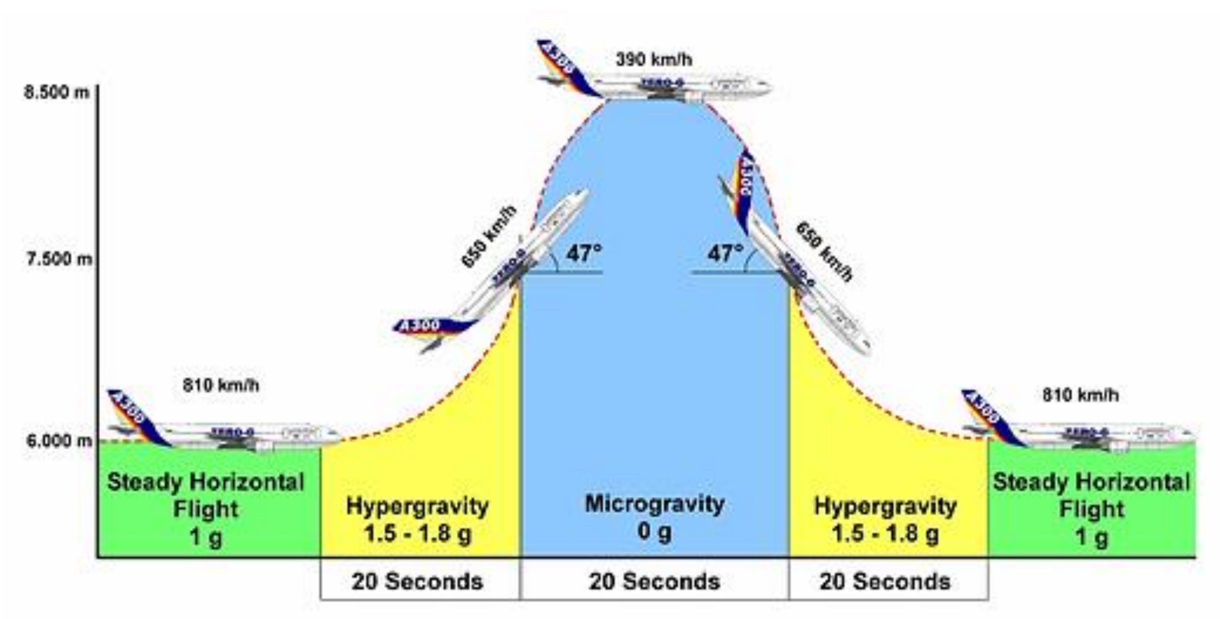

Figure 1.4: The phases of a parabolic flight

The ascent phase creates a pull of 1.8 g to 2 g, which is greater than Earth's gravity, while the descent phase induces a period of microgravity, allowing objects and occupants inside the aircraft to experience a state of near-weightlessness [5]. At the peak of the parabola, the aircraft enters a state of free fall. During this phase, everything inside the aircraft, including passengers and experiments, is essentially falling at the same rate as the aircraft itself [6]. This creates a microgravity environment within the cabin, where the gravitational forces are greatly reduced, leading to a sensation of weightlessness for about 20-30 seconds [7]. The short duration of microgravity allows for multiple parabolas during a single flight, providing researchers with the opportunity to conduct a series of experiments within a relatively short time frame. Researchers deploy experiments, including UAVs or other payloads, during the weightless phase of the parabola, providing insights into phenomena that would otherwise be challenging to study on Earth.

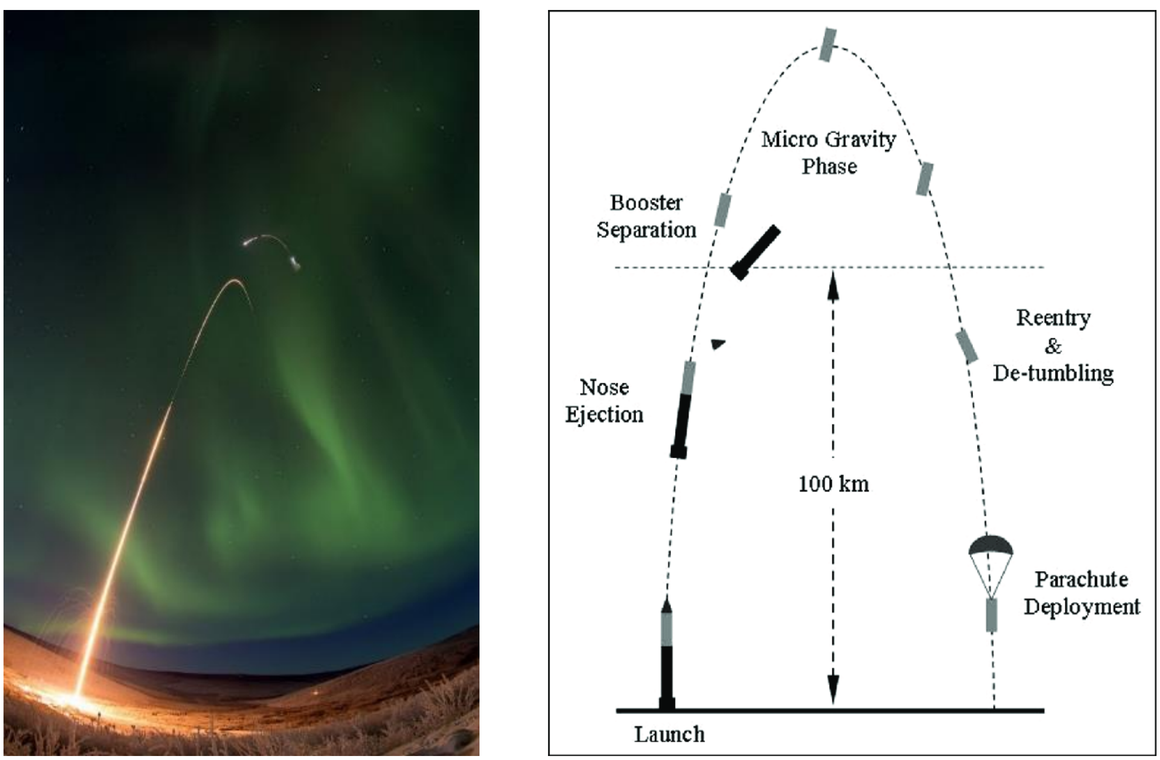

Figure 1.5: Suborbital Rocket on its trajectory (left) and its phases (right).

Sounding rockets follow a trajectory that takes them into space before descending back to Earth. They reach altitudes beyond the Earth's atmosphere but do not achieve orbit. The flight path is typically vertical or at a specific angle. Sounding rockets provide several minutes of microgravity during their ascent and descent phases. The duration depends on the specific mission and trajectory, offering researchers a relatively short but valuable period in a reduced-gravity environment. This controlled free-fall environment allows scientists to conduct experiments that simulate the effects of reduced gravity on physical, biological, and chemical systems. Parabolic flights and sounding rockets offer a more accessible and cost-effective means of experiencing microgravity compared to extended space missions or other specialized facilities. Research teams, including scientists, engineers, and even private individuals, can participate in parabolic flights to test and validate their experiments in a microgravity environment without leaving Earth's atmosphere.

Figure 1.6: Inside the “Vomit Comet” Aircraft

Aircraft like the "vomit comet" (e.g., the NASA Reduced Gravity Aircraft) perform parabolic flights, creating brief periods of microgravity by following a specific flight path [8]. During the free-fall part of the parabola, occupants experience a reduced gravitational force. Drop capsules are often used in parabolic flights, where an aircraft follows a trajectory that creates brief periods of microgravity. During these flights, experiments are placed in drop capsules that experience true weightlessness for short durations. Drop capsules are suitable for experiments requiring short-duration exposure to microgravity, and they provide a cost-effective alternative to space missions for certain types of research.

1.2.3 DROP TOWERS

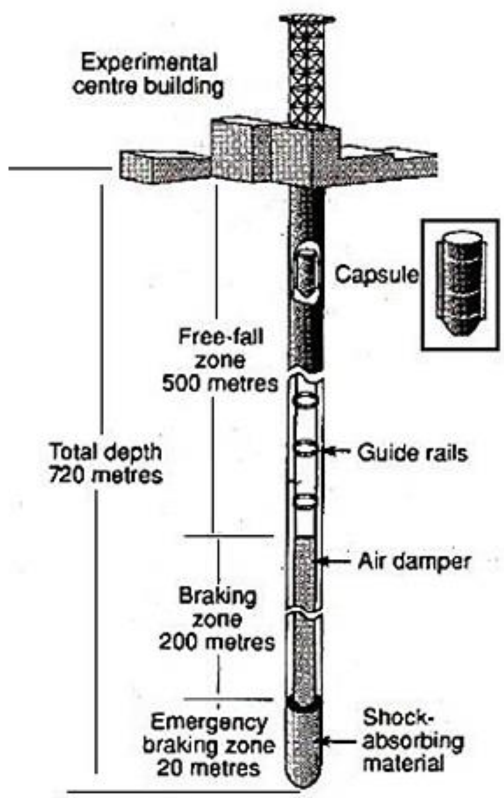

Figure 1.7: A detailed drop tower

A drop tower is a vertical structure from which experiments are dropped, creating a brief period of microgravity. Drop towers serve as unique facilities for conducting microgravity experiments on Earth. The key concept behind drop towers is the use of free fall. Objects inside the drop tower experience a state of near weightlessness as they fall under the influence of gravity but without the support force from the structure of the tower. The fall is carefully controlled, creating a brief period of microgravity during which experiments are conducted.

Figure 1.8: Bremen Drop Tower facility, Germany

Drop towers are typically tall structures with a vertical shaft. The experimental payload is placed at the top of the tower, and the entire assembly is released to fall freely under the force of gravity. The structure of the tower ensures that air resistance and other external factors do not significantly affect the free fall of the payload. Drop tower experiments are short, typically lasting a few seconds [9]. Researchers can conduct experiments in a microgravity environment without the complications associated with longer-duration microgravity platforms. While the duration is limited, the controlled conditions and rapid descent provide valuable insights into the behavior of materials, fluids, and biological samples in reduced gravity. Compared to space missions or extended microgravity platforms, drop tower experiments are relatively cost-effective. This makes them accessible to a broader range of researchers and institutions. The shorter duration of microgravity is suitable for experiments that do not require prolonged weightlessness. Drop towers are located on the Earth's surface, providing researchers with easy access to the experimental setup. This simplifies the logistics and allows for efficient preparation and execution of experiments. Researchers utilize these facilities to advance our understanding of fundamental scientific principles and to test technologies destined for space, contributing valuable data to various fields, from physics to materials science.

1.2.4 GLIDER FLIGHTS

Figure 1.9: Glider Flight

To achieve a short duration of microgravity, glider flights offer a unique relatively accessible platform for scientific research, educational purposes, etc. The glider aircraft ascend steeply exerting an upward force on the occupants and then as the glider reaches the peak of its ascent and begins its phase of controlled descent. The force of gravity acting on the occupants is counteracted by the downward acceleration of the glider allowing a momentary sensation of weightlessness. The experience of microgravity during a glider flight is short and lasts about a few seconds. It is an economical alternative compared to other methods of achieving microgravity such as parabolic flights, sounding rockets, or space stations but it requires specialized equipment, trained pilots, and operational and maintenance support leading to higher costs. Gliders heavily depend on weather conditions and airspace restrictions which impact the feasibility and safety of conducting microgravity experiments. These flights are also subject to operational restrictions such as altitude restrictions, flight duration constraints, scheduling conflicts, and availability of flight space, falling under the category of manned microgravity platform.

Figure 1.10: Neutral Buoyancy Laboratory, NASA, Houston, Texas

Facilities located underwater, such as NASA's Neutral Buoyancy Laboratory (NBL), replicate microgravity to train astronauts and assess equipment. Situated at NASA's Johnson Space Center in Houston, Texas, the NBL is a large indoor pool featuring a full-scale mock-up of the International Space Station (ISS) [10]. Its primary purpose is to prepare astronauts for extravehicular activities (EVAs) or spacewalks. Divers in the NBL fine-tune the buoyancy of astronauts and equipment using weights and flotation devices. Objects with neutral buoyancy in water neither sink nor rise, creating a simulated state of weightlessness at a specific depth. Underwater practice allows astronauts to simulate space challenges, adapting to the absence of buoyancy and the distinctive conditions of moving and working in a weightless environment. Equipped with specialized suits and gear, astronauts are immersed in the pool, which replicates the ISS structure. While the NBL isn't expressly designed for microgravity research, its training is vital for acclimating astronauts to space's microgravity conditions. Although the NBL doesn't provide true microgravity, the extensive underwater training periods provide astronauts an extended exposure to a nearly weightless setting, fostering the development of muscle memory and adaptability crucial for successful space missions.

Other methods that create conditions with reduced gravitational effects are Magnetic and Electric field Levitations where the object is suspended in mid-air using the magnetic or electric field against gravity. This approach is particularly useful for studying the behavior of materials, fluids, and biological samples in a controlled magnetic field. The European Space Agency (ESA) has explored the concept of a space-based drop tower, which involves free-fall experiments in microgravity conditions for extended durations.

1.3. UNMANNED AERIAL VEHICLES (UAVs)

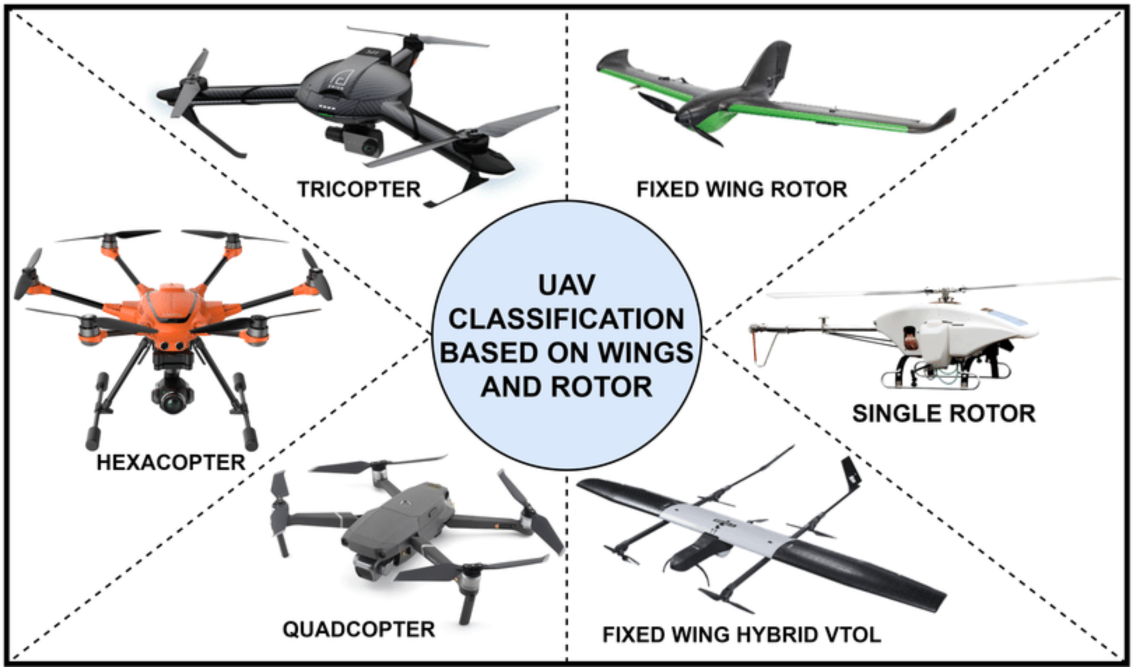

Figure 1.11: Types of UAVs

In the ever-evolving landscape of aerospace engineering, the pursuit of groundbreaking technologies has become imperative to propel scientific exploration to new frontiers. The concept of pilotless aircraft was first introduced by the Serbian-American inventor Nikola Tesla envisioned unmanned aerial vehicles for military applications as early as 1915 [11]. After its exceptional roles starting initially from surveillance, and target practice to various commercial and civilian applications like photography, inspections, agriculture, etc. has been a breakthrough in aviation technology continuing its advancements with artificial intelligence, energy efficiency, autonomy, and delivery systems. UAVs, or Unmanned Aerial Vehicles (UAVs), hold significant importance across various domains due to their versatility, cost-effectiveness, and ability to access hard-to-reach or hazardous areas. UAVs play a pivotal role in contemporary military operations, specializing in reconnaissance, surveillance, and intelligence gathering.

Figure 1.12: UAVs for military applications

They excel in monitoring enemy activities, conducting aerial surveys, and delivering real-time information to military personnel. In search and rescue missions, especially in hard-to-reach areas, UAVs equipped with cameras and thermal imaging quickly locate missing persons and assess disaster-stricken regions. For law enforcement and security agencies, UAVs enhance surveillance capabilities by monitoring crowds, borders, critical infrastructure, and public events, ensuring public safety and swift responses to potential threats. In agriculture, UAVs contribute to crop monitoring, precision farming, and assessing crop health. Farmers benefit from valuable data on crop conditions, enabling efficient resource allocation, pest control, and yield optimization. Infrastructure inspections, such as bridges, power lines, pipelines, and buildings, are streamlined by UAVs accessing hard-to-reach or hazardous locations. This reduces the need for manual inspections, improving safety and efficiency. In environmental conservation, UAVs monitor wildlife, forests, and water bodies, aiding researchers in collecting data on biodiversity, tracking ecosystem changes, and assessing the impacts of climate change. Disaster management benefits from UAVs providing rapid aerial assessments of affected areas, delivering supplies to inaccessible locations, assessing post-disaster damage, and assisting in coordinating emergency response efforts [12]. The entertainment industry has witnessed a revolution in filmmaking and photography due to UAVs, offering unique aerial perspectives previously challenging or expensive to achieve. They are now crucial tools for capturing stunning visuals in movies, documentaries, and other media productions. Companies are exploring UAV use for delivery services, particularly in remote or challenging terrains. UAVs efficiently deliver medical supplies, food, and essential items, especially in emergencies. Recreationally, UAVs have become popular, providing hobbyists with opportunities for aerial photography, racing, and exploration, making aerial technology accessible to a broader audience. Consumer UAVs have contributed to the widespread adoption of this technology for personal use.

1.4. RESEARCH OBJECTIVES

The objectives of this research are multifaceted and aim to address major aspects of creating an innovative platform for microgravity research. Initially, the study conducted an extensive literature review to comprehensively understand the existing landscape of microgravity research, UAV systems, and pertinent technologies. Subsequently, the research defined the specific design requirements and constraints, considering factors such as payload capacity, maneuverability, and safety features.

The primary focus then shifts to the conceptualization and design of the microgravity platform, including the selection of materials and integration of sensors. An integral objective is the development of a UAV system capable of precise control and stable maneuverability to accurately simulate microgravity conditions. The validation process involves conducting simulated microgravity experiments to assess the platform's effectiveness, stability, and reliability. Furthermore, the study aims to evaluate the feasibility of the unmanned microgravity platform as a cost-effective alternative for microgravity research, comparing its performance with existing methods and creating a platform smaller, affordable, and accessible for universities or research institutes to employ this method for studying the effects of microgravity. Additionally, the research seeks to optimize and refine the platform design based on experimental outcomes and feedback, ultimately contributing to the advancement of microgravity research methodologies. The final objective encompasses comprehensive documentation and communication of research findings through technical reports, presentations, and potential publications in scientific journals. Through these objectives, the research aspires to make a significant contribution to the field by providing insights into the design and development of an unmanned microgravity platform using a UAV system for scientific experimentation.

1.5. SCOPE AND SIGNIFICANCE

The scope of this research encompasses the comprehensive design, development, and evaluation of an unmanned microgravity platform using a UAV system. The significance of this study lies in its potential to democratize access to microgravity environments, enabling researchers and scientists to conduct experiments that were previously constrained by financial and logistical limitations. The developed platform could find applications in various scientific disciplines, including physics, biology, and materials science.

1.6. THESIS OUTLINE

This thesis is organized into several chapters, each addressing specific aspects of the design and development process. The subsequent chapters will delve into the literature review, design methodology, system implementation, experimental results, and conclusions drawn from the study. This thesis brings forward a method to achieve this microgravity environment for research and experiments while minimizing the cost and making it accessible, convenient, and tractable using a UAV system. The convergence of unmanned aerial vehicles (UAVs) and microgravity research presents a unique opportunity to revolutionize the way experiments are conducted without the effects of gravity. Our research endeavors to push the boundaries of conventional approaches by introducing the design and development of an Unmanned Microgravity Test Platform to achieve microgravity conditions while executing a drop test. The objective is to address the challenges associated with conducting experiments in microgravity by utilizing the agility and adaptability of a quadcopter system integrating rapid prototyping techniques streamlining the development process and customization of the test platform. By developing an affordable and adaptable unmanned microgravity test platform, this project aspires to create a platform that caters to a wide spectrum of scientific endeavors, from academic institutions to private research entities.

Allowing objects to fall freely under the influence of gravity provides a brief period of weightlessness simulating the effect of microgravity experienced in space. In this project, a drop capsule carrying the object or experiments that we intend to subject to microgravity is mounted to the UAV as a payload. To release the payload from the UAV when it reaches the desired location and altitude, a drop/release mechanism is triggered which subjects the payload to free fall under gravity. The component selection for the UAV system involves careful consideration of factors such as battery capacities, optimal choices for propeller diameter, motor rpm/volt combinations, and the design of the drop mechanism based on the objective, payload weight, and thrust capacity to achieve high flight stability and maneuverability. This research employs the technique of rapid prototyping used to quickly fabricate a scale model or prototype of a physical part or assembly. The primary goal of rapid prototyping is to enable the swift and cost-effective creation of a tangible representation of a design, allowing designers, engineers, and stakeholders to evaluate and test the concept before moving on to full-scale production. The key characteristics of rapid prototyping include speed, flexibility, and the ability to produce functional prototypes for testing and validation. The research conducts a controlled drop test to simulate microgravity conditions evaluating the structural integrity, adaptability, and functionality of the UMTP. These drop tests validated the performance of the platform while the iterative approach ensured that the final system delivered the desired goal. The duration of microgravity achieved in the drop test is relatively short depending on the height from where it is released and the design of the experiment. Even then this provides valuable insights into the behavior of objects and materials in a microgravity environment, allowing them to conduct experiments that would be challenging or impossible under normal gravity conditions.

Essentially, this study aims to advance the field of space exploration by introducing an innovative Unmanned Microgravity Test Platform. By strategically integrating drop testing and cutting-edge engineering, our objective is to elevate the capabilities of UAV systems. This endeavor paves the way for more refined and efficient experimentation within the demanding microgravity environments found beyond Earth's atmosphere.

CHAPTER 2

IDEATION & SYSTEM INTEGRATION

2.1. CONCEPTUALIZATION

Microgravity research provides unique opportunities and insights by advancing our understanding of fundamental processes in various scientific disciplines, ranging from fundamental physics to life sciences and material science. However, conducting experiments in true microgravity environments remains a complex challenge. Conventional approaches to achieving microgravity, such as parabolic flights or drop towers, present notable limitations in terms of cost, accessibility, and experimental duration. The requisites for trained crew, organizational coordination, and aircraft rental make these methods financially prohibitive, especially for smaller projects or institutions. Moreover, challenges arise from factors like air turbulence, vibrations, and temperature variations, impacting the precision and reliability of microgravity simulation. Access to these traditional test facilities is often geographically confined, posing a significant hurdle to the inclusivity of scientific exploration. Sounding rockets and parabolic flights, characterized by sudden changes in gravitational forces, introduce safety risks to both experimental setups and researchers, further complicating the feasibility of experiments. On the other hand, ground-based simulators, while more accessible, lack the flexibility and dynamic control required for a diverse range of experiments. Restrictions on the complexity or size of experiments due to space and weight limitations limit the adaptability of these simulators. Their fixed set of parameters further constrains their flexibility and applicability across various research domains. This underscores the pressing need for a paradigm shift in microgravity experimentation.

The proposed unmanned microgravity test platform, with its UAV integration, seeks to overcome these limitations by providing a cost-effective, accessible, and dynamic alternative. This innovative approach not only addresses the financial and geographical barriers but also enhances safety, adaptability, and control, ushering in a new era of inclusive and versatile microgravity research.

This research intends to address these limitations and contribute to creating a cost-effective and accessible microgravity simulation platform. The concept of employing a UAV system to establish a microgravity test platform through a carefully orchestrated drop test represents a groundbreaking approach at the intersection of aerospace technology and scientific experimentation. Leveraging the inherent capabilities of UAVs, particularly their stability, precision, and maneuverability, offers an innovative solution to simulate microgravity conditions in a controlled and repeatable manner. In this paradigm-shifting approach, the UAV system orchestrates a precisely controlled drop, creating a transient state of near-weightlessness conducive to microgravity experimentation. The unmanned aerial vehicle's capacity to navigate three-dimensional space with unparalleled accuracy allows for the creation of controlled descent profiles, enabling researchers to tailor the microgravity environment to the specific requirements of diverse experiments. By utilizing a UAV for microgravity simulations, researchers gain unprecedented flexibility, overcoming the limitations associated with traditional methods such as parabolic flights or drop towers. The autonomous nature of the UAV system, coupled with real-time data exchange capabilities, ensures dynamic adjustments during the descent phase, resulting in a more accurate and adaptable microgravity simulation platform. This approach not only extends experimental durations but also facilitates experimentation in diverse geographical locations, thereby democratizing access to microgravity research. Moreover, the UAV's ability to rapidly ascend and descend provides researchers with a unique tool to conduct iterative and efficient experiments, accelerating the pace of scientific discovery. The integration of safety features and fail-safes further underscores the commitment to secure and reliable microgravity experimentation. In essence, the fusion of UAV technology with the execution of drop tests for microgravity simulation heralds a new era in scientific research. This methodology not only pushes the boundaries of aerospace engineering but also opens avenues for advancements across scientific disciplines, from fundamental physics to biomedical research and material science. The convergence of UAV's capabilities with microgravity experimentation signifies a pioneering step towards fostering innovation, accessibility, and precision in the realm of scientific exploration. This independent and personalized microgravity test platform eliminates the need for organizational intervention, offering researchers unprecedented access to simulated microgravity conditions.

In contrast to traditional methods like parabolic flights, which entail abrupt gravitational changes, and drop towers, with their potential mechanical stresses, the unmanned microgravity test platform prioritizes safety. Through the implementation of advanced control mechanisms and fail-safes, it guarantees a secure environment for experiments, mitigating safety concerns associated with conventional approaches.

Furthermore, the adoption of UAVs in microgravity research aligns with their rapid technological evolution, rendering them more sophisticated, stable, and adaptable. This convergence of cutting-edge technology with scientific exploration underscores the commitment to pushing the boundaries of research methodologies. The democratization of microgravity experimentation achieved by this platform contributes to a more inclusive and diverse scientific landscape. Researchers, regardless of institutional affiliations or geographical locations, gain accessible and flexible means to conduct experiments, fostering innovation and collaboration across a broad spectrum of scientific disciplines. Leveraging UAV capabilities for microgravity simulation allows for extended experimental durations, enhanced control, and the elimination of geographical constraints, the design of this test platform has aimed to be lightweight, durable, and especially modular ensuring the platform's adaptability to different experimental setups and the incorporation of safety features for secure operations. Improved control, stability, and maneuverability during experiments through the integration of UAV technology into the microgravity test platform. This concept, while not uniquely original, draws inspiration from the integration of drop capsules and drop towers with UAV systems. A noteworthy precedent in this realm was set by the British startup, Gravitilab, which conducted experiments involving the dropping of microgravity payloads from altitudes ranging from 2000 to 6500 feet, facilitated by a UAV system spending thousands of dollars [13]. However, it is essential to acknowledge that this endeavor incurred substantial costs. Despite the financial investment, the experiment achieved a commendable milestone, providing a brief yet impactful 5 seconds of high-quality microgravity, showcasing the potential of such integrated systems in advancing microgravity research.

2.2. UAV INTEGRATION

This research endeavors to establish a total target weight of approximately 5 kg for the UAV and the payload, necessitating a comprehensive examination of the Thrust-to-Weight Ratio (TWR) for this flight system. The incorporation of a factor of safety is deemed imperative to attain optimal stability, control, and maneuverability. With TWR ratios typically ranging between 2:1 and 4:1, prioritizing a ratio of 3:1, gave 5 kg × 3 = 15 kg equating to a required thrust of 15 kg for the 5 kg UAV system [14]. To achieve the desired thrust-to-weight ratio, a meticulous determination for the motor-propeller combination was essential where four of these motor-propeller sets produced 15 kg thrust together as a system for the UAV i.e. each producing a minimum of 3.75 kg thrust.

2.2.1 MOTORS

Figure: 2.1 Motor (2820, 920 KV)

Notably, the choice of motor is a critical aspect with the two main categories being brushed and brushless motors. Brushless motors are more common in modern UAVs due to their efficiency, durability, and reduced maintenance emerging as a more suitable choice for the UAV [14]. Given the UAV’s configuration with four motors, the distribution of thrust and redundancy were integral considerations. The selection process involved identifying a motor boasting maximum thrust capability, efficiency, and optimal size, with specific attention to motor specifications such as KV rating, maximum current, and thrust [15]. The KV rating was calibrated by propeller size and battery voltage, adhering to the principle that lower KV motors are conducive to larger propellers and lower voltage batteries, while higher KV motors align with smaller propellers and higher voltage batteries. Considering the size and weight of the motor assumed paramount importance in preserving the UAV’s overall weight distribution. The pursuit of high motor efficiency directly impacts the increase in UAV’s flight duration. Consequently, a motor characterized by quality construction, durable materials, and an effective cooling mechanism was selected, factors known to contribute to extended lifespans. The ultimate choice arrived at a 2820 motor with a KV rating of 920 after a comprehensive evaluation of its alignment with desired flight characteristics and compatibility with the power system's voltage. This decision was informed by the intricate interplay of thrust requirements, efficiency considerations, and the constraints posed by size, weight, and budgetary considerations.

2.2.2 PROPELLERS

Once the motor was chosen, the subsequent step in the propulsion system design entails the selection of propellers, to achieve optimal UAV performance. The compatibility between the chosen motor and propeller is paramount for the harmonious functioning of the entire system. Propellers are delineated by specifications such as diameter and pitch, characteristics that significantly influence the UAV's overall performance. The correlation between motor specifications and propeller dimensions is a critical consideration in propeller selection. Typically, higher KV motors are paired with smaller propellers, while lower KV motors find compatibility with larger propellers. This relationship is crucial in ensuring the efficiency and effectiveness of the UAV's thrust generation. Diameter and pitch, as intrinsic features of propellers, determining their suitability for a given application. The diameter represents the size of the propeller, measured in inches, and larger diameters generally yield greater thrust.

Figure: 2.2 Propellers (13 inches diameter, 5 inches pitch)

Conversely, pitch signifies the theoretical forward distance a propeller should traverse in one revolution, also measured in inches. Higher pitch values denote a steeper angle of attack, rendering them suitable for high-speed applications. For larger UAVs or those tasked with transporting substantial payloads, propellers that can generate heightened thrust become imperative. Achieving an optimal balance between pitch and diameter is indispensable for realizing the desired equilibrium between thrust and efficiency. The material composition of propellers is a critical facet, impacting factors such as durability, weight, and stiffness. Various materials, including plastic, carbon fiber, and composite materials, are employed in propeller construction. In multi-rotor UAV configurations, the adoption of both clockwise (CW) and counterclockwise (CCW) rotating propellers in pairs is a common practice [16]. This practice serves to counterbalance the torque generated by the motors, ensuring stability during flight. It is imperative to ascertain that the chosen propellers are balanced adequately to mitigate vibrations. Unbalanced propellers can detrimentally affect efficiency, subject motors to increased stress, and potentially induce flight instability. The chosen propeller configuration for this study involves the selection of propellers, characterized by a diameter of 13 inches and a pitch of 5 inches. This choice is informed by a comprehensive evaluation of these specifications in alignment with the desired flight characteristics, emphasizing the importance of balancing thrust requirements with efficiency considerations.

Table 2.1: Selection chart for different propeller sizes

Prop(inch)	**Voltage(V)**	**Amps(A)**	**Thrust(gf)**	**Watts(W)**	**Efficiency(g/W)**	**Load temperature in 100% throttle**
APC13x6.5	11.1	5	500	55.5	9.009009009	50°
		8.9	750	98.79	7.591861524	
		12.9	1000	143.19	6.983727914	
		17.5	1250	194.25	6.435006435	
		23	1500	255.3	5.875440658	
		28.4	1750	315.24	5.551325974	
		37.3	2130	414.03	5.144554742	
APC12x6	11.1	5.5	500	61.05	8.19000819	58°
		9.3	750	103.23	7.265329846	
		13.9	1000	154.29	6.481301445	
		18.3	1250	203.13	6.153694678	
		24	1500	266.4	5.630630631	
		29.8	1780	330.78	5.381220146	
	14.8	4.2	500	62.16	8.043758044	
		7.3	750	108.04	6.94187338	
		10.8	1000	159.84	6.256256256	
		14.7	1250	217.56	5.74554146	
		19.1	1500	282.68	5.306353474	
		23.9	1750	353.72	4.947416035	
		29.3	2000	433.64	4.612120653	
		33.9	2250	501.72	4.484573069	
		40.4	2500	597.92	4.181161359	
		48.4	2860	716.32	3.992628993	

Table 2.1 (continued).

APC12x8	11.1	5.8	500	64.38	7.766387077	47°
		10	750	111	6.756756757	
		14.9	1000	165.39	6.046314771	
		20	1250	222	5.630630631	
		26.1	1500	289.71	5.177591384	
		32.5	1750	360.75	4.851004851	
		35.8	1880	397.38	4.730987971	
APC13x5	14.8	5.4	500	59.94	8.341675008	53°
		9.3	750	103.23	7.265329846	
		13.7	1000	152.07	6.575918985	
		18.6	1250	206.46	6.054441538	
		24.1	1500	267.51	5.607267018	
		30.4	1750	337.44	5.18610716	
		36.5	2000	405.15	4.936443293	
		42.9	2180	476.19	4.578004578	
APC11x5.5	14.8	4.5	500	66.6	7.507507508	49°
		7.9	750	116.92	6.414642491	
		11.6	1000	171.68	5.824790308	
		15.5	1250	229.4	5.448997384	
		20	1500	296	5.067567568	
		24.6	1750	364.08	4.806635904	
		30.1	2000	445.48	4.489539373	
		35.9	2250	531.32	4.234736129	
		37.3	2360	552.04	4.275052532	
APC11x7	14.8	4.7	500	69.56	7.188039103	55°
		8.2	750	121.36	6.179960448	
		12.3	1000	182.04	5.493298176	
		16.8	1250	248.64	5.027348777	
		21.7	1500	321.16	4.670569187	
		26.5	1750	392.2	4.462009179	
		33.1	2000	489.88	4.082632481	
		39.4	2250	583.12	3.858553985	
		45	2540	666	3.813813814	

Table 2.1 (continued).

APC11x8	14.8	5.1	500	75.48	6.62427133	58°
		8.6	750	127.28	5.892520427	
		13	1000	192.4	5.197505198	
		17.7	1250	261.96	4.771720873	
		23.2	1500	343.36	4.368592731	
		28.3	1750	418.84	4.178206475	
		35	2000	518	3.861003861	
		42.3	2250	626.04	3.594019551	
		48	2500	710.4	3.519144144	

2.2.3 FRAME

Figure 2.3: Frame (FPVKing 500-X4)

The choice of frame size for the Unmanned Aerial Vehicle (UAV) system holds paramount significance, directly influencing the overall stability and preventing potential interferences with selected propellers. The frame selection is done considering the motor-to-motor distance ensuring that the wake of the propellers does not interfere. The frame size depends on the mission requirement such as the payload carrying capacity. The selected frame must exhibit a delicate balance of lightweight construction, durability, and robustness. Commonly utilized frame materials for UAVs include carbon fiber, aluminum, and glass fiber. The FPVKing 500-X4 500mm (diagonal length) Carbon Fiber frame, featuring a center plate and fixed landing gear, was identified as the optimal choice. This frame, weighing approximately 475 grams, aligns with the imperative criteria of lightweight design, durability, and structural robustness.

2.2.4 BATTERY

Figure 2.4: 9200 mAh LiPo Battery

Upon finalizing the frame, motor, and propeller components for the UAV system, the selection of an appropriate battery becomes a critical consideration. The battery must provide sufficient voltage to power the motor-propeller combination within the specified voltage range of the motors [17]. The voltage of the battery is denoted by the number of cells in series (S), representing an important factor in the power supply equation. Common battery configurations encompass 3S (11.1V), 4S (14.8V), and 6S (22.2V), among others [18]. In addition to voltage considerations, battery capacity, measured in milliampere-hours (mAh), is a decisive factor influencing the duration of flight. Higher capacity batteries tend to offer extended flight times, albeit at the expense of increased weight. The trade-off between flight time and weight is a crucial consideration for maintaining optimal stability and balance in the UAV system. The Continuous

Discharge Rating (C-Rating) emerges as an indispensable metric, representing the maximum continuous discharge rate of the battery. The C-rating must exceed the current drawn by the UAV system, especially in high-demand situations [18]. Battery chemistry is another parameter requiring careful consideration, with Lithium Polymer (LiPo) batteries being the predominant choice for UAVs due to their high energy density and relatively low weight. Alternatives such as lithium-ion (Li-ion) batteries, with higher energy density but increased weight, and lithium iron phosphate (LiFePO4) batteries, renowned for stability, are also viable options. In the pursuit of an optimal battery solution, a LiPo Battery (4 Cell, 14.8V, 9200mAh, and 100C) was selected. This choice was informed by a comprehensive assessment of flight time requirements, energy demands associated with lifting the payload, and compatibility with the chosen motors and electronic components. Striking a delicate balance between flight time and weight considerations, this selection ensures the UAV's agility and responsiveness while meeting the specified operational criteria.

2.2.5 ELECTRONIC SPEED CONTROLLER (ESC)

The selection of Electronic Speed Controllers (ESCs) for a UAV demands a comprehensive evaluation of multiple factors to ensure seamless compatibility and optimal performance within the propulsion system. Commencing this process entails scrutinizing the ESCs for compatibility with the chosen motors, a crucial consideration that involves verifying voltage ratings. Specifically, the ESC’s maximum current rating should be 20 percent higher than the maximum current drawn by the motor [19]. Additionally, the voltage rating of the ESC should align with the voltage of the UAV's battery to ensure the harmonious functioning of the entire system. The current rating of ESCs is conventionally expressed in amperes (A). It is prudent to opt for ESCs with a slightly elevated current rating relative to the motor's maximum current draw, ensuring a safety margin and mitigating potential performance bottlenecks.

Figure 2.5: Electronic Speed Controller

Notably, the compatibility between ESCs and motors is contingent upon the type of ESC, with options encompassing both brushed and brushless varieties. For contemporary UAV applications, brushless ESCs have become the industry standard due to their recognized efficiency, reliability, and superior performance. The ideal configuration involves pairing brushless ESCs with brushless motors for optimal synergy. The quantity of ESCs required is equivalent to the number of motors employed in the UAV configuration. This parity is imperative for maintaining proper functionality and control in the UAV's propulsion system. Consideration must also be given to the size and weight of the chosen ESCs, ensuring a harmonious fit within the frame while preserving overall system balance. It is noteworthy that an ESC boasting a higher current rating than the motor not only ensures a safety margin but also contributes to enhanced thermal management, thereby improving overall cooling efficiency [19]. This consideration becomes particularly pertinent in mitigating potential heat-related issues during the UAV's operation. By the outlined criteria and considerations, the Electronic Speed Controller (ESC) selected for the UAV system was a 60-amp brushless motor electric speed controller for 2-4 cell LiPo batteries.

This choice aligns with the imperative factors of compatibility, optimal performance, and thermal management, ensuring a well-integrated and efficient propulsion system for our UAV.

2.2.6 FLIGHT CONTROLLER

The diligent choice of a flight controller stands as a pivotal milestone in the construction of a UAV, playing a central role in establishing a stable and reliable aerial platform. As a core component, the flight controller undertakes the crucial task of processing sensor data and orchestrating motor commands to regulate the UAV's stability and movement. It is imperative to note that flight controllers are tailored to specific configurations and sizes, ensuring compatibility with the designated number of motors.

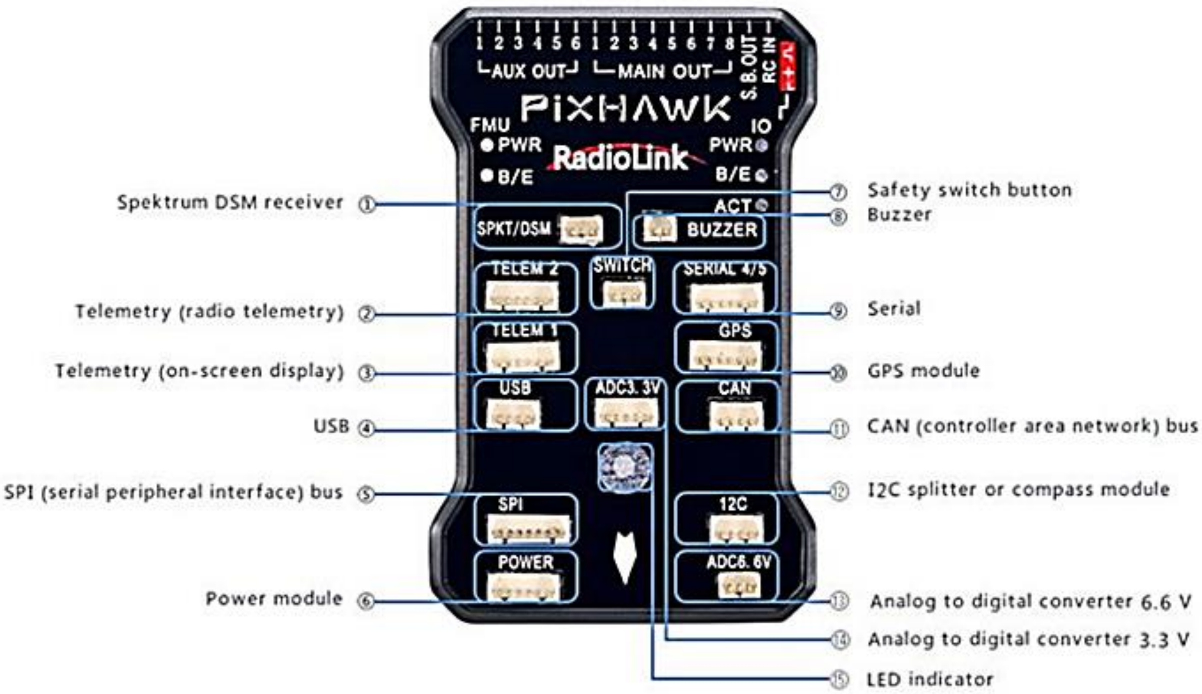

Figure 2.6: Pixhawk Flight Controller with labeled ports

A critical aspect of flight controller selection involves the range of flight modes and features it offers. Attributes such as GPS-assisted navigation, altitude hold, return-to-home functionality, and autonomous flight modes contribute significantly to the overall capabilities of the UAV. The integration of an accelerometer, measuring linear acceleration, further enhances the stability of the flight system, thereby promoting a more controlled and reliable performance. Another key consideration in flight controller selection pertains to the choice between open-source and closed-source controllers. Open-source controllers, exemplified by those based on Betaflight or ArduPilot firmware, provide a platform for customization and benefit from extensive community support [20]. Conversely, closed-source controllers may employ proprietary firmware, offering a more user-friendly interface but potentially limiting customization options.

The types and quantity of gyroscopes integrated into the flight controller emerge as crucial determinants of gyroscopic stability. An increased number of gyroscopes correlates with enhanced stability, ensuring a more robust and controlled flight experience. This consideration underscores the importance of gyroscopic stability in the overall performance and reliability of the UAV. The PIXHAWK flight controller is a highly acclaimed component in the realm of Unmanned Aerial Vehicles (UAVs), known for its versatility and robust features. It efficiently processes sensor data to govern the UAV's stability and orientation, accommodating various configurations seamlessly. With robust support for GPS-assisted navigation, altitude hold, return-to-home capabilities, and autonomous flight modes, the PIXHAWK offers enhanced control and versatility [21]. Its open-source framework, leveraging ArduPilot firmware, allows extensive customization and community-driven support. The user-friendly interface aligns with closed-source counterparts, maintaining flexibility. The incorporation of advanced gyroscopes ensures precise orientation control, contributing to a reliable and responsive flight experience. In summary, the PIXHAWK stands as a sophisticated and versatile solution, ideal for stable, reliable, and customizable UAV operations.

2.2.7 POWER DISTRIBUTION UNIT/BOARD SELECTION

The selection of a Power Distribution Board/Unit (PDB/PDU) is a crucial aspect when choosing a flight controller for Unmanned Aerial Vehicles (UAVs). Some flight controllers offer integrated PDU functionality, simplifying power distribution and enhancing the overall setup aesthetics. The inclusion of PDU is essential for efficiently distributing power to all motors via Electronic Speed Controllers (ESCs), forming a pivotal link in the UAV's propulsion system [22]. Connectivity options for the flight controller include USB, UART, I2C, and PWM ports, necessitating careful consideration to ensure compatibility with auxiliary components such as radio transmitters, telemetry capsules, and GPS units. The seamless integration of these connectivity options is paramount for establishing a comprehensive and well-coordinated communication network within the UAV system. Furthermore, the compatibility of the selected PDB/PDU with the flight controller is integral to ensuring a harmonious power distribution system. The interconnection between ESCs and the PDU plays a fundamental role in translating the flight controller's commands into motor actions, influencing the overall stability and maneuverability of the UAV.

2.2.8 GLOBAL POSITIONING SYSTEM (GPS)

The integration of Global Positioning System (GPS) technology stands as a ubiquitous and indispensable feature within contemporary UAV systems, contributing to the provision of precise location data, navigation capabilities, and various location-based functionalities. UAVs are equipped with GPS receivers, facilitating communication with satellites orbiting the Earth, collectively forming the GPS constellation. The signals emanating from these satellites determine the precise location of the UAV during its operational flights. The accuracy of GPS positioning on UAVs exhibits variability, contingent upon several influencing factors. The number of satellites in view, the geometric arrangement of these satellites relative to the UAV, and potential interference are critical determinants impacting the accuracy of GPS data which is typically about 3-5 meters [23].

Figure 2.7: GPS module

Notably, high-end UAVs often integrate advanced GPS receivers and supplementary sensors, such as differential GPS, to achieve heightened levels of positioning accuracy. UAVs commonly incorporate a Return-to-Home (RTH) feature that leverages GPS capabilities. In scenarios involving signal loss or low battery levels, the UAV autonomously engages its Return-to-Home functionality, relying on the precision of GPS coordinates. This feature ensures a safe and controlled return of the UAV to its initial takeoff location, exemplifying the critical role that GPS technology plays in enhancing the overall safety and reliability of UAV operations.

2.2.9 TELEMETRY

Figure 2.8: Telemetry module

Telemetry in the context of UAV systems refers to the wireless transmission of real-time data from the unmanned aerial vehicle (UAV) to the ground control station. This data encompasses critical parameters such as battery voltage, altitude, GPS coordinates, and system health status. The selection of telemetry for a UAV involves meticulous consideration of factors such as data transmission rate, frequency band, communication protocols, integration with the flight controller, sensor compatibility, data logging capabilities, user interface design, and the implementation of redundancy and fail-safe measures. The selection was tailored to specific operational requirements, ensuring the establishment of a reliable, efficient, and responsive telemetry interface, ultimately enhancing the overall performance and safety of the UAV.

2.2.10 POWER MODULE

The power capsule serves as a crucial component responsible for monitoring and regulating the electrical power supplied to the unmanned aerial vehicle (UAV). It typically incorporates functionalities such as voltage and current sensing, allowing for real-time monitoring of the UAV's power consumption. The selection of a power capsule involves considerations of voltage compatibility, current-handling capacity, weight, and integration capabilities with the UAV's flight controller. A judicious selection process ensures that the power capsule aligns with the specific power requirements of the UAV, contributing to stable and efficient electrical power management during operational flights [24].

Figure 2.9: Power Module

In the context of UAV power distribution, a dual-battery configuration is employed, where the primary battery delivers a direct 14.8V supply to the Power Distribution Unit (PDU). Simultaneously, a secondary branch of the power system is directed to a dedicated circuit designed to step down the voltage. This stepped-down voltage is specifically allocated to power the Pixhawk flight controller. This approach is adopted to ensure optimal power management, with the direct 14.8V supply catering to the PDU's requirements, while the regulated voltage from the secondary circuit provides the Pixhawk flight controller with a voltage level aligned with its operational specifications. This setup enhances the overall efficiency and reliability of the UAV's power distribution system, catering to the distinct voltage needs of different components within the UAV architecture.

2.2.11 TRANSMITTER & RECIEVER

The careful selection of a transmitter and receiver constitutes a critical aspect in the design and implementation of a UAV system, influencing the efficacy and reliability of communication between the ground control station and the unmanned aerial vehicle (UAV). The transmitter, commonly referred to as the radio transmitter or remote controller, serves as the interface through which the operator imparts commands and instructions to the UAV, while the receiver on the UAV interprets and executes these commands. The following section delineates key considerations and factors that guide the selection of transmitter and receiver components within the context of a UAV system. The selection is contingent upon factors such as local regulations, environmental conditions, and the presence of other electronic devices.

Figure 2.10: Transmitter & Receiver

Additionally, evaluating the transmission range is imperative, with longer ranges enhancing the operational capabilities and flexibility of the UAV system. The selection of a transmitter and receiver in a UAV system involves the evaluation of frequency, transmission range, communication protocols, number of channels, telemetry capabilities, ergonomics, redundancy, fail-safe mechanisms, and integration with the flight controller. The selected transmitter for our UAV system aligns with budgetary constraints while offering a commendable range of features. With a total of 6-10 channels, this transmitter provides versatility for various operational aspects. The primary control channels encompass throttle, roll, pitch, and yaw, each assigned to four distinct channels. In addition, the transmitter allocates four auxiliary channels to accommodate a range of supplementary functions. One auxiliary channel is designated for the flight mode selector, allowing for seamless transitions between stabilization modes such as stabilization, altitude hold, and position hold. The second auxiliary channel facilitates a switch between high-speed sports and low-speed normal control modes. Furthermore, the third auxiliary channel is dedicated to critical functionalities, including a throttle hold for hover, and a fourth one for activating the dropping mechanism servo actuating switch. This strategic channel allocation ensures a comprehensive and tailored control interface, optimizing the operational capabilities of the UAV system.

2.3. PAYLOAD POSITIONING

Positioning the payload at the lower section of the UAV serves a pivotal role in enhancing the UAV's stability during flight, a critical consideration, particularly in environments simulating microgravity where stability preservation is inherently challenging. By adopting this configuration, the payload's mass is concentrated toward the bottom, contributing to a lower center of mass and, consequently, improved overall stability dynamics. This strategic placement mitigates potential aerodynamic disturbances that may affect the system during flight, as the payload's presence below the UAV minimizes the impact of airflow. This leads to more predictable and controlled movements, crucial in scenarios where precise maneuvers are essential. Beyond stability, the choice to mount the payload underneath has additional advantages. It grants sensors and instruments an unobstructed field of view, enhancing the accuracy and reliability of data collection. Moreover, the configuration facilitates seamless deployment and retrieval procedures, proving particularly advantageous for missions involving the dropping or picking up of objects [25]. This functionality is not only operationally efficient but also expands the potential applications of the UAV, making it suitable for a diverse range of experiments.

Figure 2.11: Heavy Payload mounted at the bottom of the UAV

The flexibility offered by the bottom-mounted payload configuration extends to experiment design, accommodating various payload types and sizes. Researchers and operators can adapt the UAV to specific experimental needs, making it a versatile platform for scientific endeavors. In summary, the strategic decision to position the payload at the bottom of the UAV not only enhances stability but also optimizes functionality, making it a well-suited choice for a wide array of scientific and research missions. A mounting to be attached to the bottom of the UAV was designed to hold the payload securely while also having the release mechanism integrated into it. According to the chosen UAV frame having 2 hollow tubes at the bottom, the expected mounting to be designed must have a battery compartment, release mechanism, and payload holding ability all integrated into one design.

CHAPTER 3

DETAIL DESIGN

3.1 OVERALL ARCHITECTURE

The overarching objective was to devise a sophisticated mounting system for the UAV, complemented by its multifunctional capabilities. Serving as an integral component affixed to the UAV's underside, this mounting system was designed to fulfill the roles of housing a protective battery casing, a secure carrier for transporting the payload from the ground, a stable holding mechanism for the payload, a precision navigation tool for transporting the payload to predetermined locations, and an adept release system ensuring the maintenance of overall UAV system stability. The conceptualization and subsequent design of this mounting system were systematically executed, subjecting it to rigorous testing to validate its capacity to meet the specified requirements.

For the payload-carrying function, a secure initial engagement was established between the mounting system and the payload. This engagement was designed to carry the payload securely minimizing any unstable movements and effectively controlling the release of the payload. The ideation of the mechanism was to use a servo motor actuating mechanism, facilitating the engagement and disengagement of the payload at predetermined intervals. The payload comprised two distinct segments, an outer capsule and an inner capsule designated for carrying out experiments under microgravity conditions. The fundamental concept underlying the payload release involves the immediate attainment of zero gravity during free fall, followed by a subsequent increase in gravity as a consequence of escalating air resistance or drag. The outer capsule is specifically engineered to minimize drag, thereby mitigating the effects of air resistance on the inner capsule.

The inner capsule is meticulously designed to house and facilitate experiments undergoing microgravity conditions. Inspired by drop capsules, the payload system adopted a dual-capsule configuration, with an outer capsule encompassing an inner capsule housing the experimental payload. During descent, both capsules descended in tandem. The outer capsule decelerated due to air resistance and drag, while the inner capsule, experiencing minimal drag within the air-filled outer capsule, maintained relatively constant acceleration. Consequently, the inner capsule attained higher velocity as the outer capsule decelerated, culminating in a unique dynamic during the descent. The mounting system was further equipped to accommodate sensors and cameras on the outer capsule, providing a means to record the experimental data visually and also provide acceleration values for the outer capsule. An additional camera, strategically positioned at the bottom of the outer capsule, offered a live location feed from an aerial perspective. This live feed initiated the precise release of the payload when the UAV system attained a specific alignment above a designated catch mechanism.

To enhance data acquisition during experiments, an accelerometer was securely attached to the inner capsule. This accelerometer served the crucial function of providing real-time data on the g-force and acceleration due to gravity acting on the payload throughout its operational phases. The culmination of the experiment involved deploying a catch mechanism to safely intercept and secure the entire drop capsule system, minimizing the risk of damage. This systematic approach to testing serves as a microgravity test bench, enabling comprehensive research and analysis of the microgravity levels experienced by the experiment within the inner capsule. Ultimately, the reliability of this microgravity test bench is established through meticulous testing procedures.

3.2 ELECTRICAL COMPONENTS:

3.2.1 SERVO MOTOR

Servo systems are used as actuating mechanisms by providing precise and controlled motion through a combination of motorized components and sophisticated control systems. A servo motor, typically a DC motor drives the mechanism's motion. Integrated into the servo setup is a feedback mechanism, commonly a potentiometer or encoder, which continuously monitors the position of the motor shaft. This feedback data is essential for the servo controller, a critical component in the system, to assess the current position relative to the desired one. The controller processes this information and generates a control signal that adjusts the motor's output to minimize any positional error, ensuring the mechanism reaches and maintains the intended position accurately. The servo's responsiveness is facilitated by a signal input, often in the form of pulse-width modulation (PWM), which determines the desired position through varying pulse widths. Additionally, a power supply provides the necessary energy for the servo's operation. The servo motor is connected to the actuating mechanism through a mechanical linkage, translating the rotational motion into the desired linear or angular movement. In certain applications, limit switches may be incorporated to signal the controller when the mechanism reaches its extreme positions, preventing potential damage. This comprehensive integration of components in a servo system ensures its widespread applicability in fields such as robotics, automation, and remote control systems, where precision and control are paramount for successful actuation mechanisms. Selecting the right servo motor depends on the torque and speed requirements. Torque requirements are often influenced by the load and the desired acceleration, while speed requirements depend on the application's dynamics. The inertia of the load and the required acceleration are essential factors for determining the specifications of the servo motor. Aligned with the research objectives, due consideration was given to the inertial load, maintaining a specific value of approximately 5 kg. Simultaneously, a paramount requirement involved achieving the highest attainable acceleration.

Figure 3.1: Servo Motor and its components

The challenge was compounded by the necessity to constrain the servo's physical dimensions to a compact and minimal size while adhering strictly to a predetermined weight threshold. A 20kg Digital Servo Motor was chosen as it is characterized by high torque capabilities, further augmented by a control angle spanning 270 degrees [26]. To operationalize the servo within the system, it was seamlessly integrated with the flight controller. Subsequently, the control mechanism was established, facilitating external manipulation through a dedicated transmitter interface. This strategic amalgamation of specific servo attributes and integration methodologies was undertaken to address the nuanced research objectives effectively.

3.2.2 CAMERAS

To effectively capture the location feed, monitor the experiment's behavior during UAV flight and microgravity drops, and collect essential data on post-drop behavior, it is crucial to integrate cameras into the system. The primary camera selected for this purpose is the GoPro Hero 11 Action camera, renowned for its advanced features and high-quality imaging capabilities. Additionally, the Jadfezy sports action camera was incorporated to complement the primary camera. These cameras are chosen for their ability to capture super wide-angle views, ensuring that no vital details are missed during research observations. High frames per second (FPS) rates are also a key consideration for capturing detailed slow-motion footage and examining fast-paced events. The selected cameras offer high FPS capabilities, including rates such as 60fps, 120fps, 240fps, and higher, enabling a detailed examination of experiment behavior and UAV operations.

Figure 3.2: GoPro Hero 11 (left) and Jadfezy Action Camera (right)

The deployment of supplementary action cameras for location feed purposes enhances the comprehensive data acquisition strategy by providing multiple angles of observation. An additional action camera serves as an output backup, ensuring redundancy and safeguarding against data loss during critical recording instances. This strategic integration of various action cameras enhances the versatility and robustness of the recording setup, aligning with the overarching objectives of the research endeavor

3.2.3 ACCELEROMETER

The tri-axial accelerometer integrated into the UAV drop capsule serves as a crucial sensor designed to quantify the acceleration forces exerted upon the UAV along its three spatial axes, namely X, Y, and Z. This sensor precisely gauges the accelerative components acting on the inner capsule of the UAV, providing detailed insights into the gravitational (G) forces at play [27].

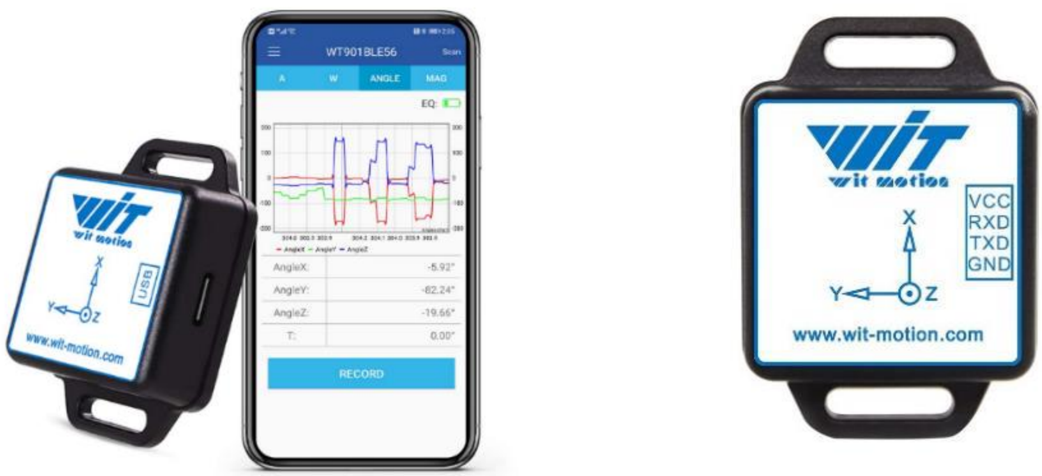

Figure 3.3: Bluetooth Accelerometer

By meticulously assessing the acceleration along each axis, the accelerometer facilitates a comprehensive understanding of the dynamic interactions between the UAV and its surrounding environment during the descent or drop process. This granular data on G forces is instrumental for researchers and operators in optimizing the capsule's design, enhancing safety protocols, and refining the overall performance of the UAV drop system in diverse operational scenarios. The Bluetooth 5.0 accelerometer with inclinometer represents a cutting-edge sensor technology designed to provide advanced motion and orientation data in a wireless and energy-efficient manner. This sensor integrates Bluetooth 5.0 technology, offering enhanced data transfer rates, increased range, and improved reliability compared to its predecessors. The Bluetooth 5.0 connectivity ensures seamless communication with other Bluetooth-enabled devices, such as smartphones, tablets, or IoT platforms. This wireless capability simplifies integration into various systems and allows for real-time monitoring and control. The increased data transfer rates of Bluetooth 5.0 enable faster and more efficient communication, contributing to a responsive and reliable sensor network.

3.2.4 LED FLASHLIGHTS

Light-emitting diodes (LEDs) flashlights are portable semiconductor devices that are highly energy efficient, durable, and compact compared to other light sources. LED flashlights have several applications such as emergency kits, hiking, camping, fishing, reading at night, security, search and rescue, and many military purposes.

Figure 3.4: LED Flashlights

To have visibility for the camera feed to record the behavior of the experiment experiencing microgravity and other movements inside the capsule, an LED flashlight was chosen as a lightweight, portable, and durable source that doesn't easily damage on drop impact.

3.3 MECHANICAL COMPONENTS

Release mechanisms represent an assemblage of components designed to securely and selectively deploy payloads or equipment from a designated platform. Diverse release mechanisms are available, each employing distinct principles for controlled payload release. The electromagnetic release mechanism utilizes an electromagnet to secure the payload, releasing it upon the application of an electric current, overcoming the electromagnetic force.

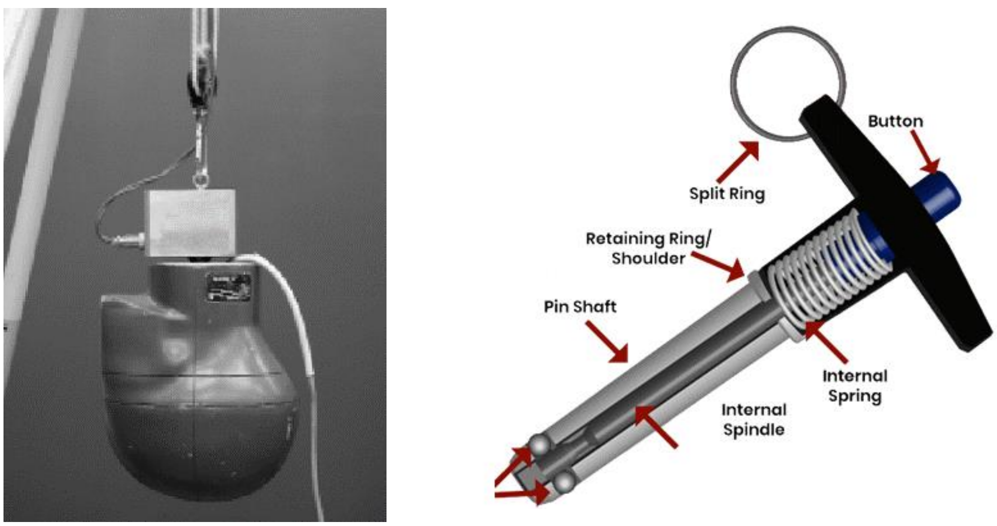

Figure 3.5: Electromagnetic (left) and Spring (right) quick release mechanisms

Conversely, spring-loaded release mechanisms employ tensioned springs to retain the payload, with rapid deployment occurring upon the release of stored energy; however, this is generally more suitable for lightweight payloads. Pyrotechnic mechanisms rely on controlled explosions to effectuate payload release, introducing safety and regulatory considerations.

Pneumatic release mechanisms, leveraging compressed air, enable controlled payload release by modulating air pressure. Other mechanisms, such as acoustic and gravity-based, exhibit specific applications and operational conditions.

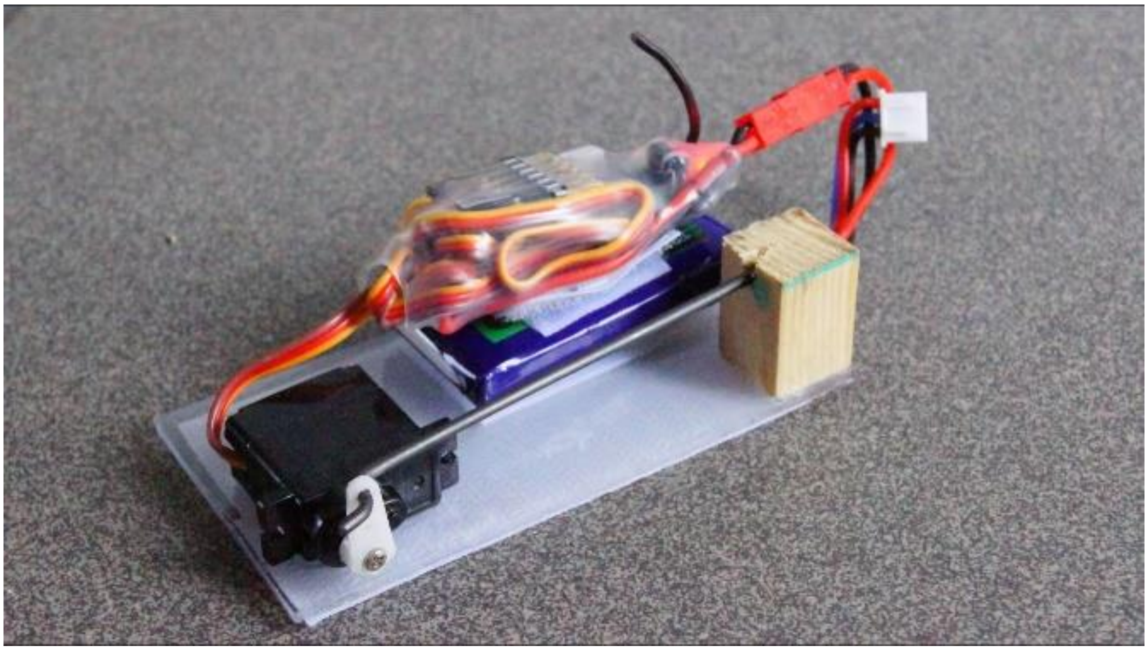

Figure 3.6: Servo actuating mechanism

In this research, a tailored release mechanism was devised by amalgamating insights from mechanical hook and servo-driven mechanisms, incorporating knowledge gleaned from drop tower experiments to ensure safety, precision, and reliability during payload release. The mounting system, tasked with both securing and releasing the payload, serves as the crucial link between the drop capsule and the UAV, accommodating the battery and release mechanism. The UAV system, integral to the research methodology, is instrumental in elevating the mounted payload to the desired height, positioning both the payload and the UAV accurately, and subsequently affecting the release of the drop capsule. The chosen mechanism design relied on a servo motor for the engagement and disengagement of the drop capsule with the UAV system. Following the assembly of the UAV and associated components, a dedicated battery holder was constructed. This casing, meticulously designed, incorporates considerations for bottom attachment to the frame and accommodates the chosen battery's dimensions to hold the battery and the entire payload securely at the bottom of the UAV.

3.3.1 MOUNTING

Following an extensive phase of research and literature review, the conceptualization of a mounting structure emerged to address multifaceted functionalities. This mounting not only securely housed the battery but also integrated the engagement and release mechanism, simultaneously providing a stable platform for the positioning of the drop capsule at its base. An initial design iteration was formulated, guided by a meticulous consideration of the battery's dimensions. The mount was specifically engineered to securely affix and support a servo motor, strategically oriented at an angle conducive for optimal functionality.

Figure 3.7: Clevis joint (left) and its components separately (right).

The servo motor converts rotary motion into linear motion, thereby effectively controlling the release of the drop capsule. The preliminary design intricately accommodated the dimensions of the battery, ensuring a precise and secure fit within the mounting structure. The release mechanism was characterized by the conversion of the servo arm's rotary motion into translational motion, facilitating the subtle control of a pin to the release process. This mechanism drew inspiration from the configuration of a clevis joint, where the system comprised a male and female lug engaged via a pin. The rotational movement of the servo arm demanded exacting measurement to ensure precision equivalence with the linear motion of the pin, orchestrating a seamless disengagement with the lug and, consequently, executing the release process with the desired accuracy and reliability. A crucial aspect of the design involved creating a dedicated space and fixation mechanism for the servo motor, conscientiously calibrated to enable its controlled movement. The servo motor's arm, positioned at an angle, played a critical role in effecting the translation of rotary motion into the desired linear motion, orchestrating the precise engagement and disengagement of a pin responsible for the release when disengaged.

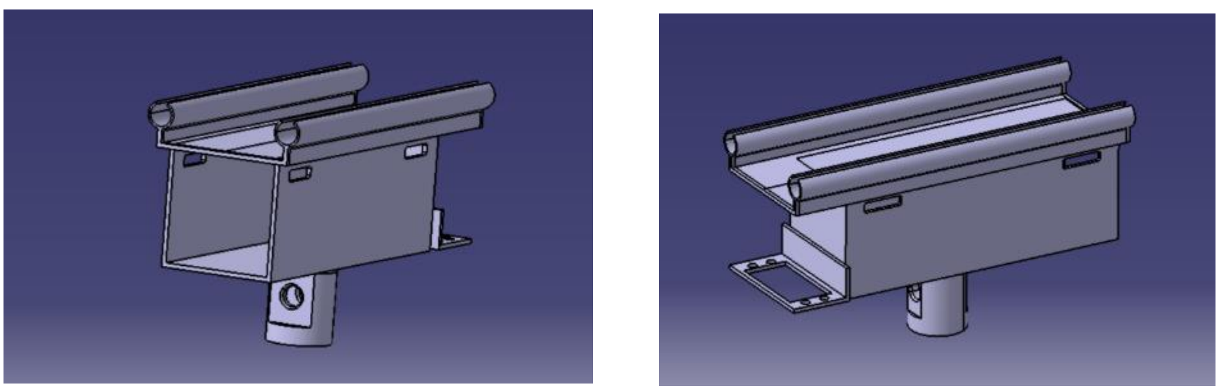

Figure 3.8: The mounting design

In the context of affixing the designed mounting structure to the UAV's undercarriage, the frame incorporated two extended cylindrical rods dedicated for attachment purposes. The tube configuration was designed with clearance to facilitate seamless attachment without interference. A strategically chosen tube structure provided the necessary accommodation for the insertion and secure fixation of the mounting onto the UAV's rods, ensuring stability and preventing inadvertent dislodgment. Battery dimensions in the design process were considered anticipating the potential bloating of the battery due to repetitive use, the casing was thoroughly crafted to accommodate such variations, ensuring a secure and adaptable fit over time. Acknowledging the criticality of maintaining the UAV's center of gravity during flight, specific provisions were made to prevent the battery from shifting within the casing. Velcro slots were integrated into the mounting structure, serving the purpose of firmly securing the battery in place and mitigating any inadvertent movements during UAV operation. To facilitate the necessary electrical connections, one side of the battery casing was intentionally left open, allowing for the seamless integration of the main lead with the flight controller. Conversely, the opposing side was enclosed, providing a secure housing for the servo motor mount on the other side. This flat side of the casing was dedicated to housing the servo motor mount, ensuring structural integrity and precision in accommodating the servo motor's role in the controlled release mechanism. The integration of these design elements within the mounting structure aimed to enhance the overall functionality, stability, and reliability of the UAV system during flights and experimental operations.

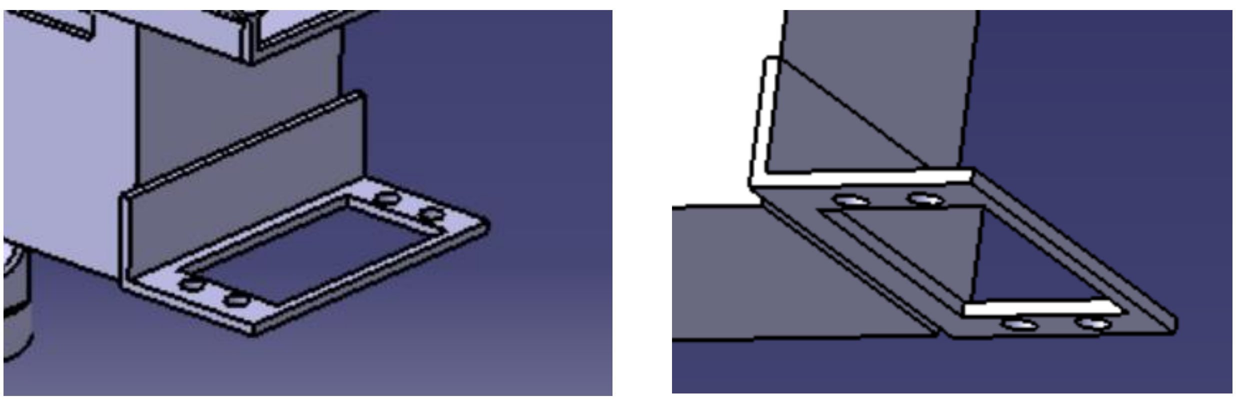

Figure 3.9: The L-shaped plate

An L-shaped plate was deliberately selected to serve as the foundational component. The L-shaped configuration, characterized by its inherent stability and versatility, provides an efficient means of securely mounting objects, particularly in confined spaces or corners. This design minimizes both shear forces (parallel to the surface) and tensile forces (pulling away from the surface), mitigating the risk of plate deformation or warping under varying loads. The L-shaped plate, with its capacity to support cantilevered loads where one end extends beyond the mounting surface, was deemed particularly advantageous for the intended application. The chosen L-shaped plate not only facilitates easy installation but also distributes the load over a substantial surface area, thereby reducing stress on the mounting point and enhancing overall stability. The height of the L-shaped plate was meticulously determined to ensure adequate space for the servo arm's rotational movement below the casing and at a secure distance from the protruded joint for the successful execution of the release mechanism. The servo mounting design specifically involved an inverted orientation, wherein the servo was placed and bolted beneath the L-shaped plate. To rigidly secure the servo motor onto the L-shaped plate, M4 holes were strategically incorporated, allowing for a robust mounting arrangement. This configuration allowed the servo arm the necessary space for unimpeded rotational movement below the battery casing, facilitating the precise and controlled release of the payload.

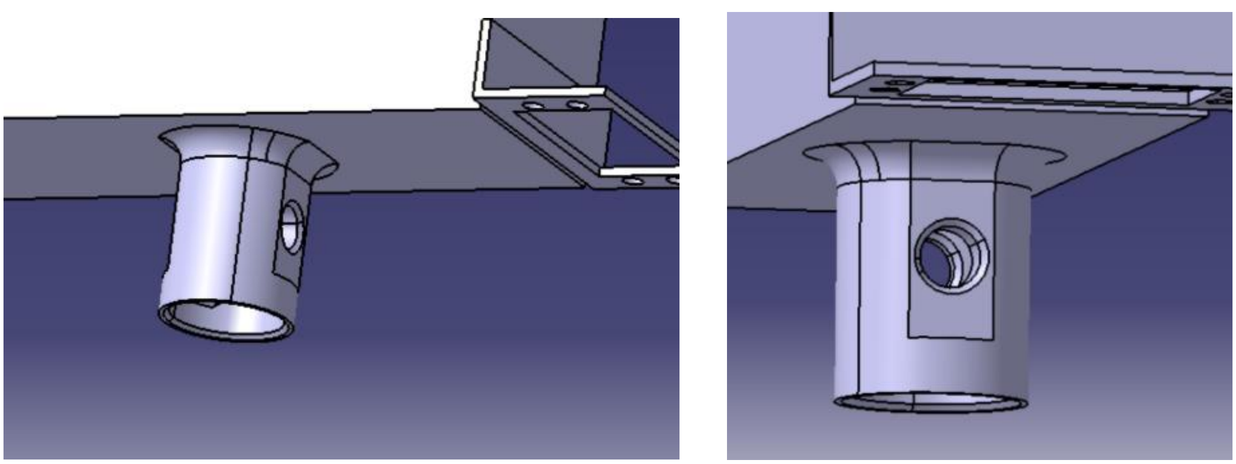

Figure 3.10: The protrusion inspired by the clevis joint configuration

Positioned at the base of the battery casing, a configuration akin to the principles of a clevis joint was meticulously devised, taking into account specific dimensions in terms of thickness, diameter, and height. A protrusion from the bottom of the battery casing acting as a mount for the drop capsules was designed as a double shear joint in the configuration similar to a clevis joint where the pin engaged was in double shear distributing the load evenly.

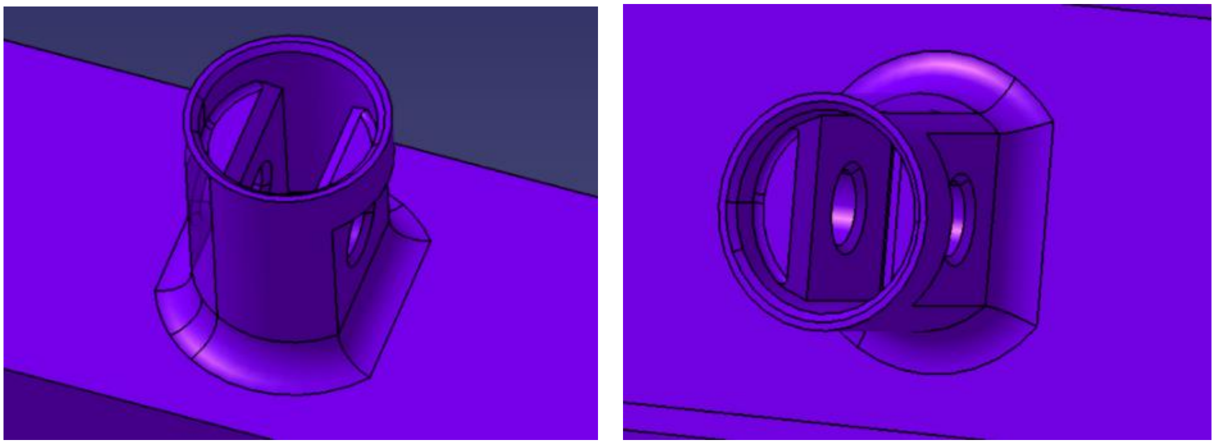

Figure 3.11: Defined protrusion

The incorporation of a configuration reminiscent of the clevis joint at the bottom of the battery casing aligns with the research-driven design principles, aiming to enhance the functionality and reliability of the release mechanism within the broader context of the UAV system.

3.3.2 CONNECTING ROD

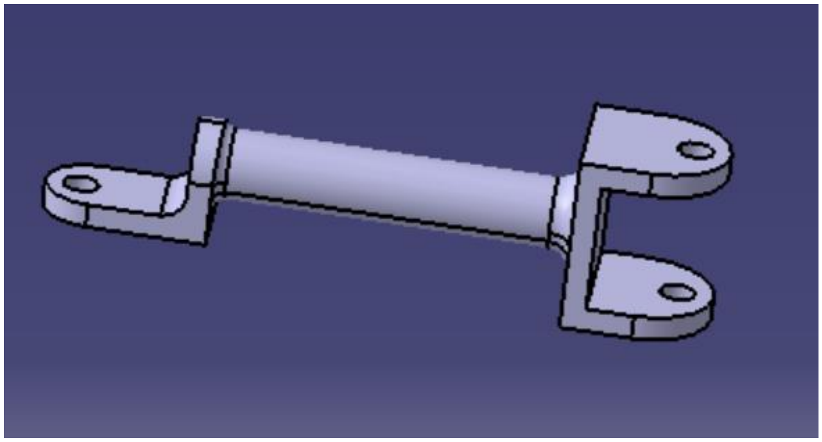

Figure 3.12: Connecting Rod Design

After the servo arm's positioning, a connecting rod was introduced, establishing a revolute joint through the use of a screw. This connecting rod featured one fork end with two flat surfaces affixed to the servo arm through a screw, creating a revolute joint configuration that allowed rotational movement. This end of the connecting rod granted freedom of rotation, ensuring adaptability to the servo arm's movements. The length of this connecting rod was meticulously considered to facilitate a connection between the servo arm and the pin intended for insertion into the lug hole of the mounting structure. The opposing eye end of the connecting rod exhibited a flat surface, establishing another revolute joint in conjunction with the engagement bolt. This carefully crafted configuration ensured that one end of the connecting rod was securely connected to the servo arm, while the other end formed another joint with the engagement pin. This strategic design choice was crucial in facilitating controlled and precise rotational movements, aligning with the intricate mechanics of the release mechanism. The connecting rod's role in transmitting motion from the servo arm to the engagement bolt was central to the successful execution of the release process within the broader context of the UAV system.

3.3.3 ENGAGEMENT PIN

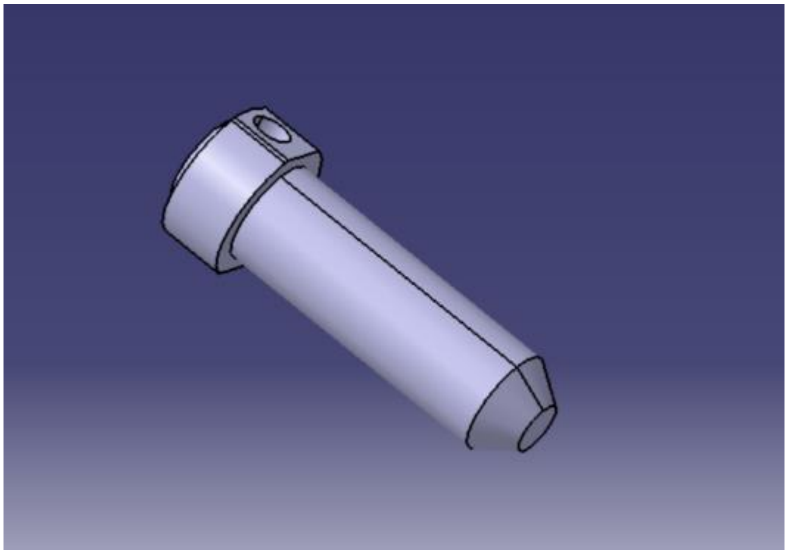

Figure 3.13: Engagement Pin

The engagement pin, integral to the release mechanism, was precisely designed with an M8 bolt configuration devoid of threads and featured a rounded head. This round head was deliberately flattened to facilitate a joint with the connecting rod through the use of an additional small screw. In the context of Degrees of Freedom (DOF) and movement terminology, this configuration allowed controlled and constrained rotational movement, ensuring precise and purposeful actions within the system. The dimensions of the head of the engagement bolt were intentionally larger than the aperture of the mounting hole to restrict its penetration. The flattened head configuration prevented it from fully entering the hole, creating a spatial constraint. This deliberate design choice ensured that the head of the pin did not completely fit into the hole, with its dimensions surpassing those of the hole. The tip of the pin slightly protruded to the other side of the mounting structure, confirming correct engagement and providing additional structural support to bear the anticipated load during the release process.

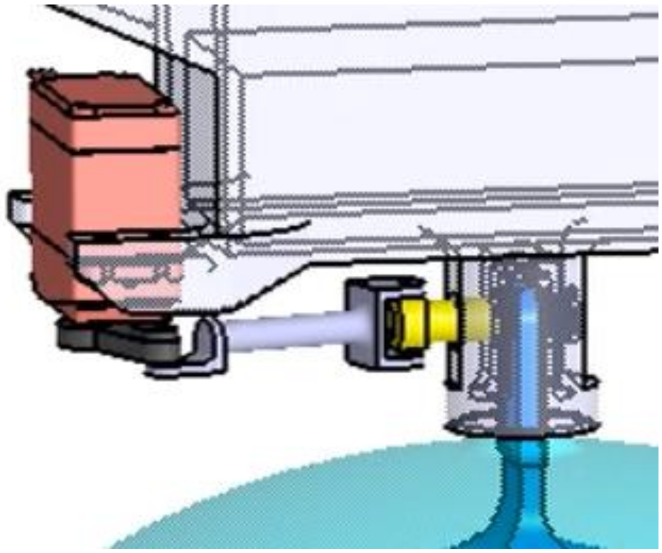

Figure 3.14: The pin securely holding the payload

This approach in the design of the engagement bolt, considering both its dimensional characteristics and constrained movement, reflects a thoughtful consideration of mechanical principles and safety factors in the development of the release mechanism. The terminology associated with Degrees of Freedom and the movement constraints employed in this design contribute to the precision and reliability of the release process within the UAV system. So on one extreme of the servo arm, where it has pulled the connecting rod far, which further has pulled the pin far and disengaged it. While, on the other extreme of the servo arm, the connecting rod was pushed towards the lug and this connecting rod pushed the pin to engage entirely.

3.4 SHAPE OF THE DROP CAPSULE

A "drop capsule" refers to a container or capsule designed for experiments conducted in a microgravity environment, often facilitated by a parabolic flight or a suborbital rocket launch. These capsules are released in a way that allows a short-duration period of reduced gravity, simulating microgravity conditions. These drop capsules are designed to protect the experiments or samples during the ascent and descent phases and ensure that they experience the microgravity environment as intended. The conceptualization focused on the design of a container, analogous to a drop capsule, intended for mounting onto a specialized mechanism. This mechanism, designed for controlled release, is affixed to a UAV system, allowing stable carriage of the container during operational phases.

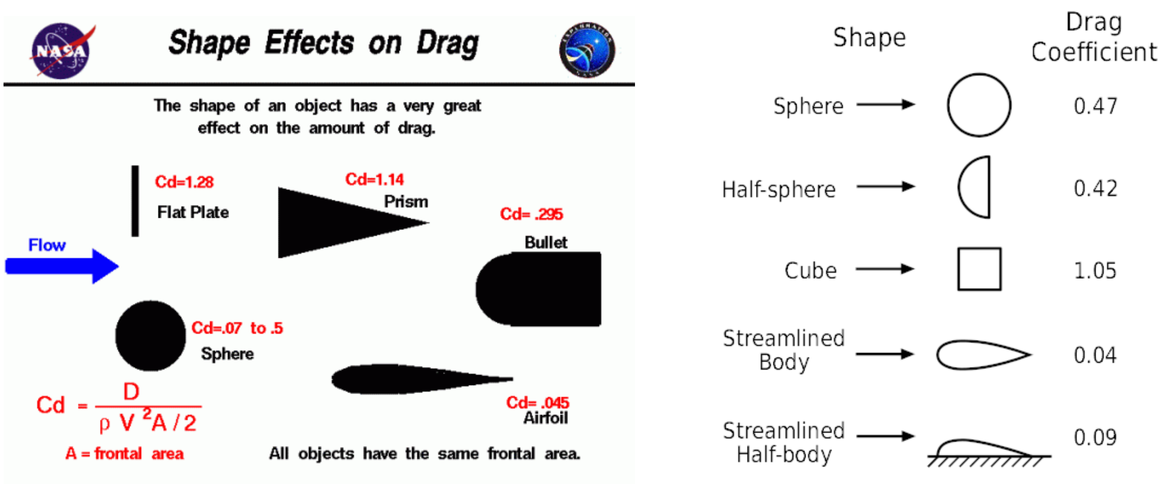

Figure 3.15: Consideration of various shapes with drag coefficient for drop capsule

The initial step involved determining the optimal shape, dimensions, and structural characteristics of the drop capsule, considering both the experiment's requirements and the outer capsule serving as a protective casing. Selecting an appropriate shape for the drop capsule necessitated a comprehensive evaluation of mission objectives, deployment methods, aerodynamics, and payload attributes. Various shapes, such as spherical, cylindrical, conical, and blunt-body, each come with distinctive advantages and constraints. Balancing considerations of stability, drag coefficient, and payload volume, a hemispherical cylinder emerged as a viable choice, amalgamating attributes of stability and low drag with ample volume. The hemispherical cylinder design offers specific benefits, including aerodynamic stability during descent.

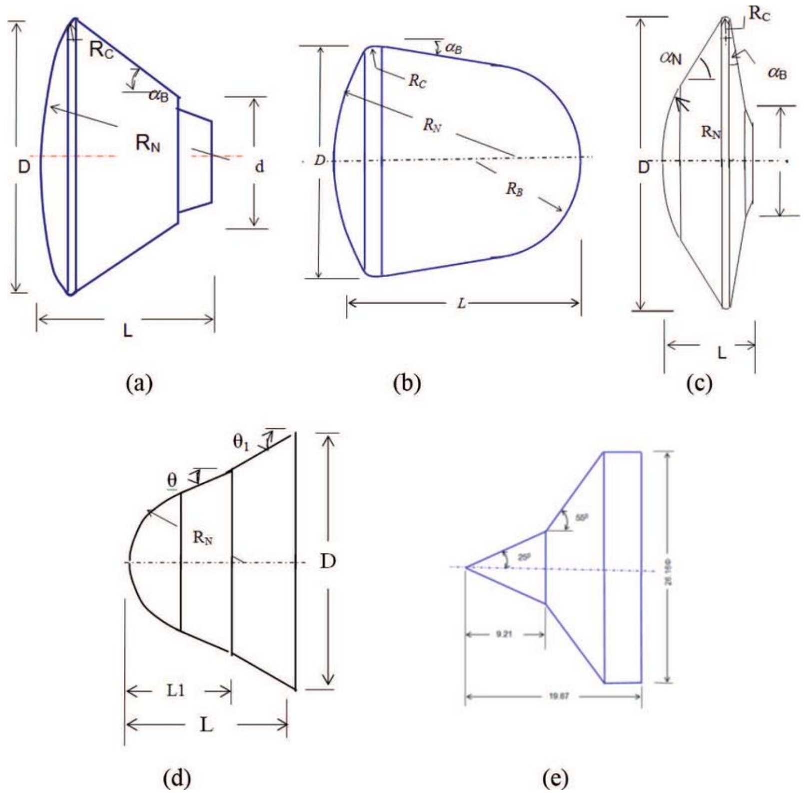

Figure 3.16: Different re-entry capsule shapes

The hemispherical ends contribute to minimizing drag, ensuring a stable trajectory during atmospheric entry. This shape not only enhances structural integrity by evenly distributing external forces but also provides sufficient time for the inner capsule's descent. Considering the simultaneous release of the inner and outer capsules, the drag-induced deceleration of the outer capsule contrasts with the inner capsule's negligible drag, resulting in the latter accelerating under gravity. To mitigate the risk of collision at the juncture of the inner and outer capsules, dimensions were cautiously chosen during the design of the cylindrical portion, adhering to modularity principles. This research elucidates the considerations behind the drop capsule design, emphasizing the interplay of aerodynamic stability, structural integrity, and controlled release dynamics. The incorporation of a hemispherical cylinder configuration reflects a strategic alignment with mission objectives and experimental requirements, contributing to the precision and reliability of microgravity simulations facilitated by the UAV system.

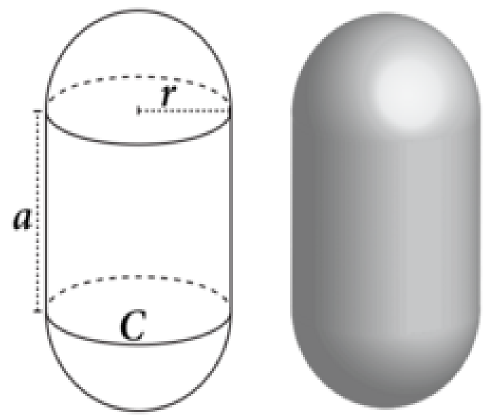

Figure 3.17: Hemispherical Cylinder shape for drop capsule

A cylinder with hemispherical ends or a capsule shape has specific design benefits such as aerodynamic stability. The hemispherical ends of the cylinder contribute to aerodynamic stability during descent. This shape helps minimize drag, ensuring a stable trajectory during atmospheric entry. The hemispherical shape distributes external forces more evenly, enhancing structural integrity, whereas the cylindrical column offers time to the inner capsule. As these capsules are released together the outer capsule slows down due to drag and the inner capsule experiences negligible drag therefore accelerating under gravity. So the velocity of the inner capsule becomes greater than the outer capsule creating a chance for collision of the inner capsule at the bottom of the outer capsule. Therefore, the dimensions to accommodate such a possibility were chosen while designing the cylindrical part modular.

3.4.1 OUTER CAPSULE

In the initial phase of design, the outer capsule underwent a segmentation into three distinct components, a strategic choice made for reasons of accessibility, modularity, and simplified mounting. This partitioning not only facilitated ease of correction for individual components during iterative changes or testing but also contributed to cost and material savings in the prototyping phase. The three constituent parts comprised the top hemisphere, the middle cylindrical section, and the bottom hemisphere.

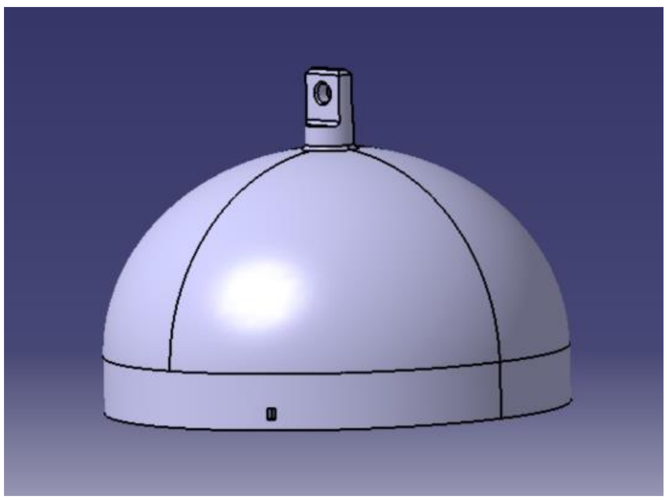

Figure 3.18: The top hemisphere

The upper hemisphere, positioned atop the assembly, featured a design facilitating attachment to the mounting beneath the UAV. A bar tailored as a female protrusion according to the dimensions of the pin and corresponding male protrusion on the mounting was incorporated. This design allowed the upper hemisphere's female protrusion to be seamlessly placed inside the male protrusion and then the pin was set to engage through the aligned holes on both the protrusions ensuring secure attachment with the mounting.

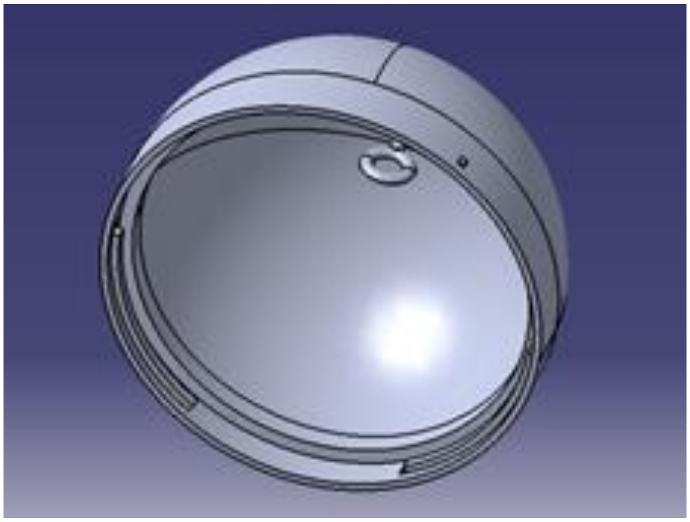

Figure 3.19: Loop created inside the top hemisphere

A loop on the inside of the top hemisphere initially served as the attachment point for the inner capsule, allowing for preliminary testing. Beneath the top hemisphere, grooves were strategically implemented to interlock with the subsequent component, the middle cylindrical section.

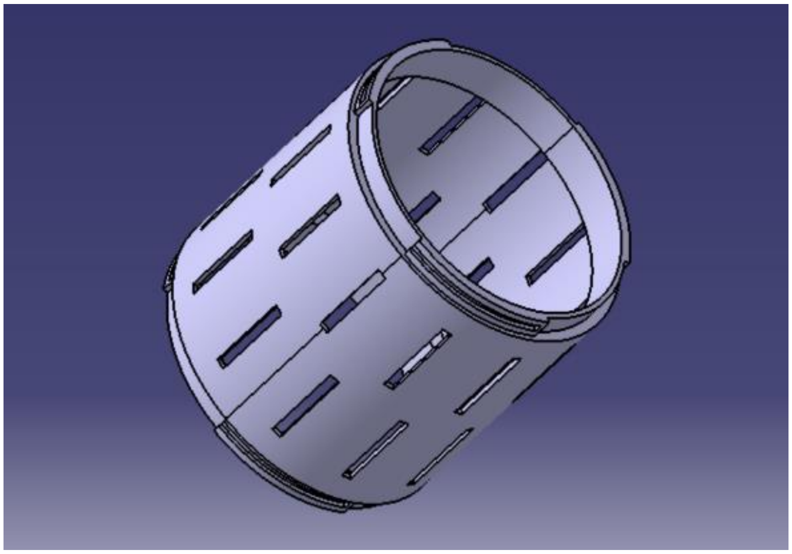

Figure 3.20: The middle cylindrical component

This hollow cylinder, designed to be both long and wide, accommodated the descent of the inner capsule. Initially featuring multiple slots along its walls to allow light into the capsule for enhanced visibility or camera feed, this component had corresponding grooves for secure connection with the top hemisphere. Additionally, a set of grooves at the bottom engaged and locked with the third component, the bottom hemisphere.

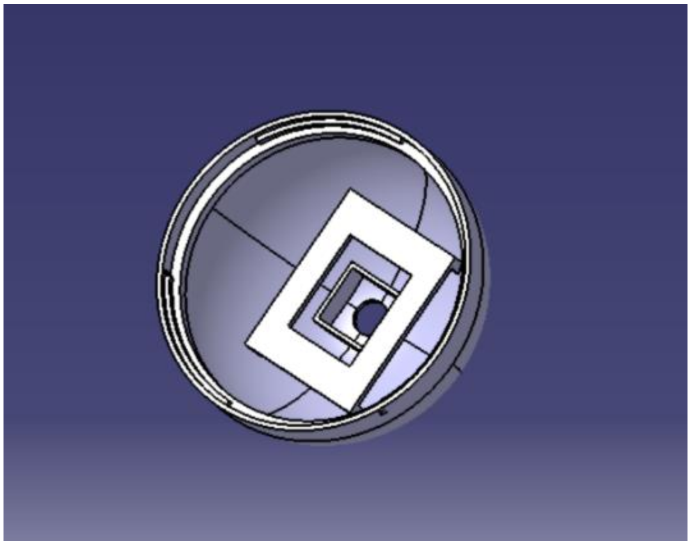

Figure 3.21: The bottom hemispherical component

The bottom hemisphere, mirroring the dimensions of the top hemisphere, featured counter grooves for seamless integration with the cylindrical section. Positioned at the exact center and bottom of the bottom hemisphere, a camera mount was strategically incorporated to facilitate the attachment of a camera for live location feed. This camera mount aimed to provide live location visuals to ensure the precise drop of the entire payload. This modular and intricately designed outer capsule underscores the significance of careful component segmentation and interlocking mechanisms to ensure a cohesive and functional system. The modular design gives further scope for adding any additional components and the feasibility of editing or redesigning a part without changing the entire outer capsule.

3.4.2 INNER CAPSULE

In a departure from the original configuration, which featured a box with a flat bottom attached to the capsule plate for separate release, the inner capsule underwent a comprehensive redesign aimed at mirroring the symmetrical and optimal structure of the outer capsule. This redesign was undertaken with the overarching objective of establishing a consistent and comparable experimental setup while concurrently streamlining the inner capsule to mitigate the effects of drag. The resultant modification involved adopting a hemispherical-cylindrical capsule design for the inner capsule, aligning seamlessly with the outer capsule's structure.

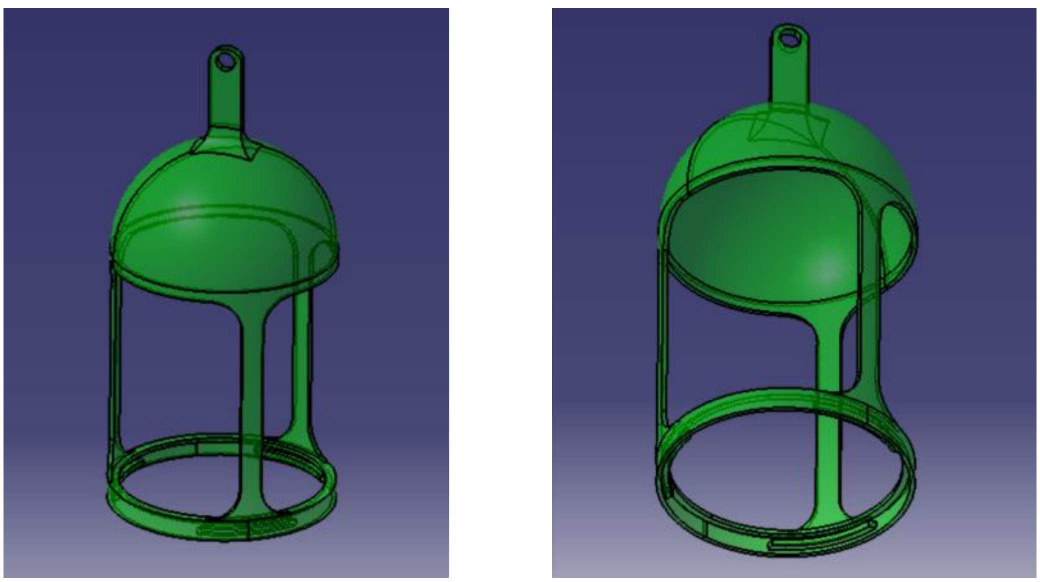

Figure 3.22: The design for the hemispherical top of the inner capsule.

The integration of this hemispherical-cylinder design with the pre-designed capsule plate ensured a symmetric and comparable configuration conducive to experimentation. This combined design extended as a protrusion from the top of the hemispherical component of the inner capsule, facilitating the independent engagement of the inner capsule onto the engagement pin. This architectural refinement allowed for controlled and autonomous release dynamics during experimentation. The inner capsule design is comprised of three distinct components. The top hemispherical component with a protrusion for connection to the engagement pin and extends below, incorporating three columns connected to a groove section for interlocking with the bottom hemispherical component.

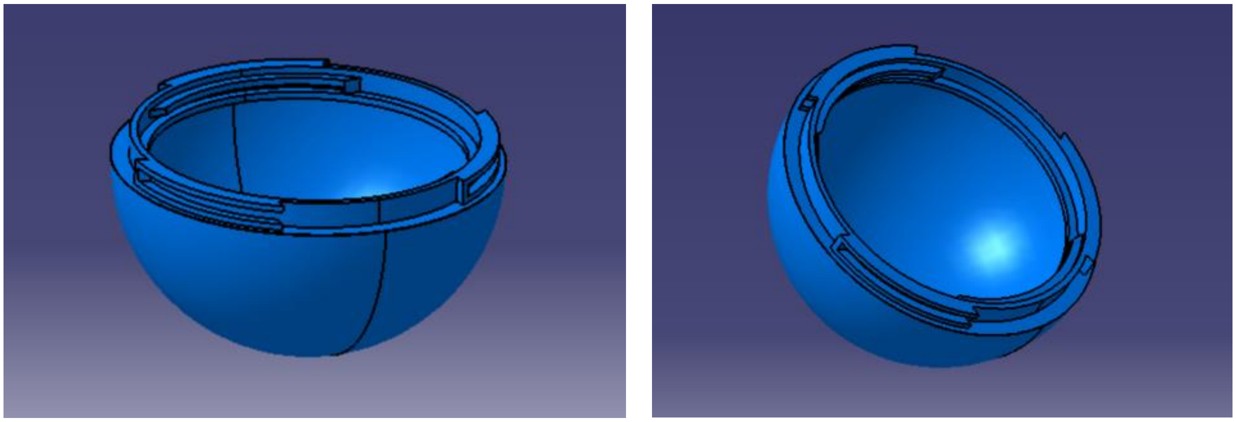

Figure 3.23: The design for the hemispherical bottom of the inner capsule.

The third component, a separate and removable plate, was designed to mount an accelerometer unit at its bottom. This plate, upon interlocking with the bottom hemisphere, served as a platform to keep the main experiment intended to study its behavior under microgravity conditions. The three columns on the upper component were strategically positioned to create wide window slots, ensuring an unobstructed camera feed for observing the experiment within. Transparent sheets covered these window structures, eliminating potential drag that could arise if the windows were left open.

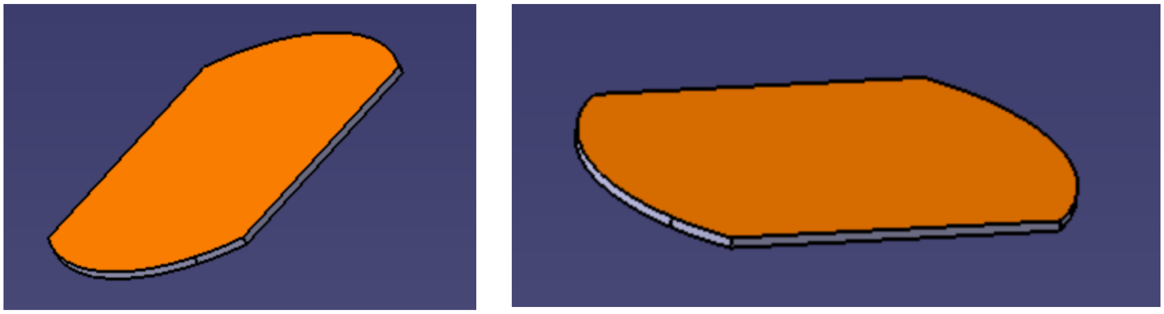

Figure 3.24: The design for the plate of the inner capsule.

The separation of these components facilitated the convenient attachment of the accelerometer to the bottom hemisphere of the inner capsule. The removable plate served the dual purpose of providing a platform for the experiment and accommodating the accelerometer mount on the opposite side. All these components seamlessly interlocked into one another, forming the integral structure of the inner capsule, which could then be independently attached to the engagement pin via the top protrusion. This modular and intricately designed inner capsule exemplifies a meticulous approach to optimizing functionality, ease of experimentation, and mitigating aerodynamic disturbances in the pursuit of precise and controlled microgravity experiences.

Figure 3.25: Assembly of the inner capsule

3.5 FILLETS IN DESIGNS

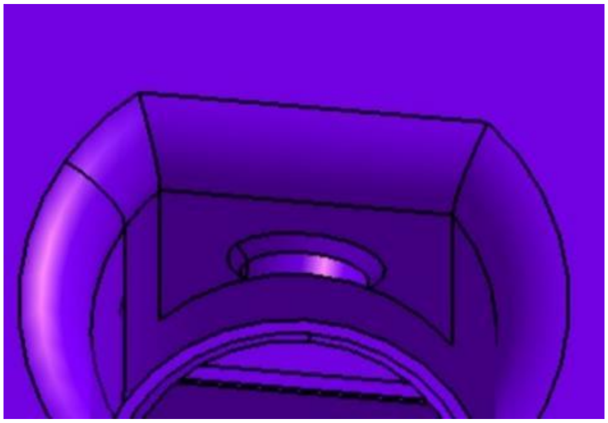 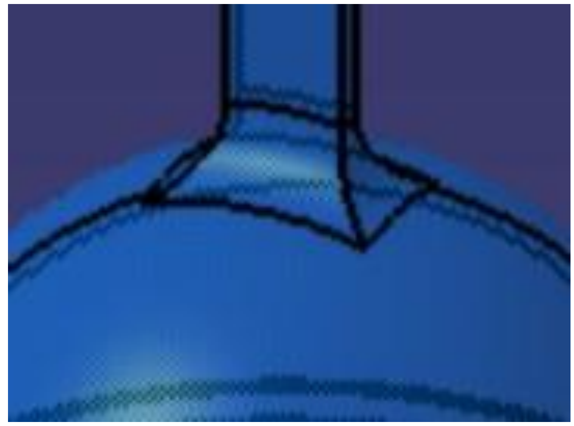

Figure 3.26: Fillets on the designed components

All the mechanical components designed had fillets i.e. a rounded interior or exterior corner, edge, or junction between two surfaces. This fillet reduces stress concentration which can lead to premature failure or crack initiation while distributing stresses more evenly enhancing the overall strength of the component. Fillets provide ease of manufacturing and streamline the process reducing the risk of defects. Sharp corners can be more susceptible to corrosion due to factors like stress corrosion cracking. They can reduce the impact of corrosive environments on a structure, improving the overall corrosion resistance. Fillets are used to improve the flow of fluids or air around a structure, reducing drag and improving overall efficiency.

3.6 KINEMATIC SIMULATION

To ensure the dimensional accuracy and functionality of the entire mechanism designed, kinematic simulation was incorporated. It analyzed the motion and behavior of the assembled components, providing valuable insights into the functioning, engagement, and release. All the mechanical components were assembled hierarchically with defined spatial relationships and constraints. The constraints include defining the permissible degrees of freedom between the assembled components. The software used was CATIA V5 which offered a wide range of joint types, such as revolute, cylindrical, prismatic, spherical, etc. enabling accurately modeled mechanical connections.

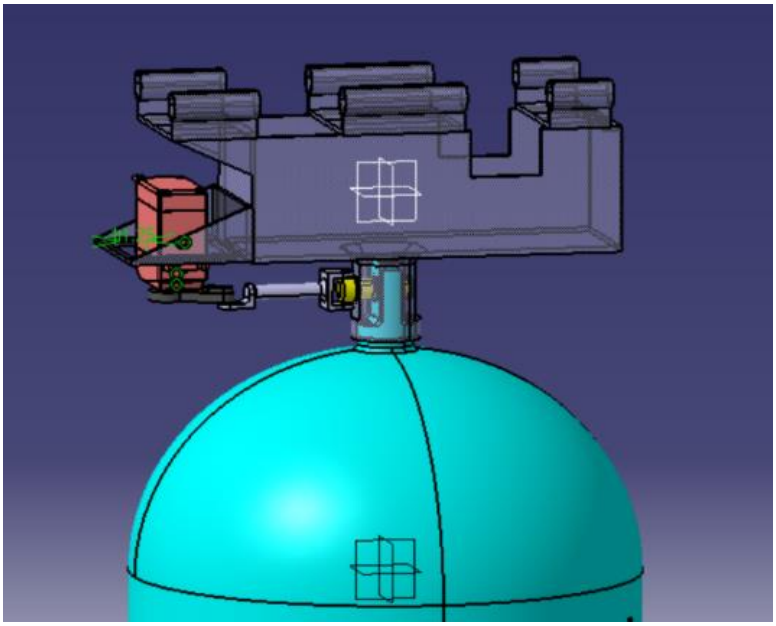

Figure 3.27: Release Mechanism

Kinematic joints allow the modeling of realistic motion between the components. The rotational motion of the servo arm to the translational motion of the engagement pin via the connecting rod was precisely simulated resulting in the virtual display of the release mechanism. Comprehensive simulation results were generated depicting motion characteristics and the interaction between the components with time which facilitated the identification of potential interferences during motion, dimensional corrections, and performance. Parameterizing various aspects of simulation, also allowed dynamic exploration of design alternatives. As, virtually testing assemblies through kinematic simulation and finding out any issues, it reduced the need for physical prototyping and minimized the cost and material waste.

3.7 STATIC VALIDATION

In the iterative process of designing the initial components for mounting, battery casing, and payload securement, rigorous focus was placed on validating the structural integrity and assessing load distribution within the proposed design for payload attachment. To accomplish this, Finite Element Analysis (FEA) emerged as a comprehensive tool, providing a virtual exploration of stress and strain distribution, thereby yielding valuable insights. Within the context of this research, FEA evaluated the response of connecting parts to anticipated loads, ensuring their resilience against the dynamic forces encountered during flight and payload release. The analytical scrutiny was specifically directed at key components, notably the connecting structures, simulating real-world scenarios to observe the design's performance under anticipated conditions.

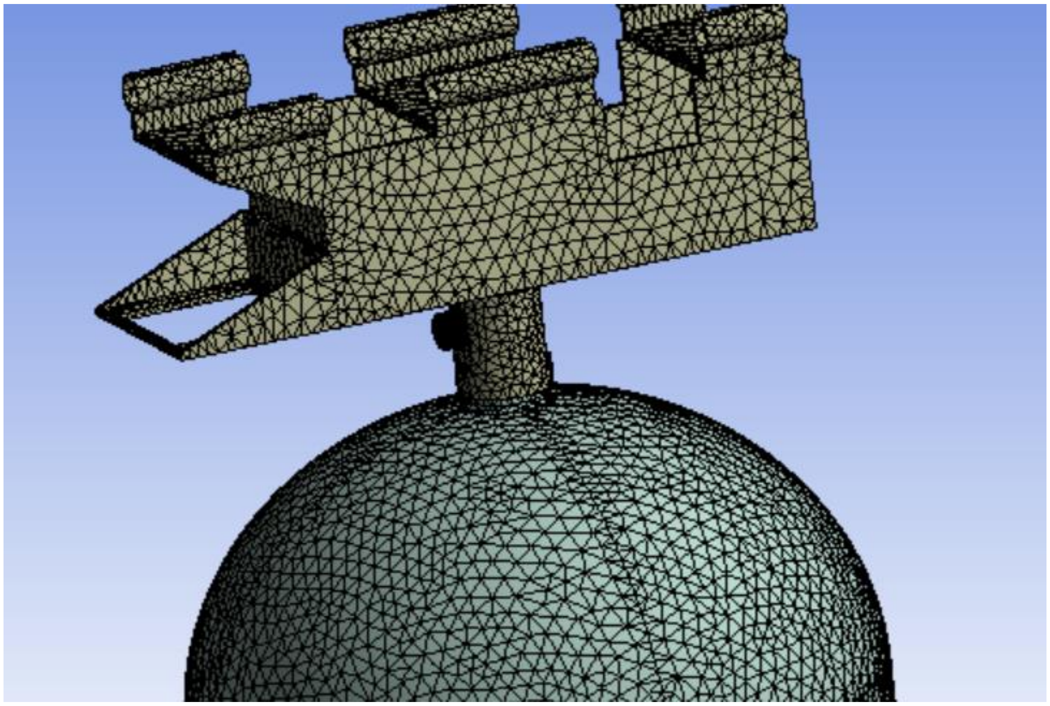

Figure 3.28: Meshed model

By applying simulated loads and constraints, FEA generated detailed stress maps, deformation plots, and other pertinent data, offering an understanding of the structural behavior of the system. The validation process was multifaceted, addressing crucial aspects such as load distribution, structural safety, optimization opportunities, and iterative refinement. FEA, serving as the linchpin in this research phase, underscored a steadfast commitment to engineering precision and safety. The insights gleaned from the analysis defined the design, ensuring that the final components were well-equipped to meet the demanding requirements of secure payload carrying, stable mounting, and reliable release mechanisms. The FEA methodology employed in this study followed a systematic approach to ensure the accuracy of the virtual representation of the UAV and its attachment components. The CAD model underwent thorough validation to faithfully mirror the physical attributes and behavior of the system. The subsequent meshing process discretized the CAD model into finite elements, creating a mesh that accurately captured the complex geometry of the UAV and attachment structure. Stratasys ABS, the material used for 3D printing the components, had its mechanical properties, including Young's modulus, Poisson's ratio, and material density, assigned to the corresponding elements. This step was crucial for simulating the material's behavior under expected loading conditions. The definition of boundary conditions established the simulation environment, incorporating constraints on degrees of freedom to replicate realistic operational scenarios, with specific considerations for UAV attachment points. The loading scenario of approximately 5kg was then simulated to assess the structural response of the payload attachment system, encompassing static loading, dynamic maneuvers, and aerodynamic forces encountered during flight. Emulating real-world operational conditions captured the inherent complexity of UAV missions.

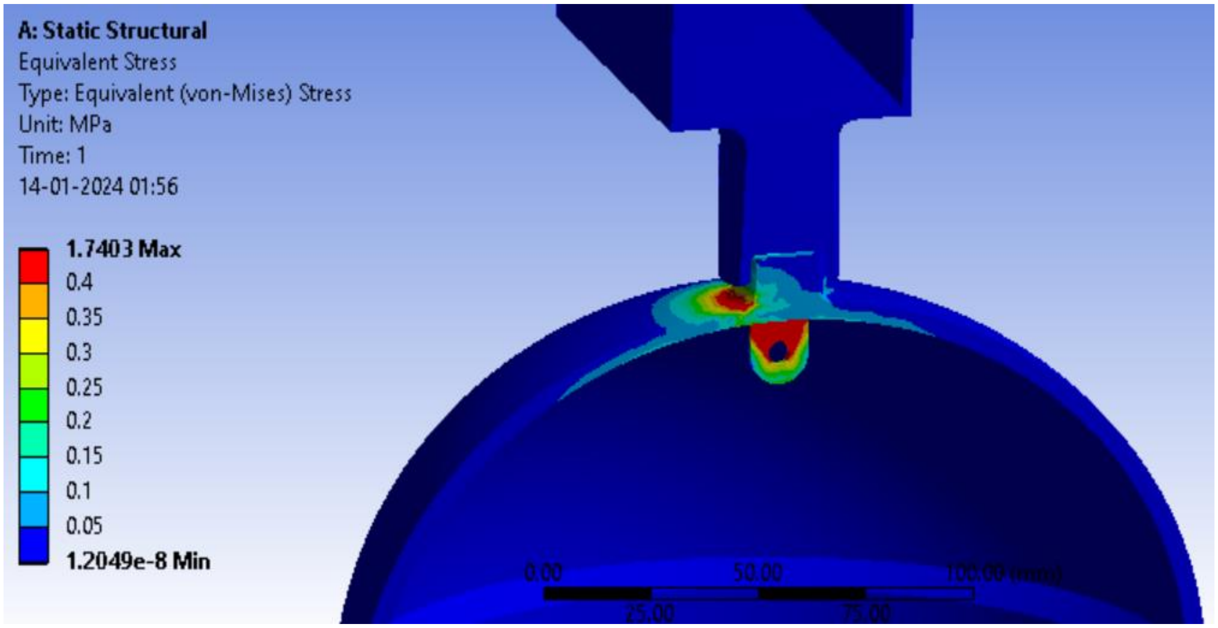

Figure 3.29: The stress distribution on the attachment area with maximum value as 1.74 MPa

The subsequent extraction of FEA results, including stress distribution, strain, and displacement, paved the way for in-depth analysis. Post-processing tools were incorporated to visualize and interpret the data, providing nuanced insights into the mechanical behavior of the payload attachment system. This comprehensive and methodical approach ensured that the study contributed not only valuable insights but also actionable data for the optimization of UAV attachment designs and the enhancement of reliability and operational safety.

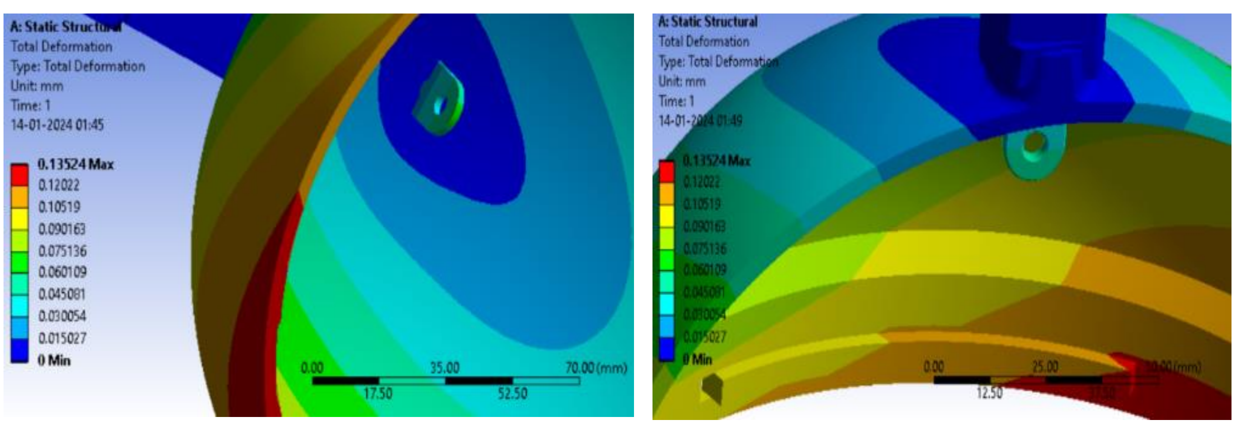

Figure 3.30: The deformation plot with maximum value as 0.13534 mm

The FEA results delivered the contour visuals of the deformation and stress values across the attachment design. The maximum stress values from the result were quite less than the material's allowable stress i.e. 44MPa Stratasys ABS (Acrylonitrile butadiene styrene) M30 filament [Matweb]. Therefore, the design was safe.

3.8 DYNAMIC VALIDATION

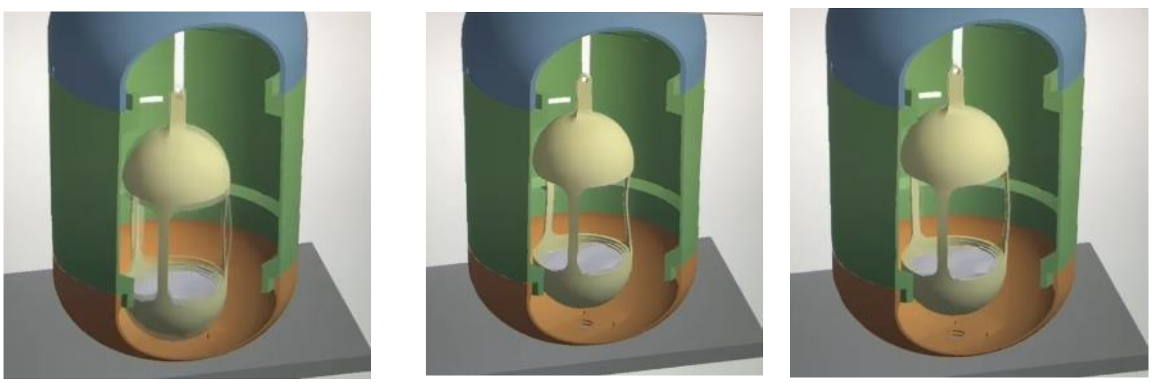

Figure 3.31: Visual representation of drop impact on the capsules

The conclusive iteration of both the inner and outer capsules underwent simulation to ascertain their response dynamics under impact conditions during drop scenarios. Traditionally, conducting simulations for drops from substantial altitudes is a laborious endeavor, necessitating considerable time investment for result attainment. In pursuit of expediting this process and optimizing efficacy, we delineated the critical pre-impact velocity threshold, leveraging this parameter to expedite result acquisition. Employing a 4 mm plate as the impacting surrogate facilitated the emulation of capsule-object interactions, thereby elucidating their behavioral intricacies. Visual analysis reveals that upon impact, the outer capsule initiates a reactionary response, inducing comprehensive capsule deflection. After the outer capsule's impact, the inner capsule comes into contact with the pre-deflected outer casing, thereby inheriting the deflective impulse. This sequential transference of deflective energy is prominently discernible in the visible deformation of the internal columns within the inner capsule, evincing subtle buckling phenomena under impact conditions.

To compute essential parameters such as the Time of fall, Maximum velocity, and terminal velocity for the payload. The simulation considered the force opposing the motion of the body in free fall, known as air resistance or aerodynamic drag force. This force is directly proportional to the velocity of the falling object.

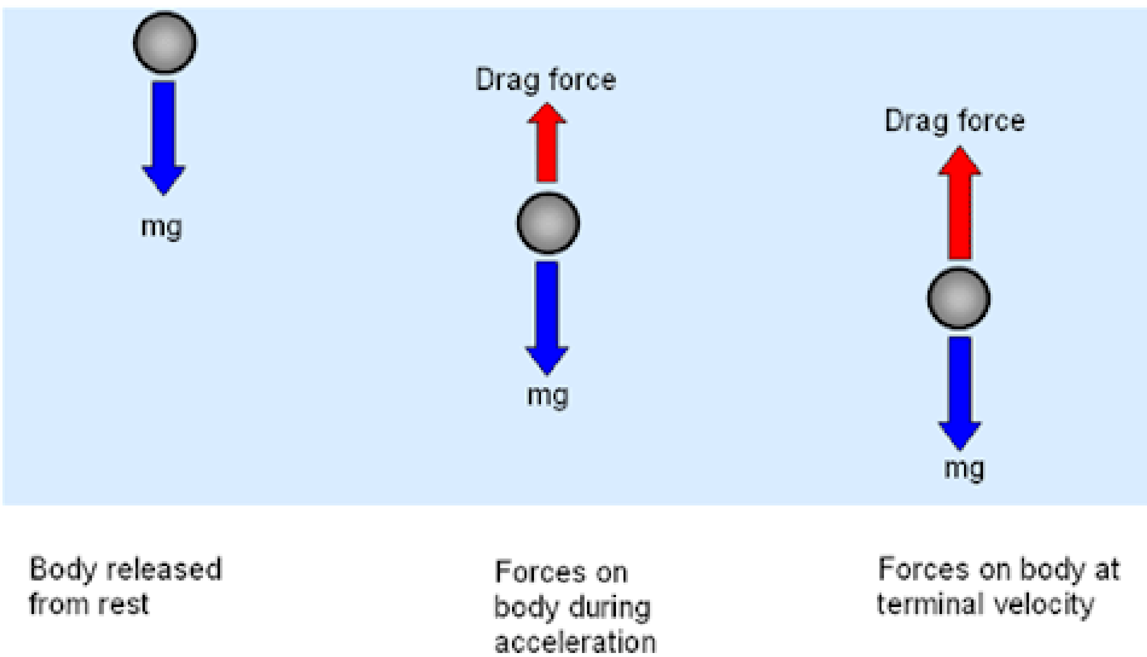

Figure 3.32: Forces on a free-falling body

As a falling object steadily accelerates during free fall, the air resistance increases with the velocity's rise. When the drag force reaches a point where it counteracts the gravitational force entirely, the object stops accelerating and reaches its terminal velocity. However, a free-falling object might reach the ground before reaching its terminal velocity, making its velocity at impact its maximum velocity. The time of fall, maximum velocity, and terminal velocity was determined by considering parameters such as mass (m), altitude (h), gravitational acceleration (g), cross-sectional area of the drop capsule, drag coefficient based on its shape, air density, and air resistance coefficient.

This maximum velocity was then utilized to simulate the Dynamic Analysis of the impact using ANSYS software, enabling a comprehensive analysis of the impact behavior of the capsules under study. The following formulas were used to determine the terminal velocity (V_t), the velocity at impact (V_{impact}), and the time to impact (T_{impact}):

C is the dimensionless drag coefficient associated with the shape of the falling body

$$F_{drag} = \frac{1}{2}\rho v^2 C_d A$$

$$F_{net} = mg - F_{drag} = 0$$

$$F_{net} = mg - \frac{1}{2}\rho v^2 C_d A = 0$$

$V_t = \sqrt{\frac{2.m.g}{C.\rho.A}}$; Terminal Velocity (Drag force = Weight of the falling object)

$\tau =$; Characteristic Time (Time when the object attains the terminal velocity)

$$V_{impact} = V_t\sqrt{(1 - \exp(\frac{-2\ g\ s}{{V_t}^2}))}$$

$$T_{impact} = \tau * \cos(h)^{-1} * \exp(\frac{s}{V_t * \tau})$$

For the outer capsule:

$V_{impact} = 16.85$ m/sec

$T_{impact} = 1.76$ sec

For the inner capsule:

$V_{impact} = 17.15$ m/sec

$T_{impact} = 1.75$ sec

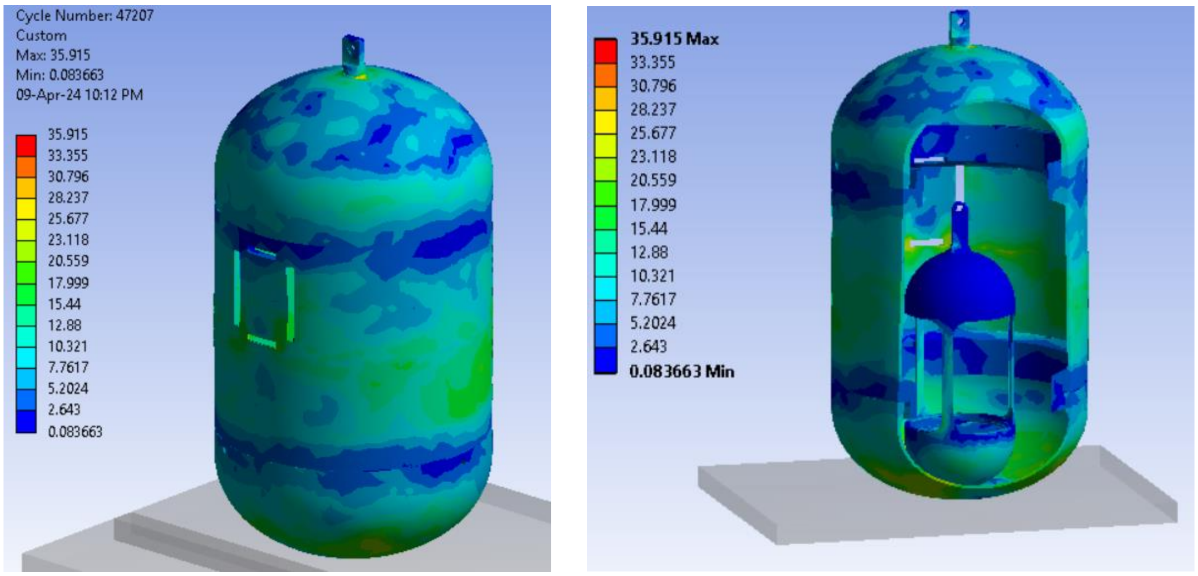

Figure 3.33: Stress value 35.915 MPa for the entire payload

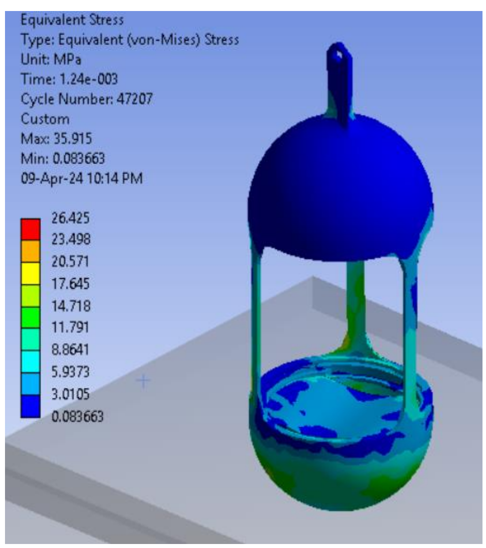

Figure 3.34: Stress value 26.425 MPa for the inner capsule.

CHAPTER 4

PLATFORM DEVELOPMENT

4.1 RAPID PROTOTYPING

Rapid prototyping is a methodology used in product development to quickly and cost-effectively create a tangible model or prototype of a product. The components were designed and the quick and iterative process of creating a preliminary version using the method of rapid prototyping was chosen as 3D printing. The primary goal of rapid prototyping is to gather feedback early in the development cycle, identify potential issues, and make necessary improvements before investing significant time and resources into the final product. For the experimentation of this research, the technique of 3D printing the components provided cost efficiency, feedback, flexibility for design, and tangible visualization of the components. 3D printing is also known as additive manufacturing as it's the process of creating 3-dimensional objects by layering material based on a digital/CAD model also with its ability to create complex shapes and structures with versatility and speed.

Figure 4.1: 3D Printing from the filament ABS-M30 (left) and seperation of the component from the filament material by dipping it in NaOH Solution (right)

To facilitate these experiments, the components of the mechanism were fabricated through 3D printing technology. This iterative approach allowed for multiple experimental iterations, providing a platform for validating the reliability of the drop mechanism and identifying potential avenues for improvement. The use of 3D printing offered a flexible and efficient means of prototyping, enabling swift modifications to be made in response to the outcomes of each trial. These early trials and subsequent iterations formed a crucial phase in the research, offering insights into the practical applicability of the drop mechanism and guiding refinements for optimal performance. The methodology of employing 3D printing for component fabrication allowed for a dynamic and adaptive approach, aligning with the iterative nature of the research and contributing to the overall development and enhancement of the drop mechanism.

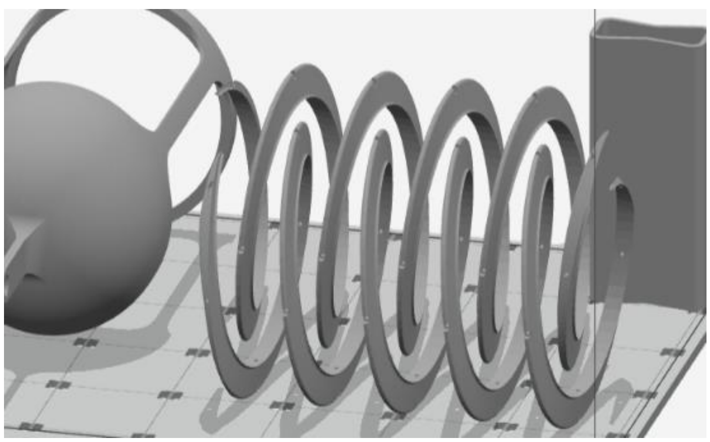

Figure 4.2: 3D Printing Simulation

The process of 3D printing was executed in a university research lab. The material used to print the components was Stratasys ABS M30 Filament. Soluble supports were used to support the parts during 3D printing. Then the parts were broken off and dissolved in sodium hydroxide (NaOH) solution to remove the attachment and to obtain the required part. On average a part of about 6x6 inches takes 24 hours to get 3D printed and ready, accordingly, bigger components took more time and smaller ones took less time. The advantage of 3D printing are speed of prototyping over other conventional methods. The 3D printing requires minimal setup and human interaction and can auto-run 24x7 according to the necessities. Parts that are produced with an accuracy of +/- 0.200mm (0.008 inches).

4.2 UAV FLYING

In the pre-flight preparation phase, meticulous attention was given to local UAV regulations, which are region-specific and stipulate criteria such as altitude restrictions, no-fly zones, and mandatory registration. These regulations, governed by the Federal Aviation Administration (FAA), encompass critical considerations such as flying within line of sight, utilizing UAVs weighing less than 55 lbs., avoiding restricted areas, and steering clear of other airborne entities [28]. Adherence to ethical standards was underscored, encompassing measures to prevent disturbance to wildlife or the public. Thorough familiarity with the UAV's anatomy, transmitter controls, and operational features was attained through a comprehensive review of manuals and pertinent documentation. Flight initiation occurred in a carefully selected on-campus location, characterized by expansive open grounds, a substantial distance from buildings, and compliance with a 20-meter proximity threshold.

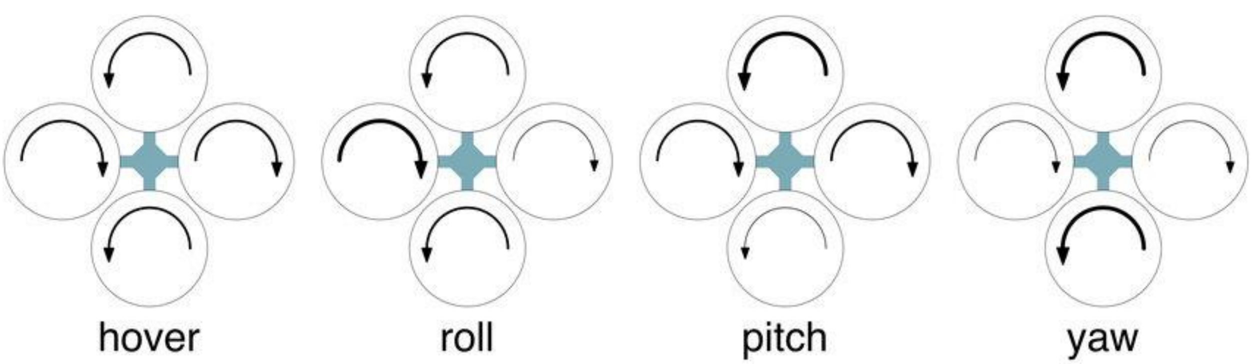

Figure 4.3: Basic maneuvers of quadcopter UAV

Figure 4.4: UAV flying in open grounds

Proficiency in basic flight maneuvers, including takeoff, landing, hovering, and directional control, was deemed indispensable. A comprehensive pre-flight inspection protocol was rigorously observed, entailing a careful examination for loose components, visible damage, or irregularities. Attention was particularly devoted to ensuring secure propeller attachment, proper battery insertion, and optimal sensor calibration for stability and precise navigation. The battery's charging status, closely monitored before and during flight, was deemed crucial to prevent untimely power loss, which could result in inadvertent UAV descent and consequential damage. The remote controller underwent charging and synchronization with the UAV, necessitating a deliberate acclimatization period to comprehend the control layout, encompassing joysticks, buttons, and switches. Fundamental controls were systematically practiced, encompassing throttle, pitch, roll, yaw, as well as essential maneuvers, within a secure and unobstructed environment.

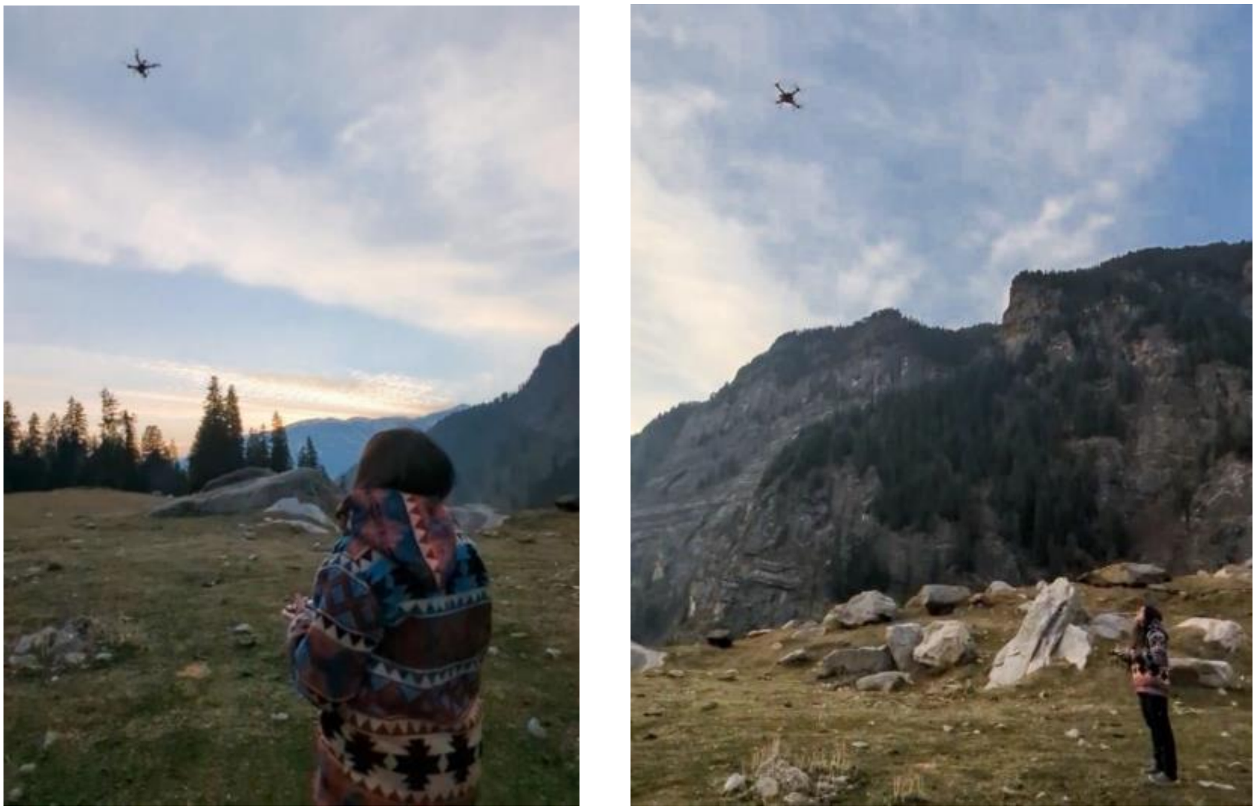

Figure 4.5: Learning UAV piloting and maneuvering

An exhaustive understanding of flight modes, including GPS mode, manual mode, and return-to-home, was acquired through the perusal of pertinent literature. Adherence to constant visual monitoring, ensuring the UAV remained within line of sight, was maintained throughout the flight trajectory, with vigilant consideration for potential obstacles. Safe and controlled UAV landing procedures were honed, emphasizing gentle descent and the avoidance of abrupt movements. Post-flight, a meticulous power-down sequence was executed by established protocols. Iterative flight sessions facilitated progressive skill enhancement and experiential learning, contributing to the refinement of piloting proficiencies over successive endeavors.

4.3 THE LAUNCH PAD

The development of an optimal UAV takeoff platform is integral to ensuring safe and effective UAV operations. Following the rapid prototyping phase of the entire capsule, it was observed that the assembled capsule exceeded the ground clearance of the UAV, necessitating the creation of a dedicated takeoff platform. To address this discrepancy, surplus materials from the laboratory were utilized, resulting in the selection of a box and a cardboard sheet. The key considerations in crafting the platform were providing a flat and level surface to ensure stability during takeoff. The cardboard sheet, chosen for its non-slip properties and cushioning capabilities, enhanced the overall functionality of the platform.

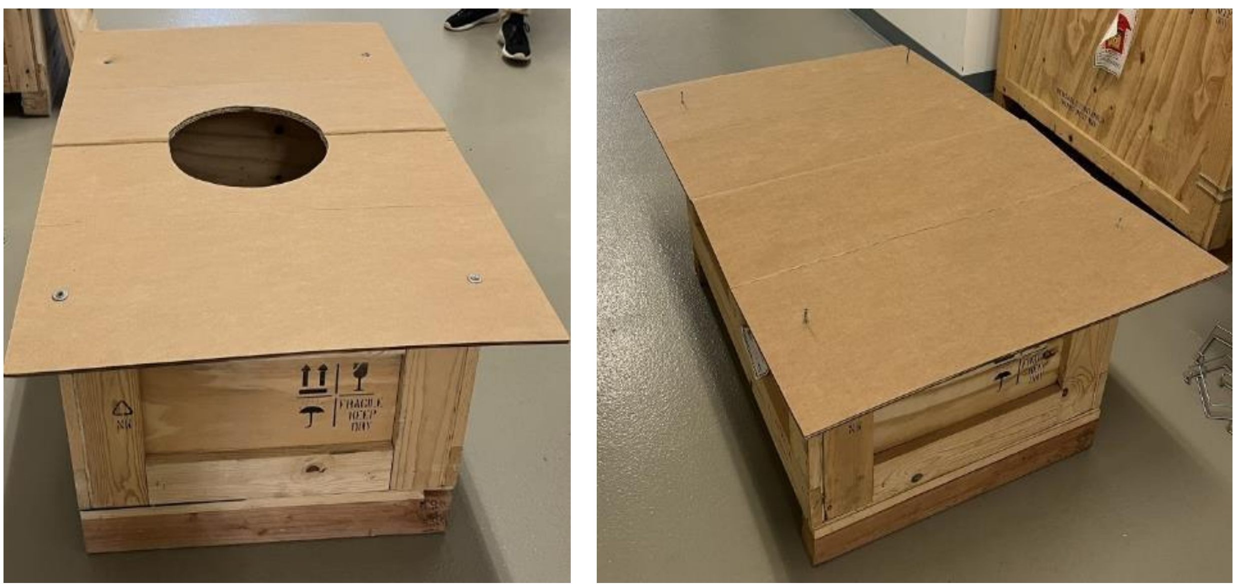

Figure 4.6: Spare Cardboard And Wooden Box

The dimensions of the box were found appropriate, with the height approximately aligning with the combined cylindrical and bottom hemispherical components when assembled. Notably, the top hemisphere extended beyond the top of the box, fitting within the clearance space between the UAV and the cardboard surface. The integration of the cardboard sheet onto the open box was achieved through secure bolting, facilitating the creation of a unified platform. A circular aperture, exceeding the diameter of the capsule, was precision-cut into the cardboard sheet. This design choice was instrumental in providing adequate clearance and robust support for the secure attachment of the entire assembly beneath the UAV. The engagement pin mechanism established a secure connection between the UAV and the capsule assembly. This meticulously crafted takeoff platform not only supported the capsule but also ensured a safe and precise takeoff, exemplifying a strategic and innovative solution to address the initial ground clearance limitations.

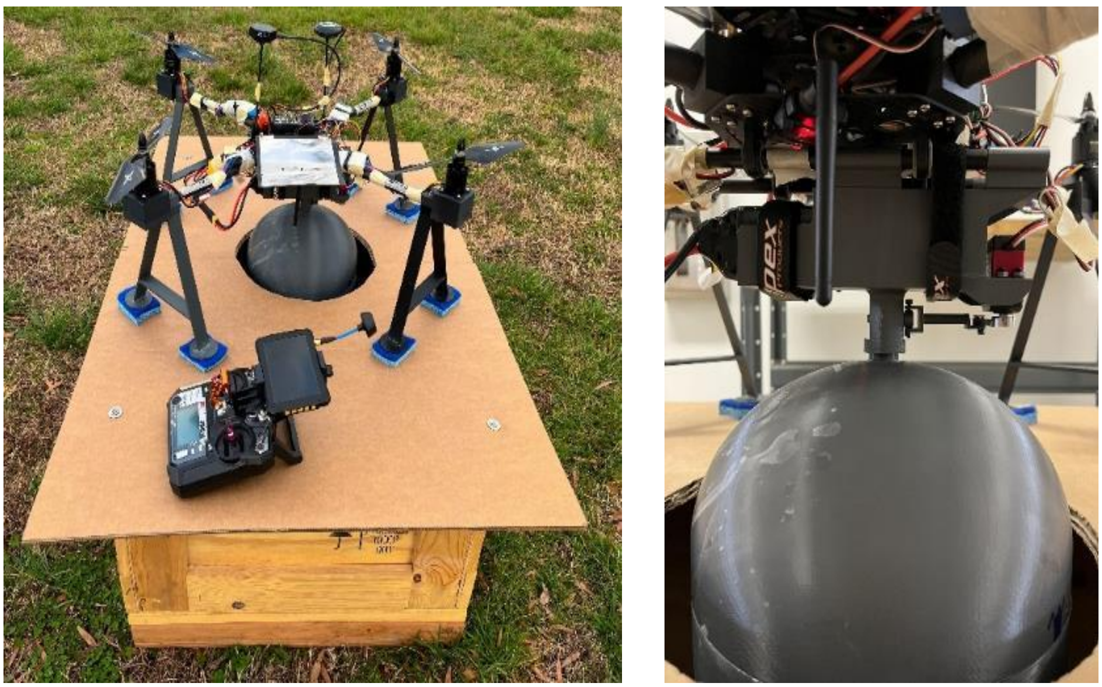

Figure 4.7: Entire assembly setup with the launch pad

4.4 DECELERATION MECHANISM

Deceleration mechanisms hold a paramount role in the realm of drop tests to facilitate a controlled and secure landing for objects or equipment undergoing examination. The primary objective is the dissipation of kinetic energy generated during free fall, thereby safeguarding the structural integrity of the tested item and ensuring the acquisition of precise data. Diverse mechanisms can be employed, tailored to the specific characteristics of the object and the unique requisites of the drop test.

Figure 4.8: Military Deceleration Parachute

Parachutes stand as a widely adopted solution for mitigating the descent speed during drop tests, providing a controlled and gradual deceleration through enhanced air resistance. Employing soft, cushioned surfaces that integrate materials such as foam, airbags, or other shock-absorbing materials proves effective in absorbing impact energy. The incorporation of springs or shock absorbers within the test rig or the object itself serves to absorb and dissipate kinetic energy upon impact, affording controlled deceleration and minimizing the potential for damage. Mid-descent deployment of retarding devices, such as drag flaps or panels, augments air resistance, achieving a more gradual deceleration. Protective structures, such as cages or frames enveloping the test object, are engineered to absorb and distribute impact forces, acting as a safeguard against direct contact with the ground and facilitating a controlled landing. Nets or webbing systems are designed to catch and decelerate falling objects, utilizing stretchable materials to absorb energy and prevent abrupt stops upon impact.

Figure 4.9 :Net & The Target Patch (Left) & Poles with Ground Anchors (Right).

Considerations like cost-efficiency and feasibility, including payload size, drop height, and experiment scale, were imperative for the strategic selection of a deceleration net. Deceleration nets, typically crafted from robust materials like nylon, polypropylene, or high-strength synthetic fibers, exhibit a flexible yet robust structure. The mesh configuration of the net plays a pivotal role, influencing its ability to deform and efficiently absorb energy upon impact. Selections of mesh sizes and configurations are made based on specific application requirements, carefully balancing the objective of slowing down the falling object while preventing it from passing through. The attachment of deceleration nets to supporting structures, such as frames or poles, is engineered to ensure stability and prevent collapse upon impact. As an object descends into the net, controlled deformation occurs, stretching and gradually dissipating kinetic energy to reduce impact forces. This paper underscores the deliberate choice of a deceleration net, considering factors such as material composition, mesh design, and attachment configuration, all of which contribute to optimizing the safety and precision of the drop tests conducted within the scope of this research.

4.5 MECHANICAL ITERATIONS

4.5.1 ITERATION 2: MOUNTING

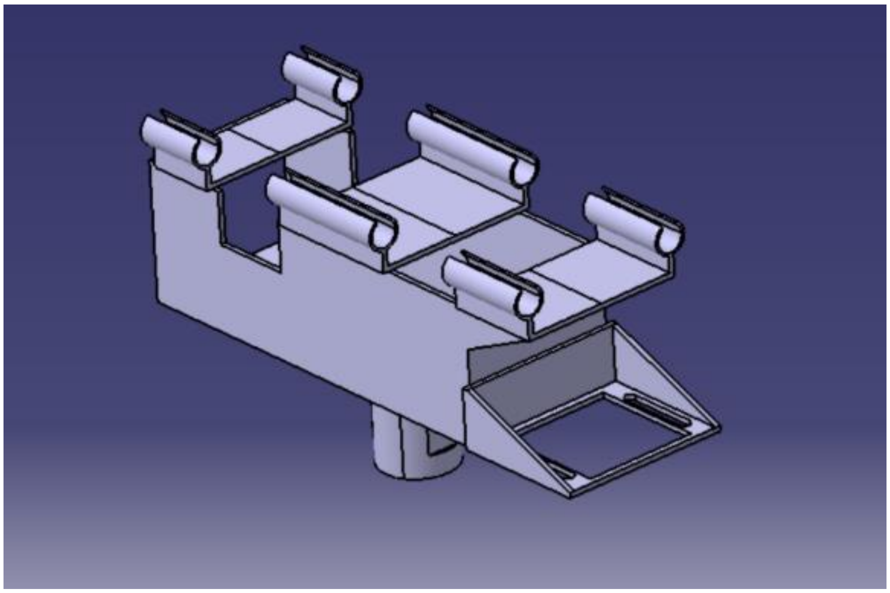

Figure 4.10: The Second Mounting Design

In the course of the assembly phase beneath the UAV, complications emerged about interference caused by two supporting structures for the cylindrical rod used in the mount. To address this challenge with precision, meticulous measurements of these structures were undertaken, leading to the incorporation of corresponding slots in the upper part of the mounting structure. This modification was implemented to alleviate interference concerns, thereby ensuring a seamless integration of the component beneath the UAV. Simultaneously, a revision was initiated for the L-shaped plate designed to secure the servo motor. In the initial attempts to affix the servo to the prior mount using nuts and bolts, an unexpected structural failure manifested in the plate. This unanticipated setback necessitated a thorough reevaluation of the plate's design and structural integrity. These encountered challenges and subsequent modifications underscore the iterative nature of the research and emphasize the significance of real-time adjustments during the implementation phase. The responsiveness to unforeseen issues and the application of practical solutions contribute to the refinement and optimization of the overall system, aligning with the research's commitment to achieving reliability and functionality. In the pursuit of enhancing the load distribution and structural support, a strategic reinforcement process was applied to the L-shaped plate. This involved the installation of two rib structures at its extremities. These ribs were strategically integrated to enhance support, stiffness, and overall reinforcement, key attributes aimed at fortifying the load-bearing capacity, minimizing deflection, and bolstering the overall strength of the L-shaped plate. The incorporation of rib structures represents a recognized engineering technique employed to optimize the mechanical properties of plates. Considering the unique requirement of mounting the servo in an inverted orientation, where the alignment of bolts presented a potential challenge, a pragmatic solution was implemented. To streamline the servo mounting process and mitigate the risk of structural failure, a channel design was introduced instead of individual holes. This design not only facilitated the alignment of bolts but also simplified the overall mounting procedure for the inverted servo configuration. In anticipation of the repetitive use of the battery, which may lead to dimensional changes and bloating, a proactive approach was adopted in the design of the battery casing. To accommodate potential variations in battery dimensions, the casing was generously endowed with better allowances dimensionally. This forward-looking design consideration aimed to ensure the adaptability of the casing to the evolving dimensions of the battery, thereby reinforcing the system's robustness and durability. These design adjustments and considerations, as delineated the importance of structural optimization and proactive measures in the iterative development of the system. The incorporation of rib structures and allowances in the battery casing reflects a commitment to ensuring long-term functionality, stability, and adaptability within the framework of the broader research objectives.

4.5.2 ITERATION 2: OUTER CAPSULE

IIn the initial phase of design iteration, the top hemisphere of the outer capsule incorporated an internal loop to suspend the inner capsule during the drop. However, subsequent testing uncovered a deficiency in achieving the desired relative microgravity conditions for the inner capsule. It became evident that true microgravity necessitated the independent release of the inner capsule from the outer capsule. The fundamental principle of microgravity lies in enabling an object to experience free fall without substantial external forces acting upon it. The initial design, wherein the inner capsule was connected to the outer capsule, inadvertently compromised the free fall experience for the experiments housed within. This interconnection introduced dependencies on the descent, timing, and responses of the outer capsule, undermining the intended conditions for achieving relative microgravity. To rectify this limitation and address the primary objective of independent free fall for the inner capsule, subsequent design modifications were implemented.

These adjustments were geared towards ensuring the autonomous release of the inner capsule, facilitating a more controlled and precise attainment of microgravity conditions during experimental drops. This strategic refinement aligns with the nuanced requirements of microgravity experiments, underscoring the importance of iterative design improvements to meet specific research goals. In response to the identified limitation, the loop within the top hemisphere, originally intended for suspending the inner capsule, was systematically eliminated. The focus then shifted towards orchestrating the sequential descent of both the inner and outer capsules, ensuring their simultaneous release from the mounting mechanism.

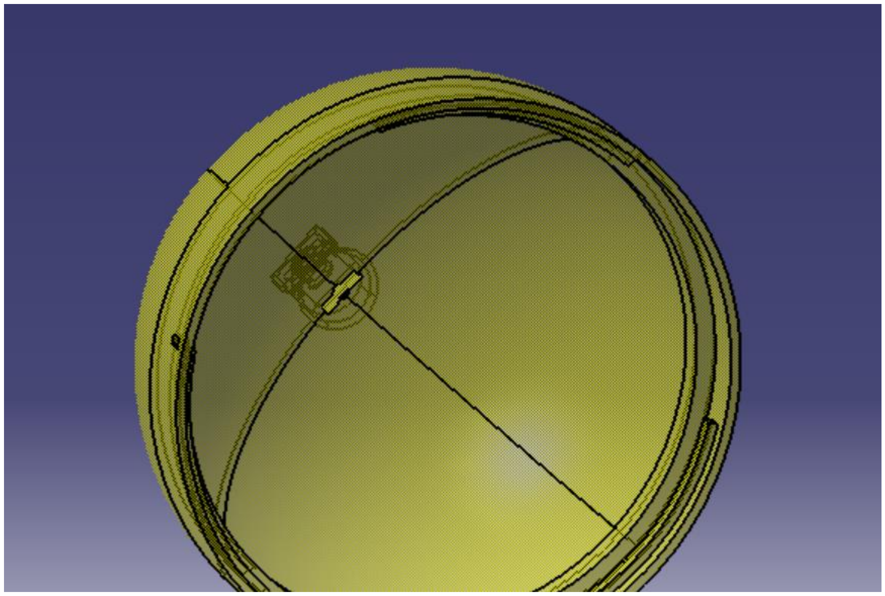

Figure 4.11 :Hemispherical top of the outer cylinder with a slot for the plate

To achieve this coordinated release, a strategic modification was introduced as a slot that was integrated inside the hemisphere of the outer capsule. This slot served as a housing for a specially designed plate, which traversed the cavity created by the slot and was securely mounted to the engagement pin. This configuration allowed the plate to operate in tandem with the outer capsule, establishing a series of connections that ensured the concurrent release of the inner and outer capsules. The design of this plate was purposefully crafted to serve the dual role of securing the experiment to be studied and facilitating the synchronized descent of the inner and outer capsules. By addressing the need for a controlled and simultaneous release, this innovative design adaptation aimed to optimize the experimental conditions, aligning with the research's emphasis on achieving precise and coordinated microgravity experiences during drop tests.

The plate's configuration was devised to incorporate two strategically positioned holes, each serving distinct functionalities within the experimental setup. The first aperture, located towards the flat surface of the plate, was purposefully designed to precisely align with the engagement pin, ensuring accuracy in both dimensions and diameter. This meticulous arrangement facilitated the secure affixation of the plate onto the engagement pin, establishing an integral connection within the series with the outer capsule.

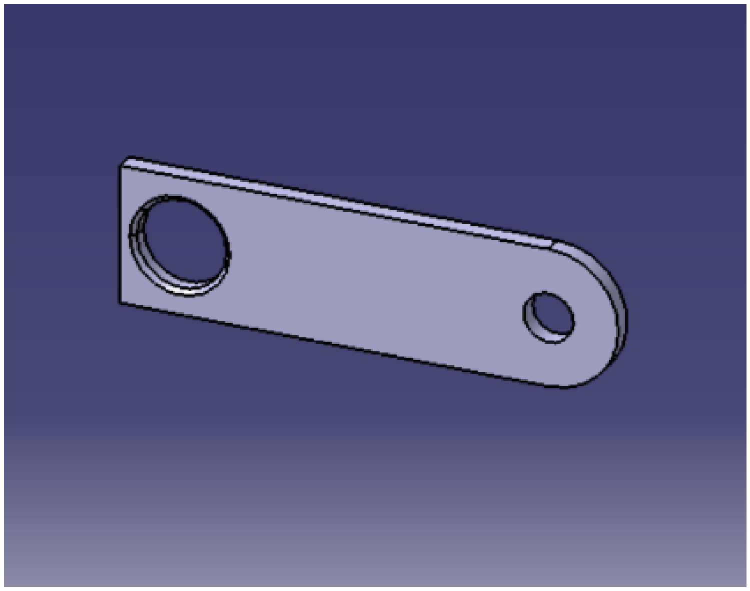

Figure 4.12: Plate design

Conversely, the second aperture was intentionally crafted to facilitate the suspension of the inner capsule from this plate. The placement of this hole was thoughtfully considered to enable the orchestrated release, contributing significantly to the achievement of the desired relative descent of both the inner and outer capsules. By leveraging these strategic hole placements, this design sought to optimize the control and synchronization of experimental conditions. During the testing phase of the second iteration, focused on achieving the relative release of the inner and outer capsules, the overall stability of the designed system and its flight dynamics were systematically monitored. The objective was to discern any potential issues that might necessitate further design adjustments. The achievement of the relative and independent release was validated, and the UAV demonstrated proficiency in executing the desired flight and release sequences. However, a subtle concern emerged regarding the stability of the entire system. The weight distribution, particularly from the battery and the mounting design, contributed to a slight shift in the center of gravity (CG) towards one end, introducing stability and balancing challenges for the quadcopter system.

4.5.3 ITERATION 3: MOUNTING

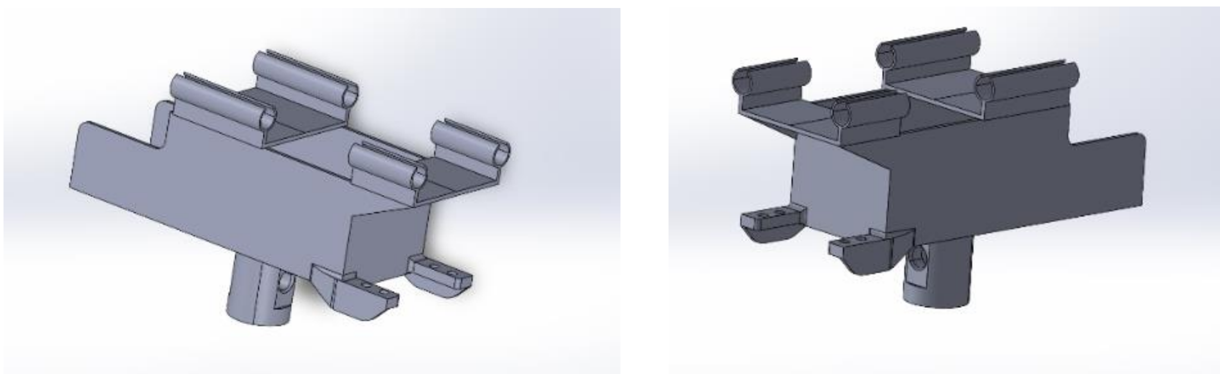

Figure 4.13: The final mounting design

To address this observed issue, a new mount design was formulated to ensure a balanced CG even after the integration of the battery and all other components. Departing from the previous design where the top hollow rods were aligned with two cut slots on the UAV, the revised design allowed for increased space to facilitate accurate manual mounting, securing a stable CG at the center of the system. The final mount design incorporated flexibility for manual adjustments to fine-tune the CG position, with limited allowances to ensure stringent constraints during flight. Simultaneously, while refining the final mount design, an additional modification was introduced for safety considerations. The initial ribbed-L-shaped plate design was replaced with two separate, robust mounts explicitly crafted for securing the servo motor. These mounts featured precise hole dimensions, eliminating any potential movement of the servo motor during flight and ensuring a secure and stable configuration. This iterative refinement process, informed by systematic testing and real-time observations, highlights the commitment to achieving optimal stability, balance, and safety in the designed system. The multifaceted approach to addressing weight distribution issues and enhancing the mounting structure contributes to the reliability and precision of the UAV system in executing the envisioned flight and release sequences.

4.5.4 ITERATION 3: OUTER CAPSULE

A critical consideration in the design optimization process was to configure the outer capsule with dimensions substantial enough to prolong the collision delay between the two capsules. After the simultaneous release of both capsules, the outer capsule was strategically designed to decelerate gradually due to drag forces experienced during descent from a specified height. This deliberate deceleration allowed the inner capsule to undergo the same drag forces, leading to its eventual acceleration surpassing that of the outer capsule. The culmination of this dynamic was envisioned to result in the collision of the inner capsule with the bottom of the outer capsule. To achieve this intended effect, the dimensions of the outer capsule were adjusted to maximize its size within the constraints of the 3D printer's maximum printable dimensions. The choice of dimensions was aligned with the inherent limitations of the 3D printer. The modifications predominantly focused on expanding the diameter of the entire capsule and the height of the cylindrical section, ensuring the outer capsule's capacity to delay the collision and enhance the experimental outcomes.

4.5.4.1 TOP AND BOTTOHEMISPHERERE

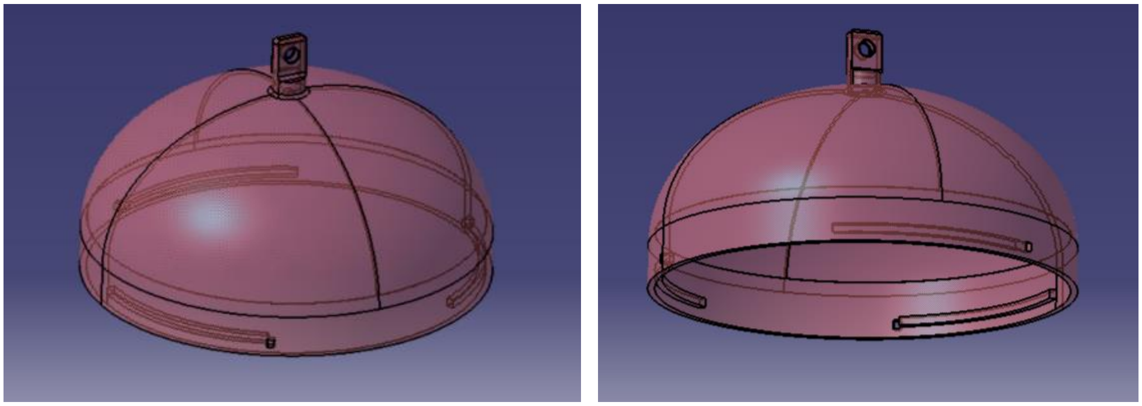

Figure 4.14: The final design for the hemispherical top of the outer capsule

The overall diameter of the entire capsule underwent a deliberate scaling and enlargement process. This meticulous adjustment took into consideration the female protrusion situated atop the upper hemisphere, intended for engaging and securely locking with the mounting apparatus. While maintaining the dimensions of the protrusion, a strategic increase in the diameter of the top hemisphere was implemented.

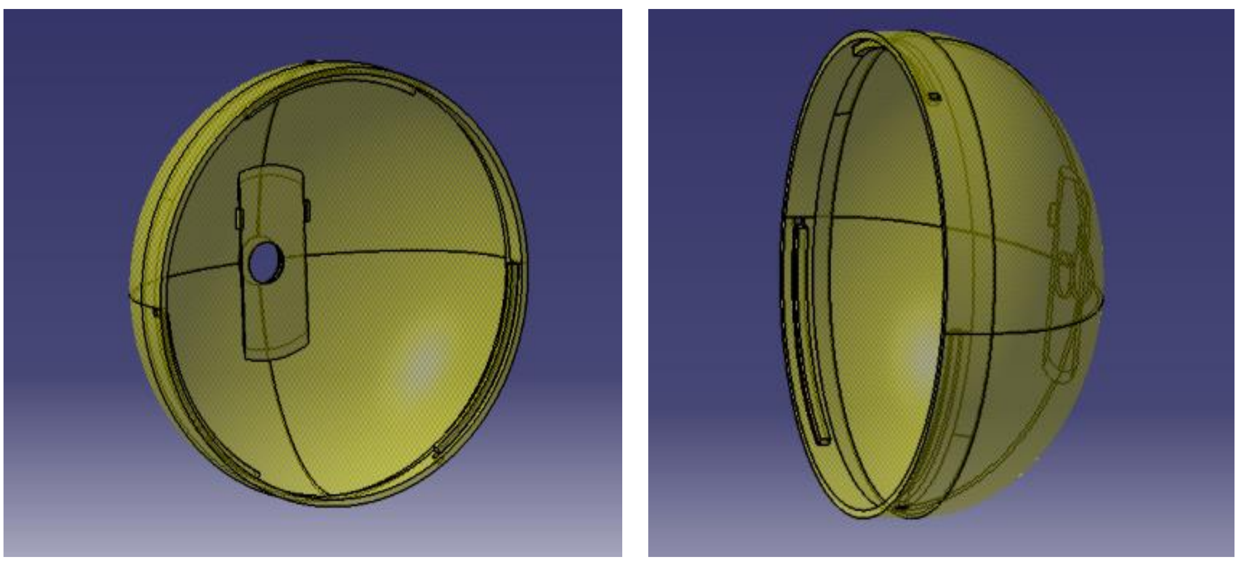

Figure 4.15: The final design for the hemispherical bottom of the outer capsule

Simultaneously, the bottom hemisphere, designated for housing a camera with a slot for location feed recording during flight, necessitated the design of a camera mount. Consequently, the dimensions of the camera mount and slot were thoroughly validated, ensuring precision, while concurrently increasing the diameter of the bottom hemisphere in a manner analogous to the modification applied to the top hemisphere.

4.5.4.2 MIDDLE CYLINDRICAL COMPONENT

In the earlier design iteration, the middle cylinder of the outer capsule featured numerous slots, primarily intended for illuminating the interior space to facilitate clearer camera feeds. However, the presence of these slots contributed to increased drag, leading to a more pronounced deceleration of the outer capsule. Slots create disruptions in the smooth flow of air around the object. As air moves over the surface of the falling object, the presence of slots can cause turbulence, leading to changes in pressure distribution and increased resistance.

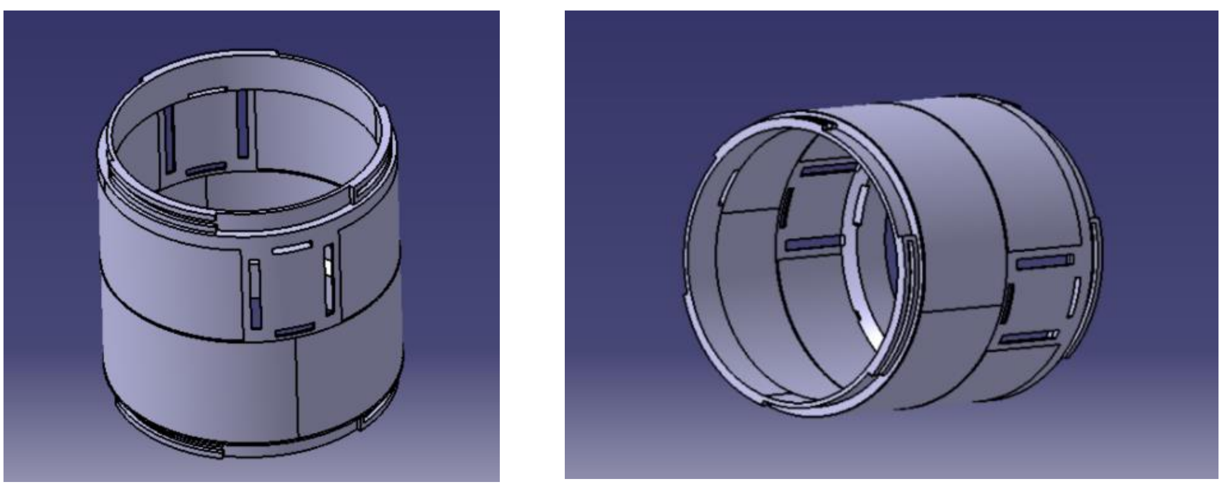

Figure 4.16: The final design for cylinder component of the outer capsule.

Slots can also induce the formation of vortices or swirling air currents creating additional drag by altering the flow patterns around the object. The presence of vortices can lead to a more complex aerodynamic environment, resulting in higher drag forces. To mitigate this drag-induced effect, a strategic modification was implemented. The majority of the slots were eliminated, and only four slots on each side were retained. These remaining slots on the opposite ends served the purpose of mounting cameras on the outer wall of the capsule while also providing a counterweight on the other side. This counterweight mitigated the risk of the outer capsule descending in a tilted orientation, a scenario that, if not controlled, could accelerate the collision between the inner capsule and the capsule wall. The comprehensive adjustments in dimensions and slot configuration reflected a nuanced approach to balancing drag considerations, collision dynamics, and experimental objectives. These refinements contribute to the precision and reliability of the outer capsule's behavior during descent, aligning with the research's emphasis on achieving controlled and impactful collision scenarios for microgravity experiments. For the final design of the outer capsule, the thickness from all three components, the top and bottom hemispheres, and the middle cylinder component, were reduced optimally maintaining the structural integrity and reducing the overall payload weight.

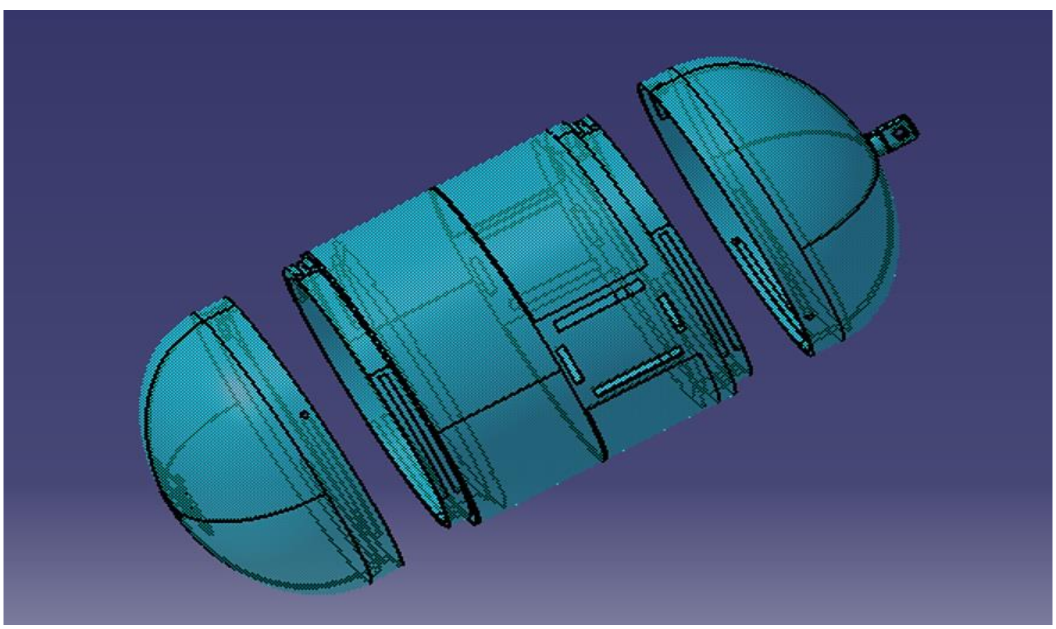

Figure 4.17: The outer capsule.

4.6 THE FINAL ASSEMBLY OF THE CAPSULES

The upper component with the protrusion interlocked with the bottom hemispherical component. The plate was further fixed with the space given at the sides for manually locking and unlocking the groove mechanism to facilitate the attachment of the accelerometer and placing the experiment inside. The assembly was successfully designed with minimum weight and utmost structural balance and integrity.

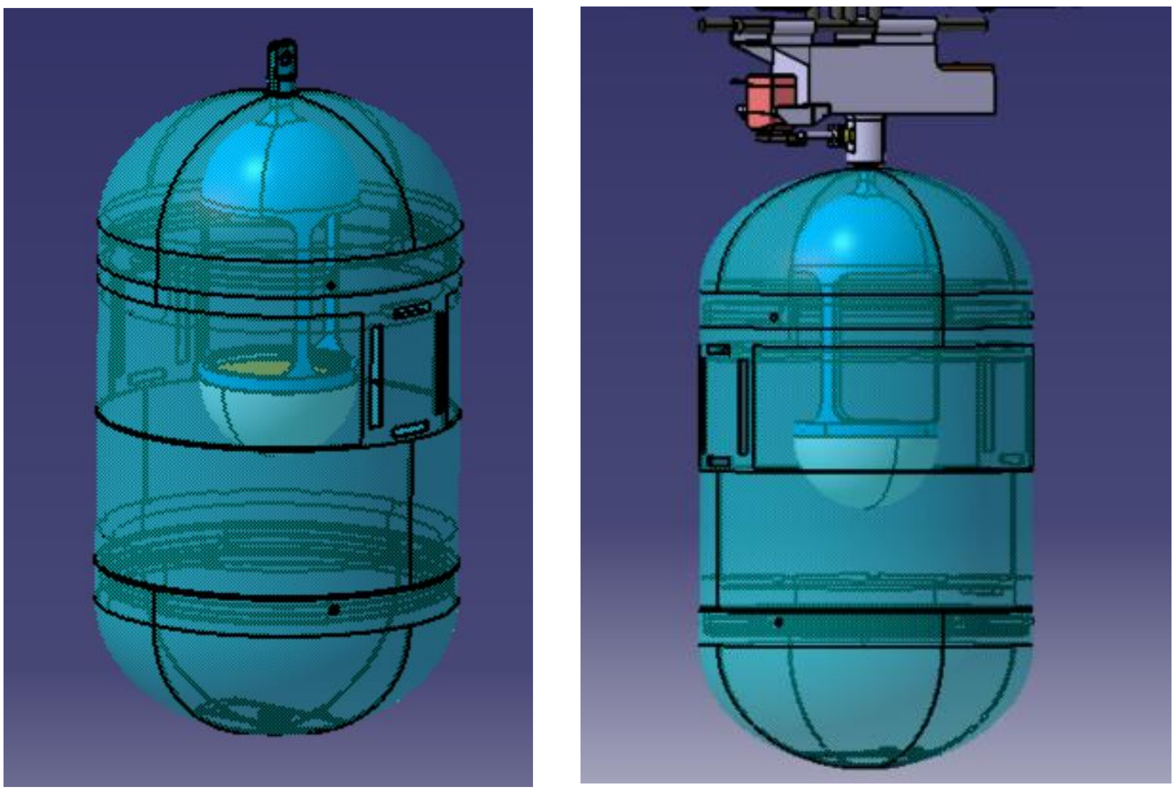

Figure 4.18: The final design for inner and outer capsules assembled

Once all the design iterations were completed and all components were corrected, the assembly of the entire design system looked as shown in the figure above. The mounting is to be attached to the UAV, holding the entire payload comprising the outer capsule and the inner capsule. Both the payload capsules have no contact between them and are independently engaged onto the pin for the release.

4.7 BILL OF MATERIAL (BOM)

Table 4.7: Bill of Materials

S NO.	PART NAME	DESCRIPTION	Quantity	PRICE ($)
1	Frame	FPVKing 500-X4 500mm Carbon Fiber Center Plate Quadcopter Frame Kit Upgrade S500 SK500 F450 with Fixed Landing Gear	1	75
2	Motors	SunnySky X2820 Brushless Motors (x4)	4	140
3	Propellers	Plastic Propeller 13x4.5 Black (CW/CCW) (2pcs)	4	24
4	ESCs	60A RC Brushless Motor Electric Speed Controller ESC 4A UBEC with XT60 & 3.5mm bullet plugs (x4)	4	116
5	LiPo Battery	HOOVO 4S Lipo Battery 9600 mAh	1	170
6	Transmitter and Receiver	FLYSKY FS-i6X 10CH 2.4GHz RC Transmitter Controller/W iA10B Receiver Upgrade Cable for RC Helicopter Plane Quadcopter Glider	1	70
7	Pixhawk+GPS+ Power Capsule+Teleme try	Hobbypower Pixhawk PX4 Flight Controller W/Shock Absorber +M8N Set OSD Capsule PPM Capsule I2C Splitter Expand Capsule Power Capsule for FPV Quadcopter Multirotor	1	260
8	Servo Motor	ANNIMOS 20KG Digital Servo High Torque Full Metal Gear Waterproof for RC Model DIY, DS3218MG,Control Angle 270°	1	16
9	Extra GPS	Radiolink M10N GPS SE100 Capsule High Positional Accuracy Works with GLONASS/BeiDou for APM Pixhawk Flight Controller DIY FPV UAV, Quad and More	1	40
10	LiPo Checker	1-8s Lipo Battery Tester Monitor Low Voltage Buzzer Alarm Voltage Checker with LED Indicator for Lipo Life LiMn Li-ion Battery (5 PCS)	1	13
11	LiPo Battery Charger	Venom Pro 2 LiPo Charger	1	77
12	LiPo safe bag	COLCASE Upgraded Fireproof Explosionproof Lipo Safe Bag for Lipo Battery Storage and Charging , NLarge Space Highly Sturdy Double Zipper LipoBattery Guard (8.46x5.70x6.5 in)	1	14

Table 4.7 (continued).

13	Go Pro Hero 11 Mini Cameras	GoPro HERO11 Black Mini | Compact | Waterproof Action Camera | with 5.3K60 Ultra HD Video | 24.7MP Frame Grabs | 1/1.9" Image Sensor | Live Streaming | Stabilization	1	260
14	Bluetooth Accelerometer and Gyroscope	Bluetooth 5.0 Accelerometer+Inclinometer | WT901BLECL MPU9250 High-Precision 9-axis Gyroscope+Angle(XY 0.05° Accuracy)+Magnetometer with Kalman Filter | Low-Power 3-axis AHRS IMU Sensor | for Arduino	2	96
15	LED Small Flashlight	COB Keychain Work Light Keychain Flashlights 4 Light Modes 1600Lumen,Keychain Light Emergency Light with Folding Bracket Bottle Opener and Magnet Base, Camping and Walking	2	9
16	Golf nets for catching mechanism	SAPLIZE Golf Net with Target Cloth and Rope, 10FT, 15FT, 20FT, 25FT, 30FT, Heavy Duty Golf Barrier Practice Net, DIY Adjustable Ball Net, Golf High Impact Net	1	90
17	Poles for mounting the nets	HIKEMAN Tarp Poles Adjustable Aluminum Telescoping Tarp Poles, Lightweight Canopy Poles Portable Tent Poles for Outdoor Camping Backpacking Awning	4	124
18	Ground anchor screws to support the poles	Ground Anchors Screw in - 12 Inch Set of 4 - Tent Stakes Heavy Duty - Trampoline Anchor Kit - Earth Anchor - Swing Set Anchors for Metal Swing Set - Trampoline Stakes Anchors High Wind	4	30
19	Mounting	3D printed part	1	82
20	Outer Capsule	Top, Middle, and Bottom Parts (3D printed)	3	378
21	Inner	Top, Bottom, and Center Plate (3D printed)	3	106
22	Connecting Rod	3D printed part	1	17
23	Engagement Pin	3D printed part	1	11
Total cost				**2218**

CHAPTER 5

TESTING & RESULTS

5.1 SENSORS INTEGRATION

The external capsule, comprising a comprehensive assembly of three constituent components, underwent meticulous orientation and interlocking procedures to ensure precise alignment during assembly. Within the lower hemisphere, a high-definition action camera was securely mounted, accompanied by safety padding to mitigate the potential impact on the camera, strategically positioned to align seamlessly with the aperture at the base of the hemispherical structure. Adjacent to the camera fixture, an accelerometer was affixed using a Velcro strap, further reinforced with supplementary safety padding to ensure stability and accuracy of readings.

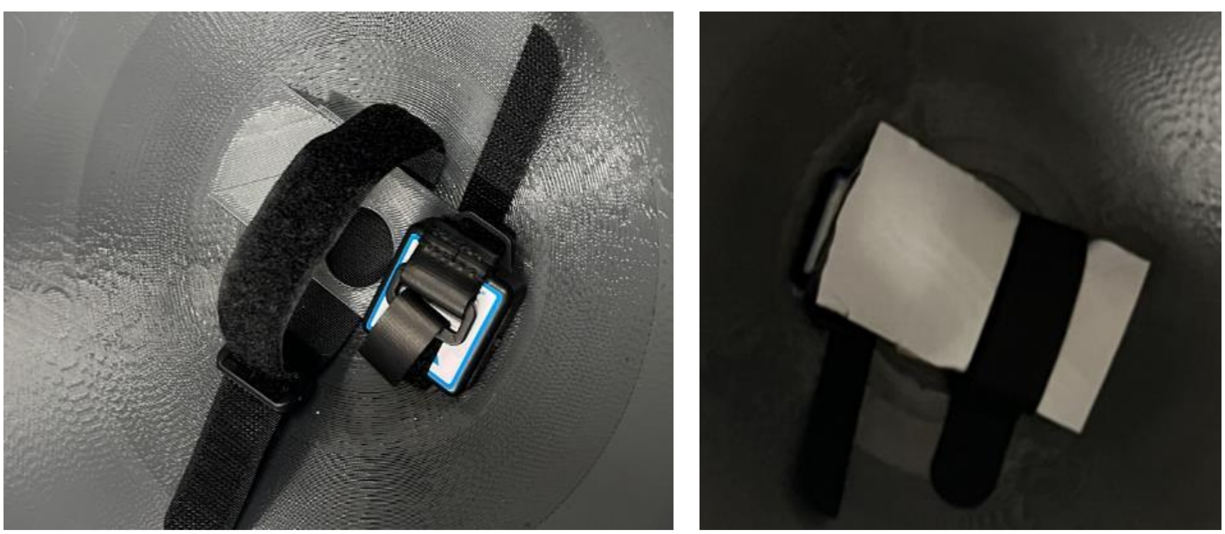

Figure 5.1: Strapped accelerometer (left) and camera strapped with safety padding (right)

Another high-definition action camera was strapped using the designated slots to capture the feed for the inner capsule suspended inside the outer capsule. To preserve equilibrium, a counterweight mechanism was affixed to the exact opposing position utilizing velcro straps.

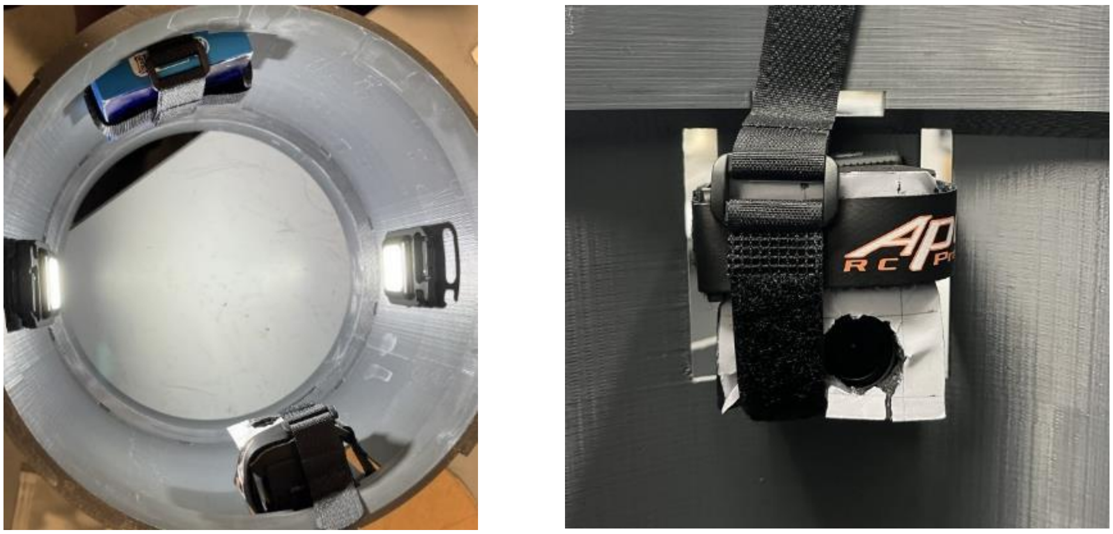

Figure 5.2: Action camera mounted with flashlights (left) and camera strapped (right)

Furthermore, two LED lights were affixed perpendicularly to the camera apparatus using double-sided adhesive tape, calibrated to ensure unobstructed illumination while verifying the compatibility of the camera feed with the activated LED lighting system. On the inner capsule's plate, another accelerometer was mounted using double-sided tape and a velcro strap to collect data separately for the inner capsule.

Figure 5.3: Accelerometer strapped to the detachable plate (left) and the plate affixed to the bottom part of the inner capsule (right)

The inner capsule was enveloped with a transparent sheet to shield its surface, achieving a dual purpose of reducing the aerodynamic drag and preventing potential dislodgment of the enclosed experiment. The deliberate selection of a transparent material aimed to facilitate unobstructed camera feed acquisition, is crucial for monitoring experimental behavior amidst microgravity conditions.

Figure 5.4: Top component covered with transparent plastic sheet

The assembly was set to be attached to the UAV via the engagement pin with the integration of accelerometers, cameras, and LED lights onto the respective capsules, and the inner capsule with the outer capsule ensued and secured by interlocking. The entire assembly was then mounted under the UAV using the engagement pin interlocking both the inner and the outer capsules suspended underneath the UAV.

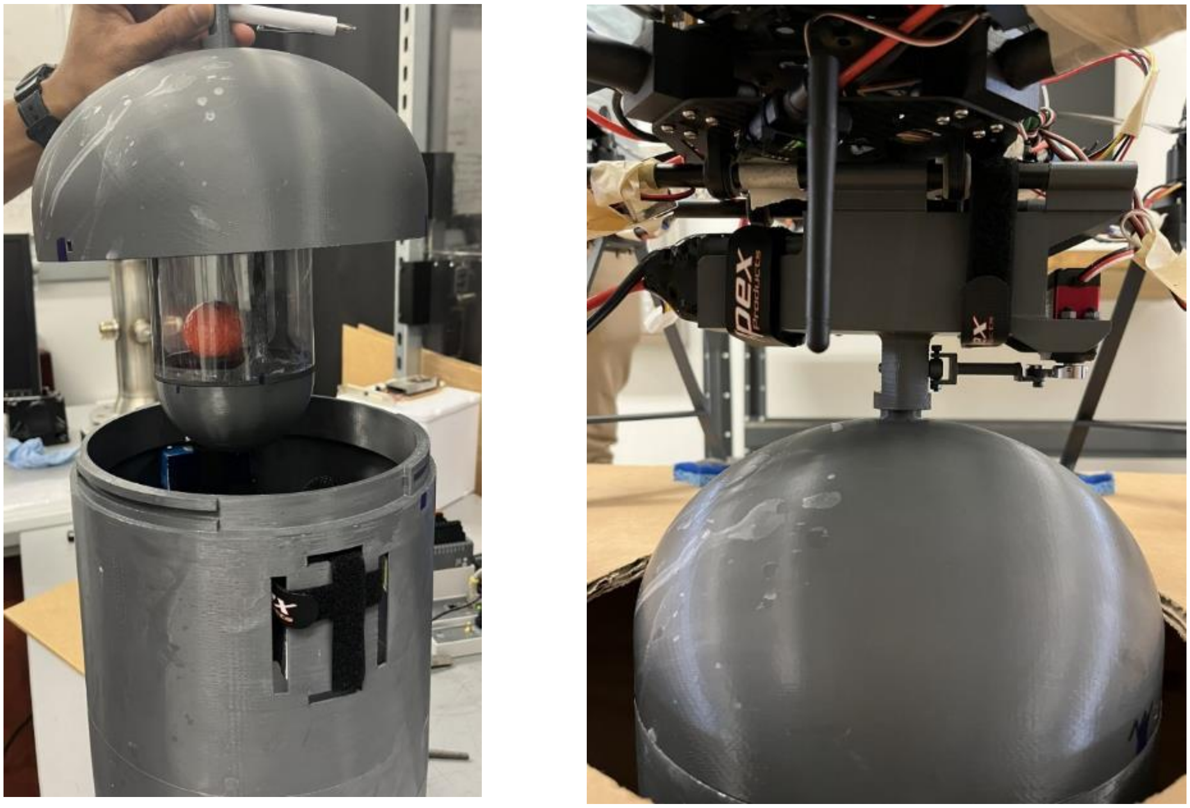

Figure 5.5: Attaching all the components underneath the UAV

5.2 MICROGRAVITY EXPERIMENT

A capillary tube with a fluid is chosen for experimenting with its behavior under the microgravity conditions. The motion of the fluid inside the tube as captured by the camera signified the microgravity experience. The fluid in a capillary tube can be used to determine gravity levels through the principle of capillarity. Capillarity refers to the ability of a liquid to flow in narrow spaces without the assistance of, or against, external forces like gravity. The height to which a fluid rises or falls in a capillary tube is influenced by the balance between adhesive and cohesive forces. Moving to different gravity levels, the effective weight of the liquid changes, impacting the balance between the adhesive and cohesive forces. The height to which it rises is influenced by the surface tension of the liquid, the tube's radius, and the contact angle between the liquid and the tube. In high gravity conditions, the weight of the liquid will be greater tending to depress the fluid in the capillary. While, the objective of this research is to observe microgravity conditions, the weight of the liquid is expected to reduce, favoring capillary rise. Testing capillary rise in a tube is an initial idea of an experiment that can be conducted on this platform as capillarity can be studied in gravity levels of order 10^{-1} to 10^{-2}.

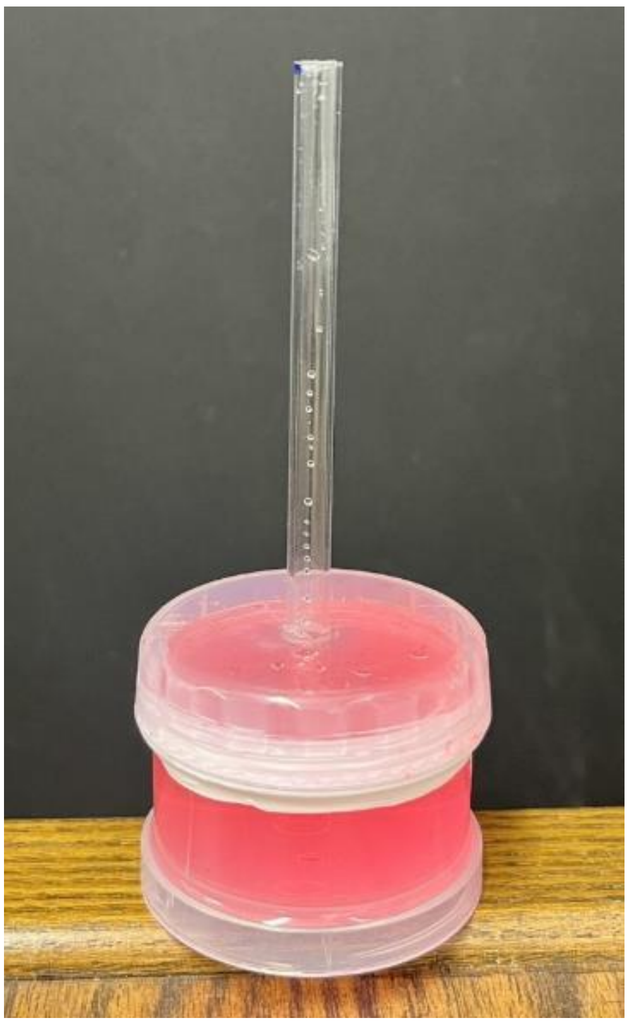

Figure 5.6: The capillary tube experiment

5.3 DECELERATION MECHANISM SET UP

The experimental setup involved a systematic procedure for preparing the catching net to facilitate drop tests. A catching net, measuring 30 feet by 10 feet, was procured to facilitate the ensuing drop tests. In adherence to UAV flying regulations and safety norms, a suitable testing environment was selected, characterized by open spaces devoid of any potential obstacles. The experimental site was prepared by laying out the net over the ground.

Figure 5.7: Deceleration mechanism equipment

To ensure stability during testing, four anchor points were strategically established, employing lightweight telescopic tarp poles. These tarp poles, adjustable due to their telescopic nature, were set to a uniform height of 1.5 meters and positioned in alignment with the dimensions of the net. The anchoring process involved inserting one end of each tarp pole securely into the ground.

Figure 5.8: Deceleration net set up using tarp poles and ground anchors

Careful attention was devoted to achieving optimal tension in the net, thereby attaining a flat and uniform surface conducive to effective drop testing. Attachment points on the net were utilized to affix its corners firmly to the tarp poles, thereby fortifying the structural integrity of the setup. After the net was attached to the 4 anchor poles, these poles were connected to the ground separately by extending the attachment using 2 ground anchor screws to hold the poles and firm upon the impact of a drop onto the net.

Figure 5.9: Ground anchors (left) and deceleration net (right)

An inspection was conducted to detect any potential loose attachments or stability issues, ensuring that the net was poised to capture the dropping capsule without incurring any damage. This systematic approach adheres to rigorous research protocols, emphasizing precision and safety in the experimental configuration for reliable and meaningful results.

5.4 GROUND CONTROL STATION:

A ground control station (GCS) for a UAV is a vital component of the UAV system, serving as the command center where operators manage and monitor the unmanned aerial vehicle (UAV) or UAV during flight operations. The GCS is typically a system comprising hardware and software components designed to facilitate safe and efficient UAV operations. The GCS has the control interface to operate and control the UAV's flight, flight planning, and auto piloting. It receives real-time telemetry data with GPS location, speed, altitude, battery status, sensor readings, etc.

Figure 5.10: Ground Control Station

Two accelerometers were used to collect data and monitor the drop for the outer and the inner capsule. For these two accelerometers on the capsules, two laptops were used simultaneously to record and monitor the data for the entire testing using the Witmotion software. These laptops were a part of the ground control station that was set at an approximate 20-meter distance from the net. The telemetry capsules were plugged into the respective laptops to collect the accelerometer data. During a microgravity drop, accelerometers capture the object's acceleration due to gravity (9.81 m/s^2). This sensor detects acceleration by the principle of inertia. It contains mass suspended by spring, hence when it experiences acceleration the mass resists this change in motion due to inertia causing deflection of the springs. Acceleration is measured along the X, Y, and Z axes and the data is typically recorded in terms of meters per second squared or gravitational unit (g), where 1 g is equal to the acceleration due to gravity.

The magnitude of acceleration for a tri-axial plane is found by the formula,

$$Resultant\ Acceleration = \sqrt{x^2 + y^2 + z^2}$$

One of these laptops was used to also run the Mission Planner software and obtain real-time flight details and feed including flight path, altitude, battery status, GPS coordinates, speed, etc [29]. Two action cameras were mounted on the payload. One was mounted at the bottom of the outer capsule to monitor live location while aligning correctly in the center of the catch net and the other one was mounted on the wall of the cylinder to record the inside happenings. While the laptops collected sensor data, personal smartphones were chosen to connect to the action cameras to monitor and collect video data. These action cameras had WiFi Technology therefore using the X-Cam app on smartphones it was easy to monitor and record the feed in real-time also enabling hassle-free download of media.

Figure 5.11: Flight Data Screen (Mission Planner Software)

The UAV is intended to run on the ArduPilot autopilot system, Mission Planner is a popular open-source ground control software (GCS). It's widely used in the UAV community and offers a comprehensive set of features for planning, monitoring, and controlling autonomous missions. Users can set parameters such as altitude, speed, and camera actions. The software provides real-time telemetry data from the UAV, including GPS position, altitude, battery voltage, speed, and attitude (pitch, roll, yaw) [30]. This information is crucial for monitoring the UAV's status during flight. It also supports various flight modes such as stabilized, altitude hold, loiter, and return-to-home. Mission Planner includes a simulation mode that allows users to test mission plans and flight parameters in a virtual environment before deploying them in the field. Once the UAV was calibrated physically while using the mission planner app it was ready to fly.

5.5 FLYING THE UAV BEFORE TESTING

The battery was checked for voltage and power levels using a battery voltage checker. The battery's connecter is connected to the specific ports on the battery checker ensuring correct polarity. Once the connection is established the battery connector displays the voltage indicating the battery's remaining charge level. Once the battery level was the desired level, the UAV was safe to be powered and fly. All the connections on the UAV were secured and checked for lost connections. For using different flight modes it was necessary to make sure the GPS was working fine. The UAV was then placed on the takeoff platform with the drop capsule assembly attached at the bottom, ready for lift-off. The launch pad was placed 15 meters away from the catch net to maintain safety and give enough space/range to the UAV to execute the flight. With enough throttle, the UAV took off from the platform and first was flown to an altitude of 6 meters approximately and then aligned exactly above the orange target patch on the net before the drop. Once it was assured that it was correctly positioned above the orange patch, it was dropped by disengaging the pin using the transmitter. The drop mechanism was successfully able to catch the entire assembly while the UAV was well capable of executing the entire mission with the given payload weight.

5.6 RESULTS

Two accelerometer sensors were employed to gather data, one from the Outer Capsule and another from the Inner Capsule. Initially, a drop test was conducted using the outer capsule containing an accelerometer sensor and a small attachment plate with the second accelerometer sensor mounted on it. Before the drop, the accelerometer measured a gravitational acceleration of

$9.81\ m/s^2$ downwards towards Earth's surface. This baseline measurement accounted for any additional acceleration due to motion or vibration. During the fall, the only acceleration experienced was due to gravity, recorded as a change in acceleration along the z-axis. The data was transmitted via Bluetooth to a computer, enabling real-time monitoring and logging. WitMotion Software was used for data interpretation, providing visual results and analyzing patterns over time. The data's three axes represent the sensor's acceleration direction, with the X and Y components indicating capsule oscillation and the Z component indicating the drop towards Earth's surface.

The initial test was performed from an altitude of 5 meters above the ground. Subsequent drop tests were then conducted at increased altitudes of 10 meters and 14 meters. Throughout these tests, the entire UAV system was manually controlled and piloted to ensure accurate positioning above the center of a catch net. Live flight data was obtained using mission planner software from the ground control station. During the flight, the altitude was not predefined but was the objective. The UAV approached the target altitude of 15 meters but dropped from a height of 14.7 meters. Precision in positioning the UAV required maneuvering to align it with the net's center. These maneuvers caused the capsules to oscillate slightly around the hinged pin, resulting in a minor loss of stability.

Once the UAV was properly positioned, a brief pause allowed the oscillation to settle before releasing the capsules simultaneously. Both accelerometers recorded gravitational acceleration ('g') values for each component (X, Y, Z) over time. The data was then plotted to analyze the test conducted from the 14.7-meter altitude, summarizing the findings from the entire testing process. The total flight duration was 1 minute and 35 seconds, encompassing the UAV's takeoff to its landing. Given that the mission was manually piloted, continuous monitoring of the flight path was necessary to ensure mission success. During the flight while the payload remained attached to the UAV, the accelerometer readings consistently measured approximately '1g' until the drop was initiated, as depicted in Figure 5.12.

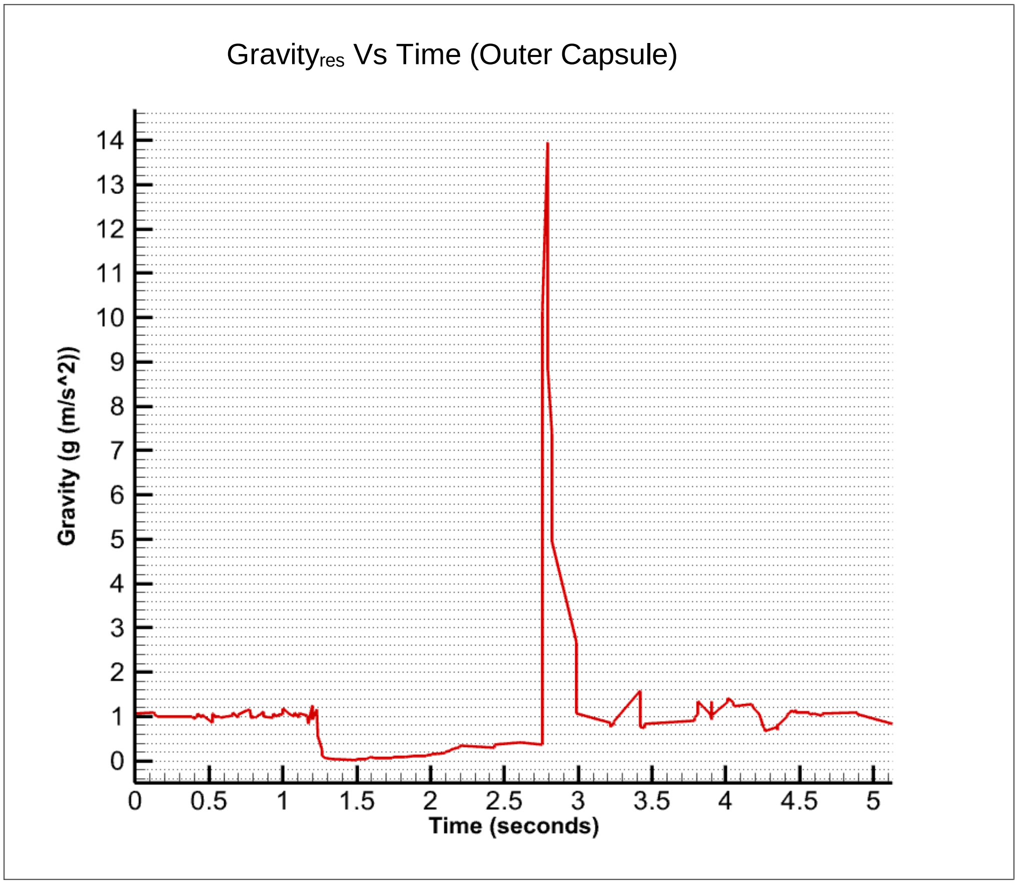

Figure 5.12: Gravity$_{res}$ Vs Time for the Outer Capsule

Referring to Figure 5.12, the payload was released at 1.2 seconds, and the drop continued until 2.89 seconds when the outer capsule made contact with the deceleration net. At this moment, there was a sudden spike in the 'g' value, peaking at '13.8g', indicating the impact of the capsule with the net, marking the end of the drop sequence. During free fall, the payload experiences consistent acceleration, leading to an increase in velocity as it nears the ground. With this increase in velocity, the drag experienced by the body will increase as well [ref] from the equation:

$$F_{drag} = \frac{1}{2}\rho v^2 C_d A$$

Theoretically,

using the 2nd kinematics equation of motion,

$$s = u * t + \frac{1}{2}a * t^2$$

s is the altitude covered or the displacement, u is the initial velocity, t is the time period and a is the acceleration of the body.

Here a = g (9.81m/s^2,) gravitational acceleration in free fall conditions

$$s = u * t + \frac{1}{2}g * t^2$$

As the initial velocity u is zero, the equation becomes,

$$s = \frac{1}{2}g * t^2$$

Dropping from an altitude of 14.7 meters (s), the time of drop can be theoretically calculated as:

$$14.7\ m = 0 + \frac{1}{2}(9.81\ \mathrm{m}/s^2) * t^2$$

Which gives, time t = 1.73 seconds.

The experimental testing revealed a drop time of approximately 1.69 seconds, which closely matches the expected empirical value.

During the drop phase, the velocity of the payload increased steadily over time, as observed in Figure 5.12 of the outer capsule's plot. Beginning around 2 seconds into the drop, there was a noticeable rise in the 'g' values, indicating the effect of drag force experienced by the outer capsule during descent.

Following the impact with the deceleration net, the 'g' values for the capsule exhibited fluctuations, reflecting the bounce on the net as it came to a complete stop and settled at a reading of '1g' at the end. The net effectively dissipated the kinetic energy of the payload, ensuring a safe landing.

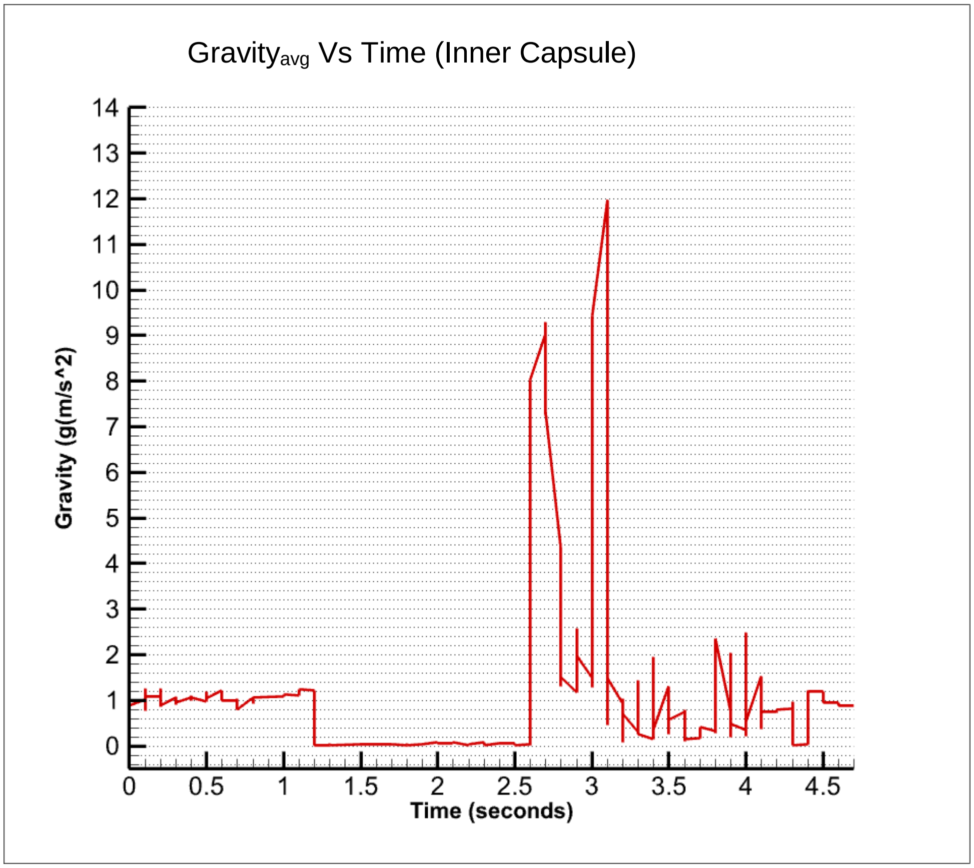

Figure 5.13: Gravity$_{res}$ Vs Time for the Inner Capsule

The data from the accelerometer inside the inner capsule exhibited a similar pattern of results to that of the outer capsule, with initial values around '1g'. As shown in Figure 5.13, the inner capsule was released at 1.2 seconds and continued to drop until 2.7 seconds when it impacted the base of the outer capsule. Notably, the inner capsule made contact earlier than the outer capsule, indicating that the inner capsule was traveling slightly faster. This difference in velocity can be attributed to the absence of air resistance affecting the inner capsule.

The plot in Figure 5.13 shows a spike at 2.7 seconds, representing the impact of the inner capsule's base with the outer capsule's base, followed by another spike at 2.9 seconds when both capsules hit the deceleration net. The irregular curve observed after impact reflects the movements and collisions of the inner capsule within the outer capsule until it came to rest, reaching a final '1g' reading. The objective of placing the inner capsule inside the outer capsule was to significantly reduce drag experienced by the inner capsule during the experiment. The outer capsule experienced drag, as indicated by the gradual increase in 'g' values with increasing velocity shown in Figure 5.12. Conversely, the 'g' values for the inner capsule remained consistently close to zero until impact, demonstrating negligible drag experienced by the inner capsule.

The placement of the inner capsule within the outer capsule proved successful in eliminating drag. It's important to note that the 'g' values shown in Figures 5.12 and 5.13 represent acceleration in all three components (X, Y, Z). To accurately determine true gravitational acceleration in free fall conditions, only the component perpendicular to the Earth's surface should be considered.

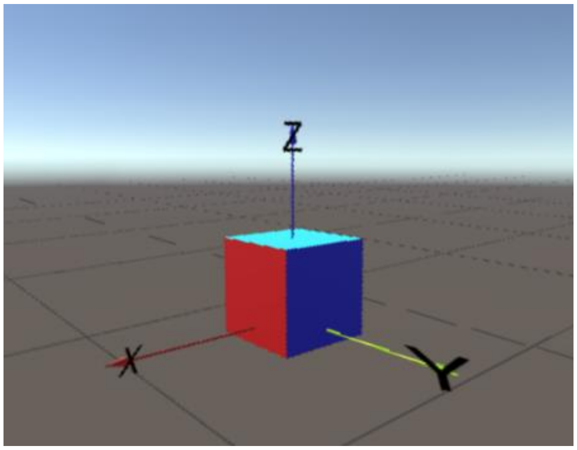

Figure 5.14: Tri-axial components (accelerometer)

Figure 5.14 illustrates the accelerometer components' directions. During free fall towards the Earth, the X and Y components correspond to horizontal motion, while the Z component conveys information about motion perpendicular to the Earth's surface. Therefore, the true 'g' values during free fall or the drop are captured by the Z-component of acceleration.

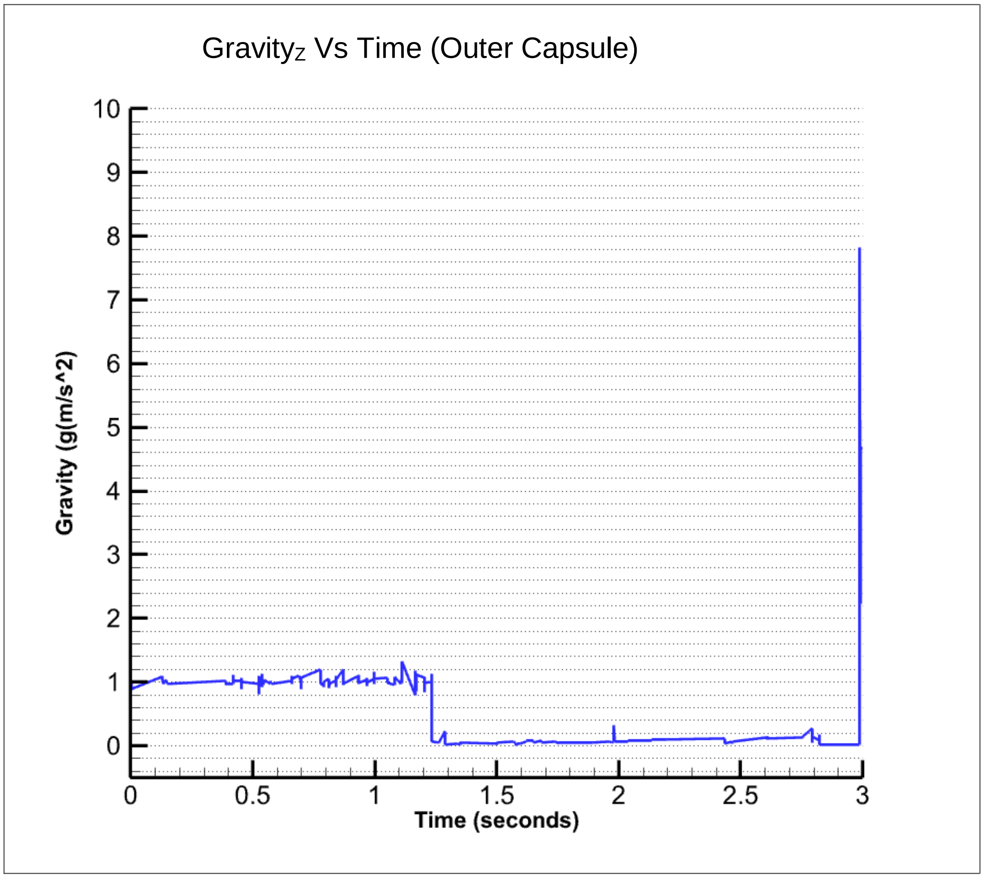

Figure 5.15: Gravity$_Z$ Vs Time for the Outer Capsule

The curve displayed represents the magnitude of the z-component over time, particularly focusing on the drop phase. Initially, the values started at '1g' until the release occurred at 1.2 seconds, continuing until impact.

During the drop phase, which lasted approximately 1.69 seconds, the average value of gravitational acceleration (g) for the outer capsule was approximately 0.0843. To better visualize the achieved microgravity levels and accurately depict the nature of the obtained values, the curve was plotted using a logarithmic scale, as shown in Figure 5.16.

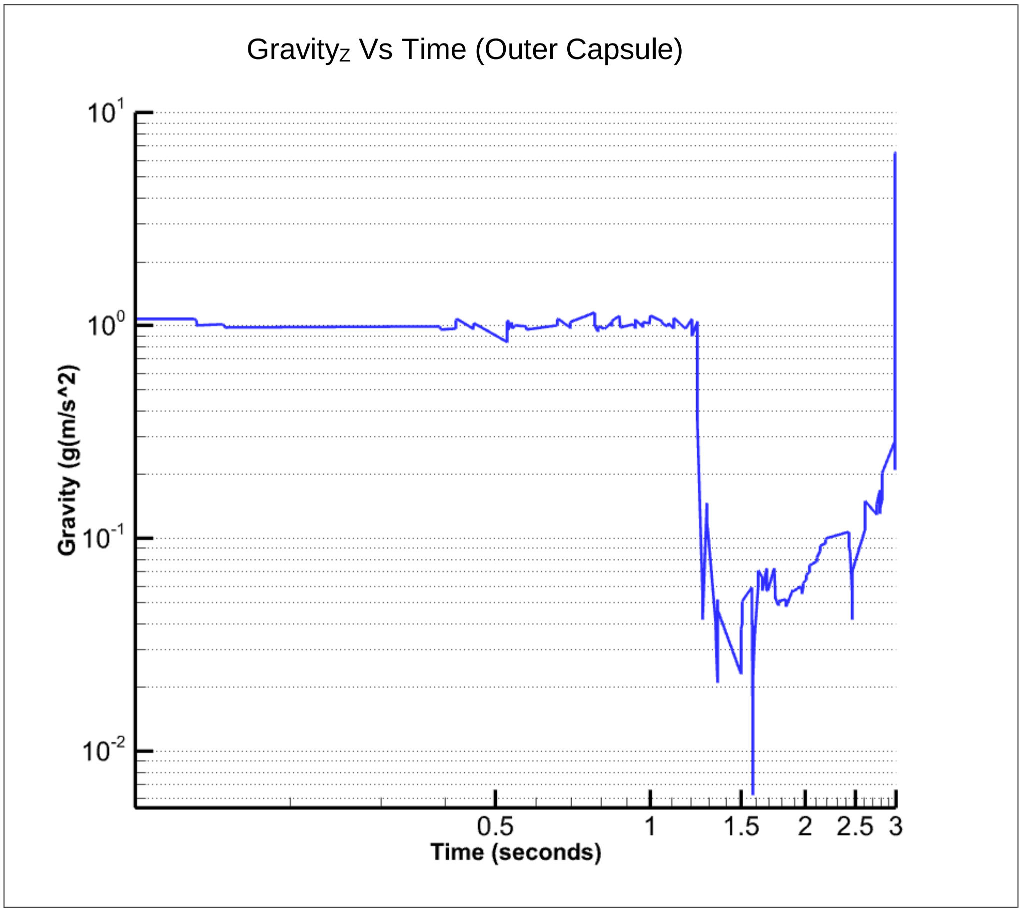

Figure 5.16: Gravity$_Z$ Vs Time for the Outer Capsule (logarithmic scale)

When plotted on a logarithmic scale, the gravity values ranged significantly between 10^{-1} and 10^{-2}. The lowest point on the curve corresponds to the minimum 'g' value achieved for the outer capsule, which is approximately around $6e^{-3}$. As the curve progresses towards impact, the values gradually increase due to the influence of drag force.

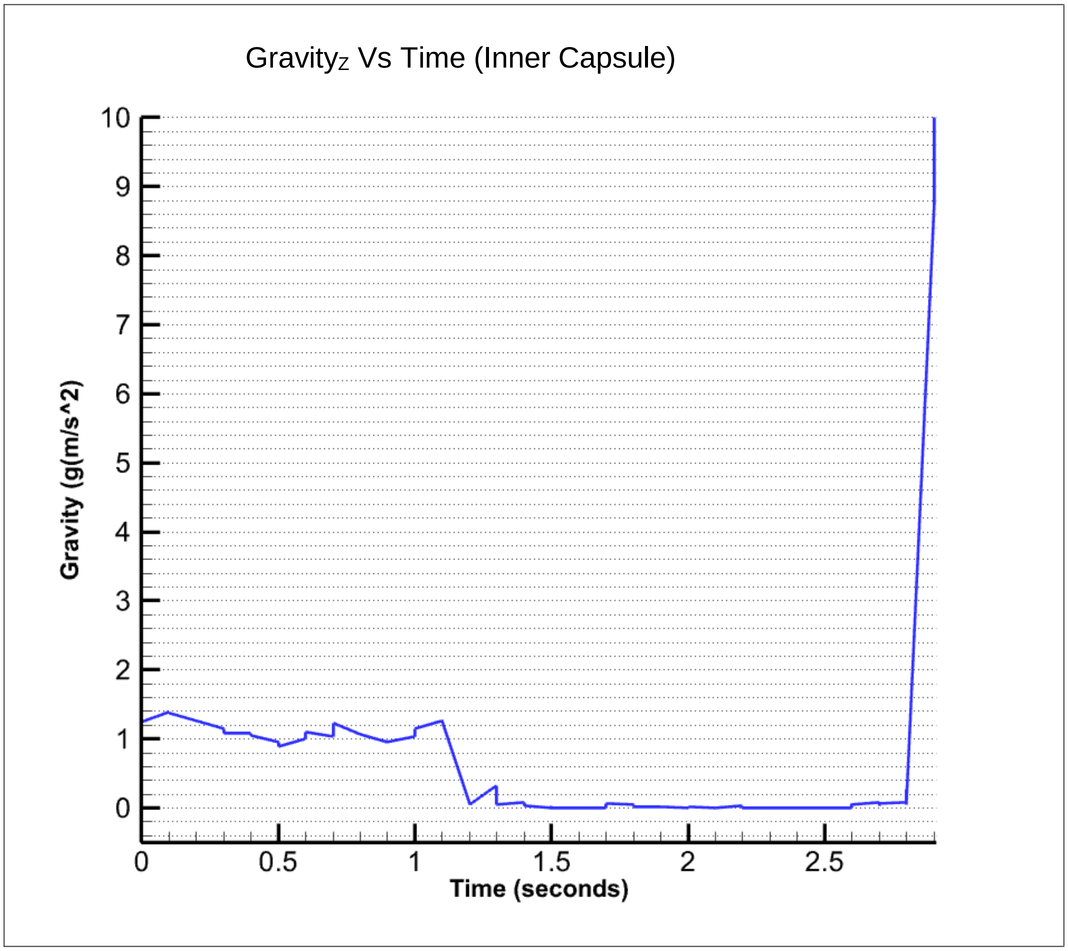

Figure 5.17: Gravity$_Z$ Vs Time for the Inner Capsule

The data curve for the magnitude of the z-component over time for the inner capsule mirrors the previous curve, showing consistent 'g' values during the drop phase. The absence of a gradual increase in these values indicates minimal drag force acting on the inner capsule.

The average 'g' value during the drop phase for the inner capsule was 0.0284 over a duration of 1.69 seconds. On a logarithmic scale, these average values for the inner capsule were around the order of 10^{-2}. The lowest recorded 'g' value for the inner capsule was approximately $2e^{-3}$.

Notably, the gravity values decrease steadily before impact for the inner capsule, maintaining a consistent trend throughout the drop phase.

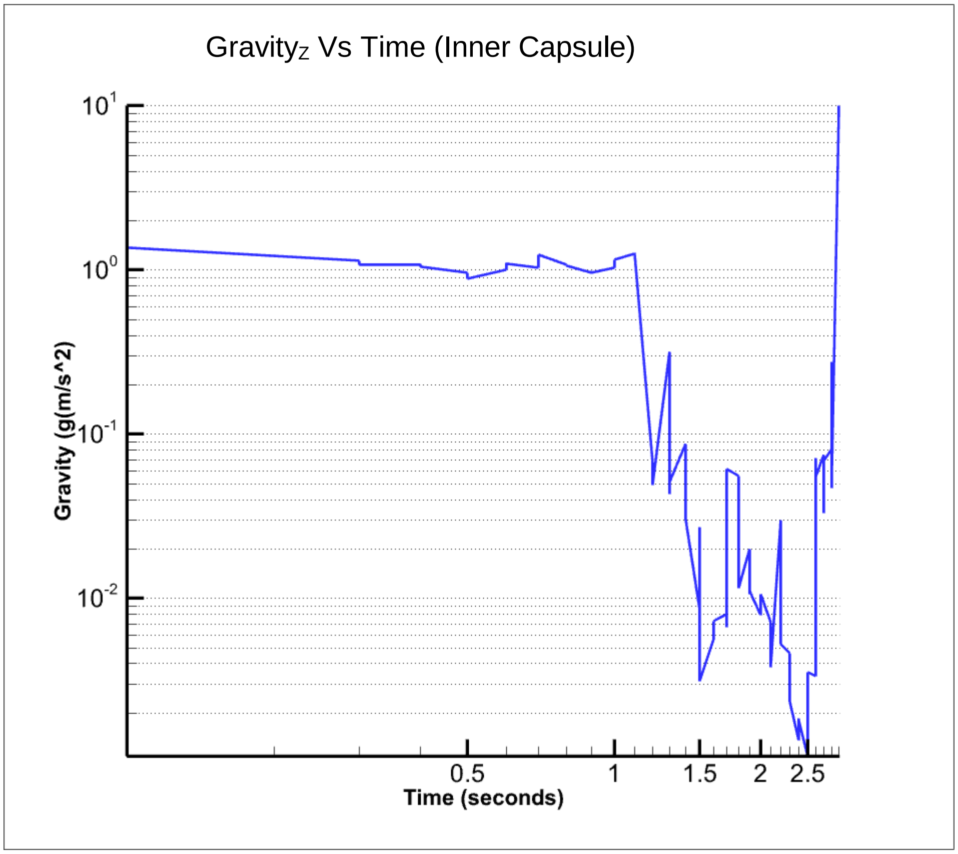

Figure 5.18: Gravity$_Z$ Vs Time for the Inner Capsule (logarithmic scale)

The 'g' values decreased for the outer capsule until it began experiencing drag, after which they increased over time. The lowest 'g' values for the inner capsule occurred before impact, while for the outer capsule, they were before it started experiencing drag. This difference in gravity values aligns with the desired outcome, with the inner capsule exhibiting lower values than the outer capsule.

The irregularities and abrupt peaks in the plots are attributed to the limited number of data points obtained from the accelerometer sensor. Achieving smoother curves would require a higher number of consistent data points.

Another insightful analysis of the results involved assessing the stability levels of the payload. To evaluate the stability of both the outer and inner capsules, the resultant of the X and Y components was calculated during the drop phase.

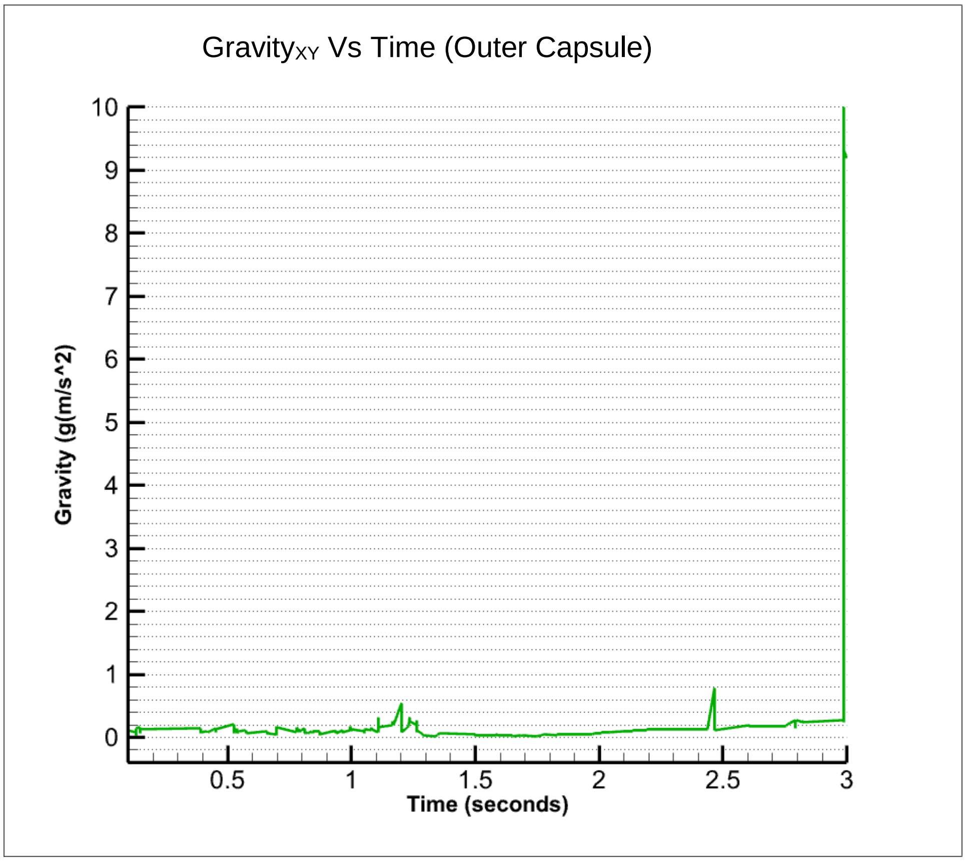

Figure 5.19: Gravity$_{XY}$ Vs Time for the Outer Capsule

In contrast to other obtained plots, these curves initially started around '0g'. The closer the values are to zero, the more stable the payload is perceived to be. For the outer capsule, as shown in Figure 5.20, the values in the plot consistently remained close to zero. A slight disturbance was observed at the time of release at 1.2 seconds, after which the values exhibited a linear behavior until impact. This indicates that our design for the outer capsule maintains stability during both flight and the drop phase.

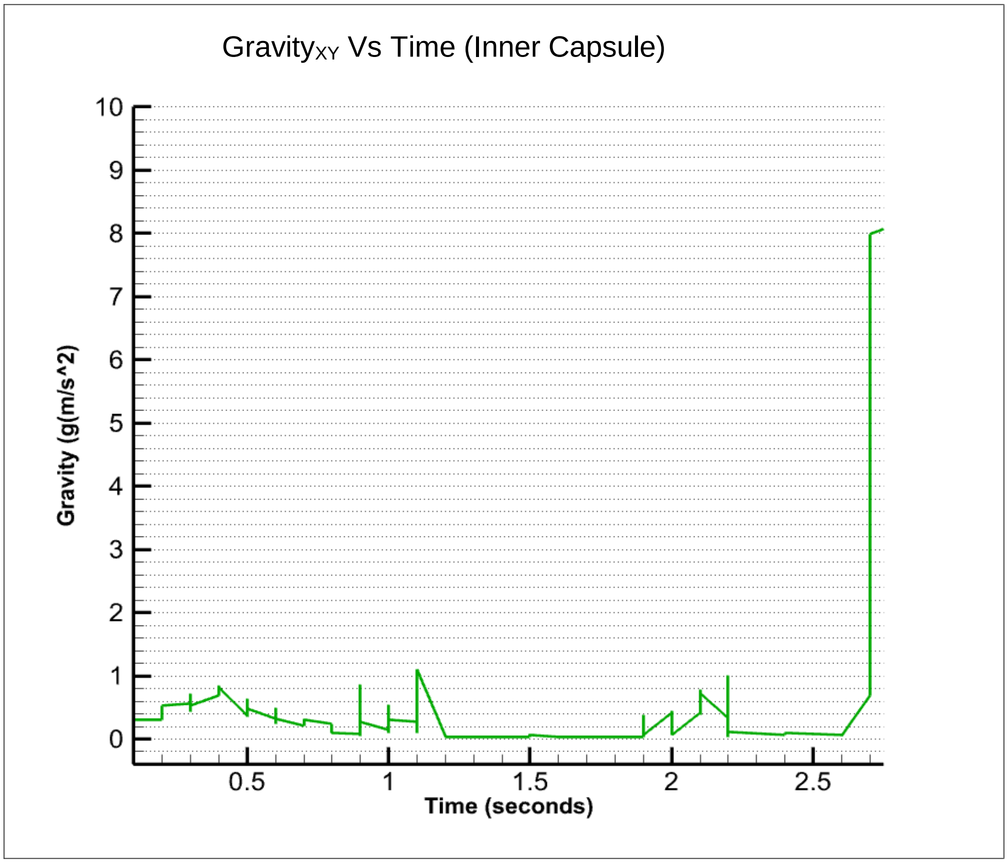

Figure 5.20: Gravity$_{XY}$ Vs Time for the Inner Capsule

The curve depicted in Figure 5.21 illustrates the stability levels of the inner capsule. Unlike the curve for the outer capsule, there are more irregularities and inconsistencies observed before the drop phase. These fluctuations indicate oscillatory movements of the inner capsule while it is engaged to the pin before release. Following the release at 1.2 seconds, the inner capsule drops steadily until around 2 seconds when it makes a slight impact with the side wall of the outer capsule from the inside. Subsequently, the inner capsule exhibits stable values until the final impact at 2.7

seconds. These findings highlight the necessity of improving the stability of the inner capsule by reducing design tolerances or implementing a design that minimizes unnecessary movements. Enhancing the stability of the inner capsule is crucial for achieving lower 'g' values, which would positively impact the overall performance of this platform.

Multiple similar drop tests were conducted to assess the performance of this microgravity test platform. From the collected data, three specific sets of results were selected to conclude the reliability and functionality of the test platform.

Table 5.1: Results for both outer and inner capsule

Test	**Altitude (meters)**	**Time (seconds)**	**Outer Capsule**			**Inner Capsule**		
			$g_{resultant}$	**z**	$\sqrt{x^2+y^2}$	$g_{resultant}$	**z**	$\sqrt{x^2+y^2}$
1	6	1.1	0.1692	0.1321	0.1063	0.2333	0.0779	0.2204
2	10	1.42	0.1984	0.1002	0.1744	0.1276	0.0575	0.1142
3	14	1.69	0.0947	0.0843	0.0433	0.0924	0.0284	0.0880

Based on the analysis of three sets of test results, it is evident that as drop altitude increases, the quality of experienced microgravity improves. The resultant 'g' values and the 'g' values from the z-component are higher for the outer capsule compared to the inner capsule, indicating minimal drag experienced by the inner capsule.

Regarding the resultant of the X and Y components, the values for the outer capsule are lower than those for the inner capsule, suggesting that the outer capsule exhibits greater stability than the inner capsule. Ideally, these values should be close to zero, indicating minimal oscillations in the horizontal plane parallel to the Earth's surface. Furthermore, the drop times for each test closely aligned with the empirical values calculated using the second kinematic equation of motion.

5.7 COMPARISON WITH THE EXISTING PLATFORMS

Existing microgravity platforms vary in terms of cost, duration, waiting period, and level of research capability. Traditional drop towers offer a relatively low-cost option for conducting microgravity experiments with short durations typically lasting seconds to minutes. These towers provide accessible opportunities for basic research and proof-of-concept experiments with minimal waiting periods between runs. In contrast, parabolic flights involve moderate to high costs due to aircraft rental and operational expenses but offer longer reduced gravity periods (10-20 seconds per parabola) and more complex research capabilities. However, scheduling and coordination often result in waiting periods of weeks to months for flight opportunities. Space-based platforms such as the International Space Station (ISS) offer the longest experimental durations lasting days to months but at an exceptionally high cost associated with space launches, mission operations, and equipment. Despite the significant financial and logistical challenges, space-based platforms enable advanced research across various scientific disciplines, leveraging prolonged exposure to microgravity conditions. The cost of the development of the UAV platform when compared to other existing platforms (as mentioned in the following table below) to conduct microgravity research is the most economical. The cost of designing and developing this unmanned test platform is approximately 2K USD.

Table 5.2: Comparison of all microgravity test platforms

Platform	μg (G)	Duration	Waiting Time	Cost	Cost of Experimentation
Space Station (ISS)	$10^{-2....-5}$	Years	> 5 years	> 10 M $	~ 1 – 5 M $
Parabolic Flights	$10^{-2....-3}$	~ 20 s	~ months - 1 year	> 1.5 M $	> 125 k $
Sounding Rockets	$10^{-4....-5}$	5-13 mins	> 2 years	> 2 M $	> 400 k $
Drop Towers	$10^{-3....-6}$	< 5 s	Months	> 10 k $	> 5 k $
Glider Flights	$10^{-1....-2}$	~ 6 s	~ days	~ 5K-50K $	~ 100 $
UMTP	$\mathbf{10^{-1....-2}}$	**1-2 s**	**-**	**2.1K $**	**0**

The existing platforms with their high cost of experimentation and limited accessibilities for smaller research groups inspired the concept of creating and developing a test platform that is highly economical, advanced, customizable, and accessible. The order of microgravity achieved with the initial testing is similar to that of a glider flight used to simulate microgravity conditions. This research was an initial step to create a first-of-its-kind microgravity test platform that holds a huge scope of advancement and improvement in the future. This research endeavor has established the possibility of making microgravity research accessible, remote, and economical which is an amalgamation of innovative ideas and technologies. Once developed and integrated, this platform has no waiting time to conduct research, has high repeatability, and can be easily operated. Improving this platform further can result in better quality of microgravity and increased time.

CHAPTER 6

CONCLUSION & FUTURE SCOPE

6.1 CONCLUSION

The primary goal to contribute to the advancement of microgravity experimentation to create a very accessible, sophisticated, versatile, and customizable platform has resulted in the successful research and development of an unmanned microgravity test platform addressing free fall conditions. This research opens up opportunities for research across various disciplines, from fundamental physics to materials science and biotechnology. By providing a controlled environment where experiments can be conducted in microgravity, our platform offers researchers a powerful tool to explore phenomena that are inaccessible or difficult to study under Earth's gravity. Through a comprehensive review of relevant literature, thorough analysis of existing microgravity platforms, and the application of advanced engineering principles, this thesis has outlined the conceptualization, design, and realization of a novel unmanned microgravity test platform. The platform's successful construction and testing demonstrate its viability as a tool for conducting experiments in microgravity conditions, with the potential to advance research across various scientific disciplines. The process involves details research and planning, innovative design ideas, rigorous development, and testing involving several iterations to address the shortcomings, embracing modifications to enhance structural integrity, reduce drag, and ensure the reproducibility of microgravity conditions. In the design phase, meticulous attention was paid to the structural integrity, propulsion system, and control mechanisms of the UMP. This iterative approach reflects the commitment to achieving optimal performance and functionality. The modular architecture of the unmanned microgravity test platform contributes to its adaptability and ease of use. The separation of components within the inner and outer capsules not only facilitates experimentation by providing a platform for various instruments but also allows for the convenient attachment of sensors and devices. Proactive design considerations, such as allowances in the battery casing and the integration of rib structures for reinforcement, demonstrate a forward-looking approach. These considerations ensure the adaptability and robustness of the system, anticipating potential variations and challenges that may arise during prolonged usage. Aerodynamic considerations and the mitigation of drag emerged as critical focal points in the design philosophy.

The incorporation of innovative features, such as the deceleration net and the redesigned inner capsule, exemplifies our commitment to pushing the boundaries of conventional microgravity test platforms. These features not only contribute to the controlled release dynamics and enhanced safety of experiments but also underscore our dedication to introducing novel solutions to longstanding challenges in microgravity experimentation. In conclusion, the design and development of this unmanned microgravity test platform stand as a testament to the multidisciplinary efforts, innovative thinking, and rigorous engineering that define aerospace research. As we look to the future, we anticipate further advancements, collaborations, and applications of this platform in diverse scientific domains, ultimately pushing the boundaries of our understanding of physical phenomena in microgravity environments. The assembly of a UAV with all its components selection and integration into the desired platform to carry payload, and conduct a drop test to simulate microgravity incorporating a drop capsule concept. Later, the design underwent rapid prototyping and development, and tests were created to check the reliability of this UMTP for microgravity testing.

The outcomes of this dissertation underscore the feasibility and efficacy of the Unmanned Microgravity Platform as a tool to address scientific queries associated with microgravity. By providing a controlled and reproducible environment, the UMP opens up new avenues for researchers to explore phenomena that were previously difficult to study, thereby contributing to advancements in various scientific fields. One notable future scope lies in the continuous refinement and optimization of the platform based on ongoing technological advancements. Integration of advanced sensors, improved materials, and enhanced communication systems can elevate the platform's capabilities, allowing for more sophisticated and diverse experiments in microgravity environments. Collaborations with space agencies, research institutions, and commercial entities present an exciting prospect, fostering the exploration of outer space and contributing to the broader field of space science. Furthermore, the platform's adaptability positions it as a valuable tool for educational purposes, providing students and researchers with hands-on experience in microgravity experimentation. As the platform gains recognition and usage expands, it may catalyze the development of standardized protocols for microgravity experimentation, fostering a collaborative and standardized approach in the global scientific community. The future holds immense potential for this unmanned microgravity test platform to be at the forefront of cutting-edge research, education, and advancements in our understanding of the effects of gravity on various physical phenomena.

6.2 FURTHER IMPROVEMENTS

To advance our microgravity experiment, we are utilizing a modular outer capsule design that allows for the attachment of additional middle cylindrical components. This expansion increases the volume within the outer capsule column, delaying the collision with the inner capsule during descent. The custom-built UAV encountered stability issues during manual piloting tests, particularly when aligning precisely above the drop location on the catch net. This caused increased oscillatory movement of the inner capsule. To address this, we plan to modify the engagement design between the inner and outer capsules by optimizing tolerances in their interlocking cavity, enhancing stability during operations. Additionally, the development of a new outer capsule design is in process with camera mounts on the outer surface of the capsule to provide more internal space and improve sensor data capture by avoiding collisions. The wider camera angle achieved by mounting the camera at a distance from the inner capsule will enhance observation capabilities. During certain tests, the payload's orientation was affected by wind or weather conditions. To address this issue, surface modifications such as adding fins can be implemented to aerodynamically stabilize the payload for a vertical drop. If the payload's orientation shifts during descent, the tri-axial plane may change, causing either the x or y component to become the vertical axis instead of the z component perpendicular to the Earth. To manage increased payload weight without exceeding safe battery voltage limits, options such as integrating a larger battery to boost motor-propeller performance can be explored. Alternatively, two 9200 mAh batteries can be used simultaneously. Redesigning the battery mounts will accommodate these changes effectively. Automation will play a key role in optimizing flight control. By programming the UAV for automated takeoff, precise positioning, and drop initiation, we eliminate the need for manual adjustments, thereby improving stability. Finally, upgrading to advanced sensors like high-resolution accelerometers will enhance data collection accuracy, providing valuable insights for refining our experiment.

6.3 FUTURE SCOPE

Increasing the platform's payload capacity will expand its utility, enabling researchers to conduct experiments with larger equipment and diverse setups. This enhancement will broaden the scope of potential studies and accommodate a wider range of scientific inquiries. Incorporating advanced autonomous navigation systems will augment the UMP's ability to operate in dynamic environments. Features such as obstacle detection and avoidance mechanisms will make the platform more adaptable, allowing for greater flexibility in mission profiles and expanding its applicability. The implementation of artificial intelligence for real-time data analysis and decision-making processes holds the potential to optimize the UMP's performance during experiments. This integration could lead to more efficient data collection, quicker response times, and improved overall mission outcomes. While the platform has already demonstrated its potential, ongoing research and development efforts are imperative to refine its capabilities further, making it an indispensable tool for researchers and scientists in unraveling the complexities of microgravity. Establishing collaborations with established space agencies can provide opportunities to integrate the Unmanned Microgravity Platform into existing space research programs. Such partnerships would foster international cooperation, increase visibility, and expand the platform's reach and impact on a global scale. The journey does not conclude here; rather, it serves as a springboard into an exciting and dynamic future in microgravity exploration.

References

[1] E. Blaler, H. Marcal and B. P. Burns, "Bioastronautics: The Influence of Microgravity," *Astrobiology,* vol. 10, no. 5, 2010.

[2] S. Iwase, N. Nishimura, K. Tanaka and T. Mano, "Effects of Microgravity on Human Physiology," *Chapter metrics overview,* 2020.

[3] J. R. Cowles, R. Lemay and G. Jahns, "Microgravity effects on plant growth and lignification," *Astrophysical Letters and Communication,* 1988.

[4] J. Uri and V. Cooley, "International Space Station - A unique place for research," in *IEEE Aerospace Conference*, 2003.

[5] F. Karmali and M. Shelhamer, "The dynamics of parabolic flight: flight characteristics and passenger percepts," *Acta Astronautica,* vol. 63, no. 5-6, pp. 594-602, 2008.

[6] A. Spaeth, "A brief guide Parabolic Flights," AeroReport, 12 2022. [Online]. Available: https://aeroreport.de/en/good-to-know/a-brief-guide-parabolic-flights.

[7] C. E. Carr, N. C. Bryan, K. N. Saboda, S. A. Bhattaru and G. R. &. M. T. Zuber, "Acceleration profiles and processing methods for parabolic flight," *npj microgravity,* 2018.

[8] N. T. Tillman, "Space.com," 25 August 2017. [Online]. Available: https://www.space.com/37942-vomit-comet.html.

[9] C. Welch and B. Osborne, "Short Duration Reduced Gravity Drop Tower Design and Development," *Journal of the British Interplanetary Society,* 2012.

[10] "Neutral Buoyancy Laboratory," NASA, [Online]. Available: https://www.nasa.gov/johnson/neutral-buoyancy-laboratory/.

[11] S. Franco, "The first drone was invented 16 years prior to the world war 1 by Nikola Tesla," 14 July 2022. [Online]. Available: https://www.warhistoryonline.com/military-vehicle-news/nikola-tesla-drone.html.

[12] S. A. H. Mohsan, M. A. Khan, F. Noor, I. Ullah and A. H. Mohammed, "Towards the Unmanned Aerial Vehicles (UAVs): A Comprehensive Review," *Drones,* vol. 6, no. 6, 2022.

[13] "Tech : Watch a drone drop a microgravity capsule," Space.com, 2 February 2023. [Online]. Available: https://www.space.com/gravitilab-first-drone-based-microgravity-experiment-video.

[14] D. P. Blogs, "Selecting Quadcopter Motors: A detailed Guide 2021," 16 December 2020. [Online]. Available: https://robu.in/selecting-quadcopter-motor-a-detailed-guide-2021/.

[15] N. Agnihotri, "How to select drone motors," Engineers Garage, [Online]. Available: https://www.engineersgarage.com/how-to-select-drone-motors/.

[16] D. Kotarski, P. Piljek, M. Pranjić, C. G. Grlj and J. Kasać, "A Modular Multirotor Unmanned Aerial Vehicle Design Approach for Development of an Engineering Education Platform," *Sensors (Basel)*, vol. 21, no. 8, 2021 April.

[17] Danae, "How to choose the best battery for my drone," 10 12 2020. [Online]. Available: https://www.grepow.com/blog/how-to-choose-the-best-battery-for-my-drone-uav.html.

[18] "All About Multirotor Drone Batteries," Get FPV, 8 February 2018. [Online]. Available: https://www.getfpv.com/learn/new-to-fpv/all-about-multirotor-fpv-drone-battery/.

[19] "Electronic Speed Controller (ESC)," 8 December 2023. [Online]. Available: https://www.jouav.com/blog/electronic-speed-controller-esc.html.

[20] C. Bergquist, "How to build a drone," Drone DOJO, 23 March 2019. [Online]. Available: https://dojofordrones.com/build-a-drone/.

[21] C. Bergquist, "Selecting a drone flight controller," 28 march 2019. [Online]. Available: https://dojofordrones.com/drone-flight-controller/.

[22] "All About Multirotor Drone FPV Power Distribution Boards," Get FPV, 3 February 2018. [Online]. Available: https://www.getfpv.com/learn/new-to-fpv/all-about-multirotor-fpv-drone-power-distribution-board/.

[23] "RTK GPS Correction," Ardupilot, [Online]. Available: https://ardupilot.org/copter/docs/common-rtk-correction.html.

[24] "Common Power Module," Ardupilot, [Online]. Available: https://ardupilot.org/copter/docs/common-3dr-power-module.html.

[25] D. Daly, "Drone Payloads Vs. Performance: A balancing Act," [Online]. Available: https://consortiq.com/uas-resources/how-to-balance-your-drones-payload-performance---.

[26] "Servo Motors," Real Digital , [Online]. Available: https://www.realdigital.org/doc/d0c3c99063edf31ea853d517847ac488.

[27] "Physics: Accelerometer," Vedantu, 22 March 2024. [Online]. Available: https://www.vedantu.com/physics/accelerometer.

[28] "Unmanned Aerial Systems (Drones) Guidelines in Raleigh," 9 Feb 2024. [Online]. Available: https://raleighnc.gov/services/parks/drones-guidelines-raleigh-parks.

[29] "Choosing a ground station," Ardupilot, [Online]. Available: https://ardupilot.org/plane/docs/common-choosing-a-ground-station.html.

[30] "Mission Planning," Ardupilot, [Online]. Available: https://ardupilot.org/copter/docs/common-mission-planning.html.

[31] V. Plester, N. Frischauf, R. laufer and D. Cohen, "Parabolic flights with gliders as an innovative low cost platform for microgravity and hypergravity research," in *68th International Astronautical Congress*, Adelaide, Australia, 2017.

APPENDICES

Appendix A: MATLAB Code

The code was created in MATLAB to convert the data point obtained from the accelerometer sensor to time to be plot gravity values with respect to time.

```
clc

clear

close all


Time = [];

g_X = [];

g_Y = [];

g_Z = [];


filename = 'Outer_capsule.txt'; %%%%%%%% INPUT NEEDED %%%%%%%%%

fid = fopen(filename,'r');


ST = textscan(fid,'StartTime: %s %s');

Start_Time = strcat(ST{1,1}, {' '}, ST{1,2});

Start_Time = datetime(Start_Time, 'InputFormat', 'yy-M-dd HH:mm:ss.SSS');
```

```
%Advance 1 lines:

% skipping the column titles line

for ii = 1:1

    fgetl(fid);

end



%Advance x lines:

linesToSkip = 25500; % skipping unnecessary data lines/rows %%%%%%%%% INPUT
NEEDED %%%%%%%%%

for ii = 1:linesToSkip

    fgetl(fid);

end




n = 600; % Data lines to read  %%%%%%%%% INPUT NEEDED %%%%%%%%%



for i=1:n



    C = textscan(fid,'0x50 %s %f32 %f32 %f32 %f32',1);
```

```
    T = datetime(strcat(ST{1,1}, {' '}, C{1,1}), 'InputFormat', 'yy-M-dd mm:ss.SSS');
    Time = [Time; seconds(T - Start_Time)];
    g_X = [g_X; C{1,2}];
    g_Y = [g_Y; C{1,3}];
    g_Z = [g_Z; C{1,4}];

end

fclose(fid);

g_Total = sqrt(g_Z.^2);

Time = Time - Time(1);

figure(1)
plot(Time,g_Total,'r')
ylabel('Gravity (g m/s^2)')
xlabel('Seconds (s)')
grid on
title('g Vs Time')
```

```
ylim([-1 15])

figure(2)
plot(g_Total,'b')
ylabel('Gravity (g m/s^2)')
xlabel('Number of Data Points')
grid on
title('g Vs Number of Data Points')
ylim([-1 15])

%%%%%% Saving Data File %%%%%%%%

table = [Time, g_Total];
savefilename = 'g_Outer_capsule_.dat'; %%%%%%%% INPUT NEEDED %%%%%%%%%

writematrix(table, savefilename, 'Delimiter', ' ')
```